Materials Horizons

ROYAL SOCIETY OF CHEMISTRY

REVIEW

View Article Online
View Journal | View Issue

Cite this: *Mater. Horiz.*, 2021, 8, 2387

Metal–organic frameworks for chemical sensing devices

Joseph F. Olorunyomi,[ab] Shu Teng Geh,[ab] Rachel A. Caruso *[a] and Cara M. Doherty *[b]

Metal–organic frameworks (MOFs) are exceptionally large surface area materials with organized porous cages that have been investigated for nearly three decades. Due to the flexibility in their design and predisposition toward functionalization, they have shown promise in many areas of application, including chemical sensing. Consequently, they are identified as advanced materials with potential for deployment in analytical devices for chemical and biochemical sensing applications, where high sensitivity is desirable, for example, in environmental monitoring and to advance personal diagnostics. To keep abreast of new research, which signposts the future directions in the development of MOF-based chemical sensors, this review examines studies since 2015 that focus on the applications of MOF films and devices in chemical sensing. Various examples that use MOF films in solid-state sensing applications were drawn from recent studies based on electronic, electrochemical, electromechanical and optical sensing methods. These examples underscore the readiness of MOFs to be integrated in optical and electronic analytical devices. Also, preliminary demonstrations of future sensors are indicated in the performances of MOF-based wearables and smartphone sensors. This review will inspire collaborative efforts between scientists and engineers working within the field of MOFs, leading to greater innovations and accelerating the development of MOF-based analytical devices for chemical and biochemical sensing applications.

Received 14th April 2021,
Accepted 21st June 2021

DOI: 10.1039/d1mh00609f

rsc.li/materials-horizons

1 Introduction

The field of porous materials has undergone significant growth within the last 25 years and has seen the emergence and rapid development of metal–organic frameworks (MOFs).[1,2] MOFs,

[a] *Applied Chemistry and Environmental Science, School of Science, RMIT University, Melbourne, Victoria 3000, Australia. E-mail: rachel.caruso@rmit.edu.au*
[b] *CSIRO Manufacturing, Clayton, Victoria 3168, Australia. E-mail: cara.doherty@csiro.au*

Joseph F. Olorunyomi

Joseph Olorunyomi received his bachelor's and Master of Philosophy degrees in Chemistry from Obafemi Awolowo University, Ile-Ife, Nigeria and the University of Hong Kong, Hong Kong, respectively. He is currently a PhD candidate at RMIT University, Australia under the joint supervision of Prof. Rachel Caruso and Dr Cara Doherty, Commonwealth Scientific and Industrial Research Organisation (CSIRO), Australia. His research interest is in the implementation of metal–organic frameworks in portable devices for smart sensing of toxins.

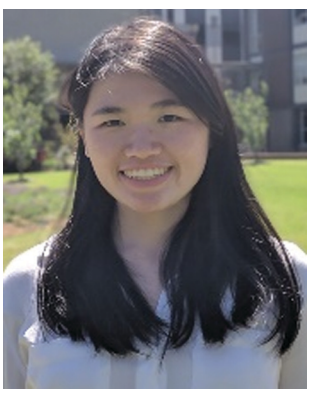

Shu Teng Geh

Shu Teng Geh received her BEng (Hons) in Chemical Engineering from Monash University, Australia in 2019. She is currently pursuing her Masters by Research at RMIT University, Australia in the RMIT/CSIRO Masters by Research Program under the joint supervision of Prof. Rachel Caruso (RMIT), Prof. Leslie Yeo (RMIT) and Dr Mustafa Musameh (CSIRO, Australia). Her research interests include metal–organic frameworks, biosensors and electrochemistry.

also known as porous coordination polymers, are a class of advanced porous materials constructed from inorganic clusters and organic ligands.[3] They are characterized by large internal surface areas, highly organized porosity and vast structural diversity with a range of chemical and physical properties.[4–6] Consequently, MOFs have shown great promise in various applications including ionic/molecular adsorption,[7,8] separations,[9] electrochemical energy storage,[10] catalysis,[11,12] chemical and biosensing.[13]

Chemical sensing is a process that uses analytical devices having sensitive components which undergo chemical changes upon interactions with chemical substances and a transducer that transforms the chemical changes into measurable physical signals. Chemical sensing is one of the most promising applications of MOFs due to the large libraries of metal centres and readily functionalized organic cages that render them responsive to different chemical and biological stimuli.[13–15] The publication trends and the associated citations that are related to MOF sensing topics over the last decade is shown in Fig. 1. The number of published articles on the sensing applications of MOFs increased and the citations followed a similar trend over this period. The sustained citation growth over this period highlights the significant potential of MOFs as sensitive materials to different chemical and biochemical stimuli. Hence, this development has driven the desire to fabricate MOF-based analytical devices that can provide immediate information on the occurrence of specific substances in a complex sample.[16] The construction of analytical devices starts with the fabrication of films of MOFs (which are primarily obtained as powders) either through the deposition or coating of substrates with MOF crystals.[17]

Many excellent reviews have been written on the development of film fabrication technologies. In 2009, Fischer and coworkers reviewed studies on the direct MOF growth over various functionalized substrates and thickness control through layer-by-layer (LbL) deposition.[18] In 2012, Bétard and Fischer provided a comprehensive critical appraisal of the processing methods used for the fabrication of MOF thin films.[19]

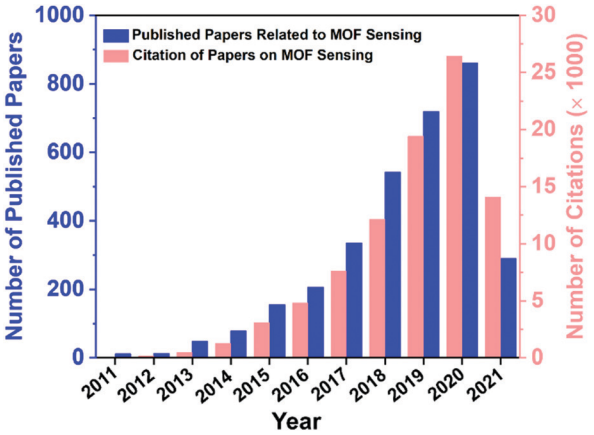

Fig. 1 The number of published papers with their corresponding citations on topics related to MOF sensing in the 2011 to 2021 period, using the search terms ("metal–organic framework") AND (sens*) AND (detect*). Source: Web of Science. The asterisked 'sens*' was used to include papers containing keywords such as 'sensing', 'sensor', 'sensors', 'sensitive' and 'sensitivity'. Similarly, 'detect*' was added to the search terms to include papers containing keywords such as 'detect', 'detection' and 'detecting' in the search.

In the same year, Bradshaw *et al.* presented their assessments on the fabrication techniques for MOF composite thin films.[20] Later studies reported systematic MOF crystals positioning on substrates, film patterning and lithography, which were reviewed by Falcaro *et al.* in 2012[21] and 2014[22] and to advance the prospects of MOF films for device applications. Also, Dong *et al.*,[23] Zhao *et al.*,[24] Wang *et al.*[25] and Chakraborty *et al.*[26] reviewed the recent progress in the film fabrication processes using 2D MOF structures with potential toward various sensing applications. Updated recent reviews from 2021 include Crivello *et al.*,[27] Ren and Jen[28] and Faustini[29] on advanced technologies for MOF film fabrication.

Furthermore, the reviews written by Allendorf *et al.*[17] in 2011 and Stassen *et al.*[30] in 2017, highlighted studies aimed at the implementation of MOF films in electronic devices. The reviews addressed the important requirements and challenges for the

Rachel A. Caruso

Rachel Caruso is a materials chemist and has expertise in the area of advanced porous materials. She has led teams of scientists at the Max Planck Institute of Colloids and Interfaces (Germany), The University of Melbourne, CSIRO and RMIT University (Australia). Her research interests include mesoporous oxides, perovskites and carbon materials for energy and environmental applications. She is currently the Director of the Advanced Materials Enabling Capability Platform at RMIT University.

Cara M. Doherty

Cara Doherty received her BSc degree in Applied Physics from Curtin University and her PhD in Physical Chemistry at The University of Melbourne, Australia. She is currently leading a research team at CSIRO focused on the applications of advanced porous materials. Her research interests include metal–organic frameworks for chemical sensing, bioremediation, biomineralization and device fabrication for energy and environmental applications. She is currently a Veski Inspiring Women Fellow.

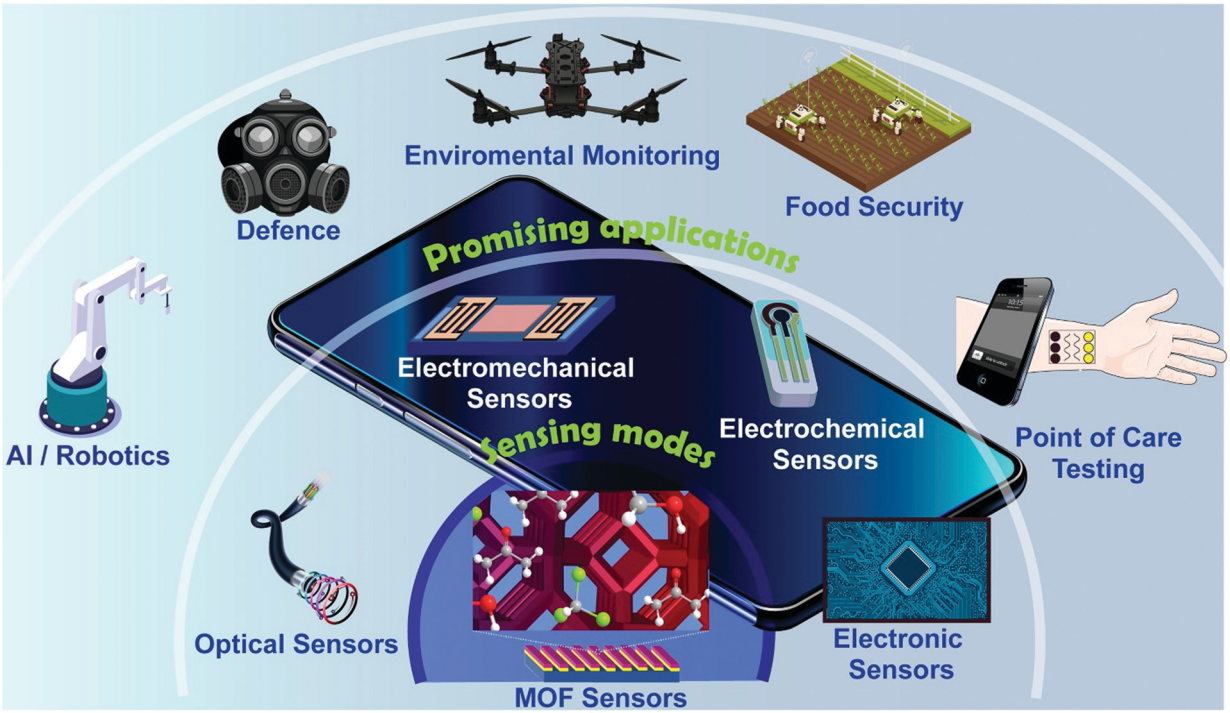

Fig. 2 Schematic showing MOF sensors that can recognise molecules through different sensing modes including electrochemical, electronic, electromechanical and optical platforms. Five major areas of application of MOF devices including point of care testing, food security, environmental monitoring, defence and artificial intelligence are illustrated. The background smartphone highlights the current research trend towards portable platform technologies utilising MOF sensors and bringing the future of sensing to the individual.

electronic application of MOF films and their interface with electronic components of a device.[17,30] Several more focused reviews have highlighted key progress on MOF device fabrication for sensing applications.[25,26,31–43] Therefore, the current review will appeal to researchers beyond the MOF community because it reveals insights into the future direction of sensing and highlights areas that are rising in importance across the materials and sensing fields. The aim of this review is to provide a complementary overview of the latest research on MOF integration into different sensing platforms. As illustrated in Fig. 2, this review will first highlight the latest MOF-based proof-of-concept sensors developed since 2015 across the four major sensing platforms, namely: electrochemical, electronic, electromechanical and optical modes. Finally, the progress and prospects of MOF sensors for field-deployable applications such as in point-of-care diagnosis, food security, environmental monitoring, defence and artificial intelligence will be discussed.

2 Proof-of-concept MOF devices from different sensing platforms

Many studies have shown interesting performance of MOFs towards the detection of chemical species and have demonstrated some proof-of-concept devices across various sensing platforms.[31,33,41,44] It is noteworthy that the progress recorded in combining various film fabrication and patterning techniques to MOF syntheses is currently driving the development of MOF sensors. Some examples of those sensors and devices reported since 2015 are shown in Table 1. These representative proof-of-concept devices highlight the potential of MOFs in the development of wearable and field-deployable sensor technology. An overview of the latest research on the application of electrochemical, electronic, electromechanical and optical sensors are discussed in this section.

2.1 Electrochemical sensors

Electrochemical sensors are a class of sensors that provide direct and selective detection of organic and inorganic compounds that can be easily oxidized or reduced.[72] They are promising due to several advantages including ease of operation, rapid detection and low production cost.[73] One of the most common electrochemical sensing technique is an amperometric method that uses current as the sensing response from the analyte.[74] Typically, the rate of the electrochemical reaction with the target analyte will determine the sensitivity of the amperometric sensors. Since electrochemical reactions can only occur on the surface of the electrode, the surface should be modified by immobilizing the electrocatalyst.[74] This would provide more catalytically active sites for the electrochemical reaction with the target analyte. Hence, resulting in a faster reaction rate and higher sensitivity toward the analyte.

MOFs are attractive for sensing owing to their unique properties such as high surface area, exceptional porosity and

Table 1 Representative proof-of-concept MOF devices for chemical sensing application

Sensing device	Active MOF film	Film deposition method	Sensing application	Ref.
Wearable sweat sensor	Copper isonicotinate	Direct growth on graphene-loaded carbon fibre.	Sweat glucose and lactate	45
Enzymatic biofuel cell sensor	ZIF-8	Biomimetic fabrication: direct assembly of ZIF-8@enzyme on the surface of cellulose acetate functionalized MWCNTs/Au electrode.	Bisphenol A and glucose	46 and 47
On-chip capacitive sensor	Mg–MOF-74	*In situ* growth with energy supply from thermally activated platinum (Pt) interdigitated electrodes.	CO_2 and benzene	48
Capacitive sensor	MOF-199	Electrochemical deposition[49] and drop-casting.[50]	Organic volatiles	49 and 50
Capacitive sensor	MFM-300 (In)	Solvothermal synthesis on a prefunctionalized interdigitated electrode with an OH-terminated self-assembled monolayer.	SO_2	51
Capacitive sensor	Yttrium fumarate MOF with **fcu** topology	Solvothermal synthesis on a prefunctionalized interdigitated electrode with an OH-terminated self-assembled monolayer.	H_2S	52
Capacitive sensor	Yttrium naphthalene dicarboxylate MOF with **fcu** topology	Solvothermal synthesis on a prefunctionalized interdigitated electrode with an OH-terminated self-assembled monolayer.	NH_3	53
Resistance-switching memory sensors	ZIF-8	Direct synthesis on a polyethylene terephthalate substrate.	Alcohols	54
Conductive textile	Ni_3HHTP_2 and Ni_3HITP_2	*In situ* growth of conductive MOFs on cotton.	NO, H_2S and H_2O	55
Conductive textile (inter-digitated textile electrodes)	MIL-96(Al)	Langmuir–Blodgett technique.	Humidity with organic volatile interferences	56
Impedance sensor	MFM-300 (In, Al, Fe or Sc)	Drop-casting of MFM-300 suspension on an interdigitated electrode.	I_2	57
Liquid-gated field-effect transistor (FET)	$Ni_3(HITP)_2$	*In situ* growth of Ni–MOF layer on the FET device.	Gluconic acid	58
MOF-on-SLG transparent electronic device	$Ni_3(HHTP)_2$	Epitaxial growth.	NH_3	59
Hybrid resonant acoustic (HYDRA) device	HKUST-1	Surface acoustic wave (SAW)-induced wetting of piezoelectric surface with HKUST-1 precursors and subsequent nebulization of the wetted surface.		60
SAW device	HKUST-1 Fe-MIL-88B	Microfluidic centrifugation induced by SAW irradiation.		61
Microcantilever sensor	ZIF-8	Direct growth of ZIF-8 on ZnO/Si cantilever.	Alcohols	62
Wearable sweat sensor	DUT-101 and Ag^+/Eu^{3+}@UiO-67	Cotton fabric immersed in the MOF suspension.	Cl^- monitoring through fluorescence	63
1-D photonic crystal	NH_2-MIL-101(Cr)	Spin coating on TiO_2 substrate.	Methanal/ formaldehyde	64
A bioactive 3D-printed MOF flow sensor	ZIF-8	Biomimetic fabrication: direct assembly of ZIF-8 crystals on the surface of bioactive 3D-printed device.	Methyl parathion	65
Optical fibre long-period grating MOF device	ZIF-8 and HKUST-1	Layer-by-layer growth.	CO_2 and organic vapours	66–68
Optical fibre MOF sensors	ZIF-8	Layer-by-layer growth.	Small inorganic gas molecules	69
Optical fibre-single MOF crystal	HKUST-1	Direct attachment of a single crystal to one end of the optical fibre.	Nitrobenzene	70
Photonic microring resonator	ZIF-8	Layer-by-layer growth followed by patterning *via* lithography.	Organic vapours	71

$Ni_3(HHTP)_2$ = Ni_3(2,3,6,7,10,11-hexahydroxytriphenylene)$_2$, $Ni_3(HITP)_2$ = Ni_3(2,3,6,7,10,11-hexaiminotriphenylene)$_2$, SLG = single-layer graphene.

highly tunable pore size and shape. The porosity of MOFs can be tuned by selecting the appropriate metal ions and ligands, making them highly selective to the desired analyte during electrochemical sensing.[75] However, most MOFs are electrically insulating and have poor electron-transfer ability, which often hinders the direct use of MOFs for electrochemical sensing. To overcome this limitation, conducting materials such as metal nanoparticles (NPs) and carbon-based nanomaterials (*e.g.* carbon nanotubes (CNTs) and reduced graphene oxide (rGO)) are usually incorporated with the MOFs to accelerate the electron-transfer rate between the MOF composites and the electrode.[76,77] The assembly of metal NPs such as gold and silver into MOFs have also been reported to increase the catalytic activity.[78,79] On the other hand, the combination of MOFs and carbon nanomaterials like CNTs not only improve the electrical conductivity but also the mechanical strength of the composites.[80]

In electrochemical sensing, MOFs are typically deposited on glassy carbon electrodes (GCE) for standard laboratory testing, but other substrates are also desirable to promote the integration of MOFs with portable electrochemical devices.[81–83] MOF films are fabricated using controlled parameters to achieve desired film properties such as low roughness and variable thickness ranging from nanometres to a few micrometres.[27] It is worth noting that the properties of the MOF films such as the crystal size and thickness, affect their electron-transfer kinetics and adsorption ability.[27] In other words, these properties will impact the performance of the electrochemical sensor as well. Thus, it is important to control the quality of MOF films by moderating the fabrication parameters. In this section, the

recent development of electrochemical sensors based on MOF films for the detection of analytes, such as hydrogen peroxide, glucose and nitrite will be discussed.

2.1.1 MOF films for detection of inorganic analytes

(a) Detection of nitrite. Nitrite is a preserving agent that is often used in the manufacturing of meat products. The amount of nitrite in food must be measured and controlled as an excess amount is harmful to humans.[84] Several materials, such as Au NPs and porphyrin, have been widely used for the detection of nitrite owing to their excellent electrocatalytic ability.[85,86] For instance, the uniformly grown MOF constructed from hexazirconium nodes and porphyrin linkers, *i.e.* MOF-525 thin film, was first developed by Kung *et al.* to detect nitrite in aqueous KCl solution.[87] The MOF-525 thin films were grown on hydroxyl functionalized fluorine-doped tin oxide (FTO) *via* a solvothermal method, shown in the scanning electron microscopy (SEM) images, Fig. 3a. In MOF-525, the porphyrin ligands served as the active sites for the electrooxidation of nitrite. The current density doubled after the MOF-525 film was exposed to 0.5 mM nitrite ion and showed extraordinary sensing performance compared to the bare FTO, which shows negligible current response with nitrite. Furthermore, a linear increase in peak current was also observed upon the addition of nitrite when the MOF-525 film was used, confirming its electrocatalytic activity for the oxidation of nitrite (see Fig. 3b). In this study, nitrite ions were expected to diffuse through the pores of the MOF film, where oxidation of nitrite occurred within the film. The current response during the detection was attributed to the charge-hopping between the linkers. The electrochemical sensor exhibited a linear range from 20 to 800 μM, sensitivity of 95 μA mM^{-1} cm^{-2} at 0.9 V and limit of detection (LOD) of 2.1 μM (S/N = 3). However, the sensing performance deteriorated due to the sluggish linker-to-linker charge hopping process in MOF-525. Sensitivity can be further enhanced by improving the electrical conductivity of the MOF composites because it will increase the charge transport rate. This can be achieved by incorporating conductive materials into the MOFs.

Kung *et al.* further improved the electrochemical sensing performance of the nitrite sensor by interconnecting the MOF-525 with graphene nanoribbons (GNRs).[88] As shown in Fig. 3c, the GNRs acted as conductive bridges to facilitate charge transport between the linkers, thus, accelerating the overall rate of electrocatalysis of the MOF-525 thin films. This improved version of MOF-525/GNRs sensor achieved a comparable sensitivity at a lower applied potential, *i.e.* 93.8 μA mM^{-1} cm^{-2} at 0.85 V, compared to the previously reported MOF-525 thin film sensor. Furthermore, a much wider linear range of 100 to 2500 μM nitrite and a lower LOD of 0.75 μM (S/N = 3) were also achieved by the modified MOF-525/GNRs film.

(b) Detection of hydrogen peroxide (H_2O_2). H_2O_2 functions as the major transmitter of redox signals during electrochemical processes[90] and is also frequently detected for MOF-based sensing. For instance, a high-density cross-linked copper-based MOF (Cu–BTC) film for the non-enzymatic detection of H_2O_2 was fabricated by Zhou's group.[91] The Cu–BTC film was

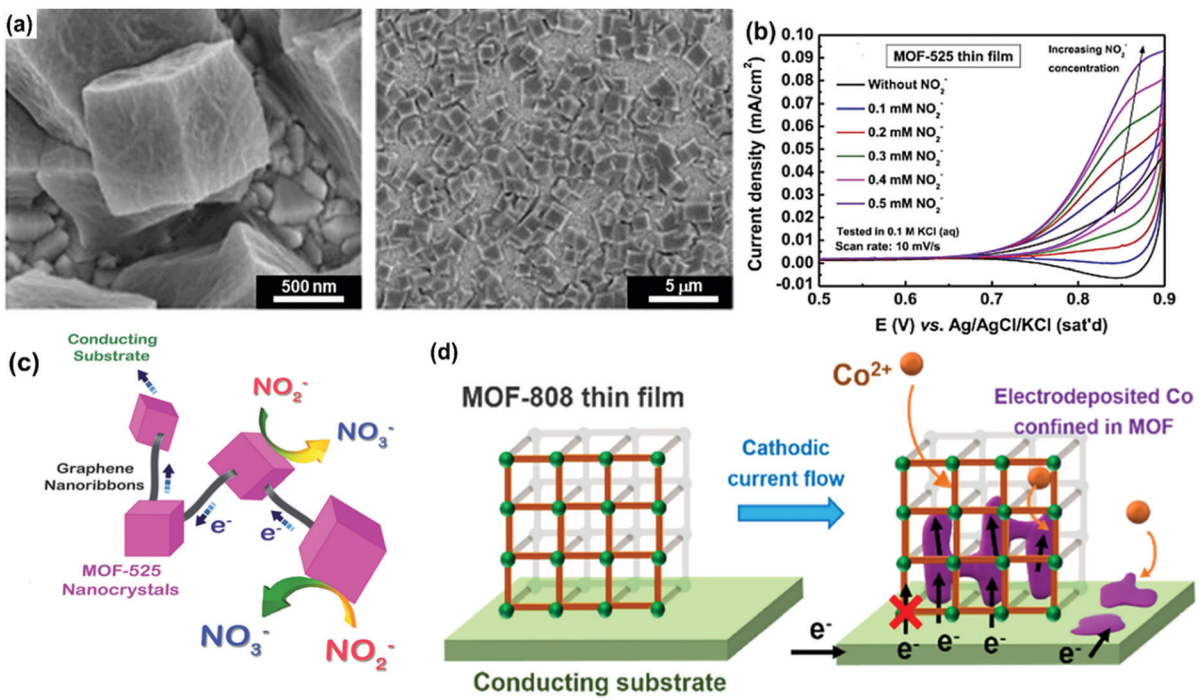

Fig. 3 (a) SEM images of the surface of MOF-525 thin film showing MOF-525 crystals at high and low magnifications. (b) CV curve of the MOF-525 thin film with increasing concentration of nitrite. Adapted with permission.[87] Copyright 2015, Elsevier. (c) Schematic drawing of the MOF-525/GNRs composite for the electrooxidation of nitrite. Reproduced with permission.[88] Copyright 2016, the Royal Society of Chemistry. (d) Schematic illustration for the electrodeposition of cobalt ions in MOF-808 thin film, starting from the MOF/substrate (FTO) interface. Reproduced with permission.[89] Copyright 2020, Elsevier.

prepared on a carboxylated graphene-modified GCE surface, where functional groups including –OH, –COOH and C–O–C were used to promote the oriented growth of the MOF.[92] Based on the electrochemical analysis of the fabricated sensor, it was concluded that only the Cu^{2+} ions possessed good catalytic activity toward H_2O_2 reduction. Moreover, the sensor also displayed a fast response time of less than 10 s, indicating that the analyte molecules could reach the electrode surface in a short time owing to the outstanding porosity of MOFs. The highly porous Cu–MOFs also displayed high selectivity toward H_2O_2 by providing a molecular sieving effect during the detection. The sensor showed high sensitivity of 792 μA mM^{-1}, LOD of 0.067 μM and a wide linear detection range from 0.2 to 185 μM. These promising performances are mainly attributed to three factors, namely: the excellent conductivity of graphene, high porosity of MOF structures and the electrocatalytic activity of the copper ions.

Besides graphene, electroactive substances such as metallic cobalt are an alternative to enhance the conductivity of MOFs, resulting in superior performances of the fabricated sensor. Since most MOFs possess high porosity, the conductivity of MOFs can be improved by inserting the electroactive material in their pores. In a study conducted by Chang *et al.*, electrochemically active cobalt was confined to the pores of an insulating zirconium-based MOF, MOF-808.[89] The electrodeposition of cobalt ions was initiated from the MOF/substrate (FTO) interface, while the porous structure of MOF-808 promoted the diffusion of cobalt ions throughout the MOF film. This should provide more electrically conductive sites for the electrodeposition of cobalt ions within the MOF pores (see Fig. 3d). Furthermore, the rigid structure of MOF-808 in acidic and neutral pH aqueous media can prevent the electrochemically induced aggregation of Co^{2+} during sensing. The resulting Co@MOF-808 thin films were applied for electrochemical H_2O_2 sensing. It was observed that the pore-confined cobalt exhibited a much higher electrochemical activity than the flat cobalt and the presence of the MOF thin film does serve as a template to assist the electrodeposition of cobalt. In the presence of MOF-808, the amount of deposited cobalt was approximately 10 times higher than that deposited on bare FTO. The porosity of the framework also created more exposed surfaces for the confined cobalt, resulting in its superior electrocatalytic activity. The proposed electrochemical sensor displayed a sensitivity of 382 μA mM^{-1} cm^{-2}, LOD of 1.3 μM and a linear range of 10 to 450 μM H_2O_2.

2.1.2 MOF films for biosensing applications

(a) Enzymatic H_2O_2 and glucose detection. Zeolitic imidazolate frameworks (ZIFs) are attractive for the fabrication of electrochemical sensors owing to their high surface area, negligible cytotoxicity and exceptional chemical and thermal stability.[93] For biosensing applications, ZIFs are compatible with most biomolecules and have been deployed in biomimetic mineralization as protective shells for biomolecules.[94] Fan *et al.* first demonstrated the fabrication of a ZIF-8 thin film with encapsulated horseradish peroxidase (HRP) for the enzymatic detection of H_2O_2.[95] To overcome the poor electronic conductivity of ZIF-8, rGO was combined with ZIF-8@HRP and the biocomposite film was coated on an indium-tin oxide (ITO) substrate through the layer-by-layer (LbL) method. When assembling the ZIF-8@HRP composites *via* the LbL method, it was crucial to optimize the film thickness to achieve an optimum sensing performance. For instance, the content of HRP increases with increasing number of layers, which provides more active sites for the target analyte and enhances the sensitivity of the sensor. However, thicker assembled layers will obstruct the substrate diffusion and increase the electron transfer resistance, thus, deteriorating the performance of the sensor. For the best sensing performance, a maximum of four layers was fabricated in this study. The enzymatic bioactivity of HRP was well maintained as the enzyme was enclosed and protected within the ZIF-8 framework. In addition, ZIF-8 had good permeability for H_2O_2, which allowed the sensor to reach a stable response in less than 5 s upon addition of H_2O_2. The resultant enzymatic electrochemical sensor presented excellent anti-interference ability and long-term stability with a wide linear range of 0.02 to 6 mM H_2O_2 and a LOD of 3.4 μM H_2O_2 (S/N = 3).

A different approach was adopted by Zhang *et al.* who prepared a biocomposite film without adding conducting carbon to maximize mass transfer of the analyte. They directly deposited a glucose oxidase (GOx)–ZIF-8 biomineralized composite on a gold substrate for electrochemical glucose detection. GOx–ZIF-8 was assembled by *in situ* synthesis of ZIF-8 in the presence of the enzyme, followed by the cast-coating of the biocomposite on a Au electrode as schematically represented in Fig. 4a.[96] It is interesting that the presence of the enzyme accelerated the growth of ZIF-8 such that the GOx–ZIF-8 biocomposite has larger crystal size than the pristine ZIF-8 (Fig. 4b and c). The GOx–ZIF-8/Au sensor showed linear amperometric response to glucose from 0.01 mM to 1.5 mM with a sensitivity of 21 μA mM^{-1} cm^{-2} and detection limit of 2.2 μM. The GOx–ZIF-8/Au electrode exhibited stability under various testing conditions. The sensor was further shown to be promising for selective detection of glucose in the presence of other forms of sugar that are present in food samples, such as those present in red wine. The stability of the electrode is due to the protective function of ZIF-8 towards GOx and the strong attachment of GOx–ZIF-8 on the Au substrate owing to strong Au–N coordinate bonding.[97]

(b) Enzymatic biofuel cells for bisphenol A and glucose detection. Biofuel cells are devices that generate electricity from enzyme-catalysed redox reactions between organic molecules as fuels and oxidants and they can be endowed with sensing capability to develop self-power generating Enzymatic Biofuel Cell (EBFC) sensors.[98] They are promising for the future advancement of self-powered wearable electrochemical sensors.[99]

MOFs are attracting attention to encapsulate enzymes *via* a biomineralized pathway with the pores allowing transport of the substrate.[46,47,100] Wei's group have investigated the prospects of biomineralized ZIF-8 materials in the application of

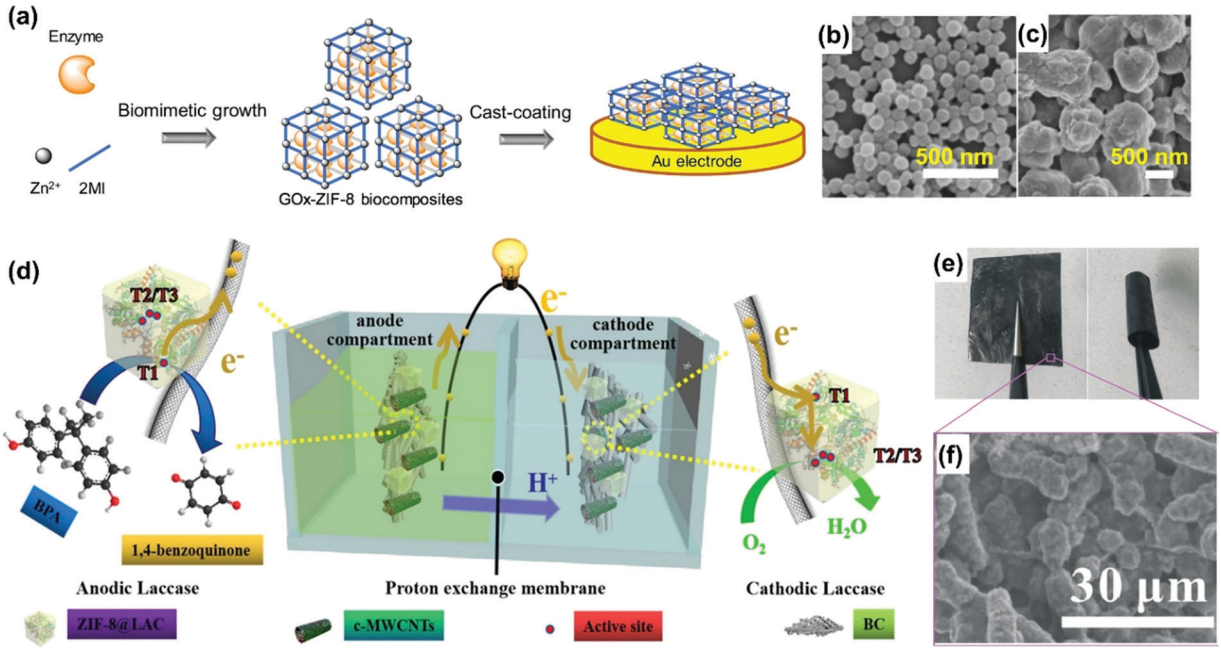

Fig. 4 (a) Illustration of the preparation of GOx–ZIF-8 biocomposites and the fabrication of the electrochemical biosensor. SEM images of (b) ZIF-8 and (c) GOx–ZIF-8. Adapted with permission.[96] Copyright 2018, Elsevier. (d) Schematic representation of processes within an ZIF-8 based enzymatic biofuel cell sensor for the detection of bisphenol A (BPA). Reproduced with permission.[46] Copyright 2020, Elsevier. (e) Optical images of flexible CA/ZIF-8@enzyme/MWCNTs/Au electrode and (f) SEM image of the surface of the flexible CA/ZIF-8@enzyme/MWCNTs/Au electrode. Reproduced with permission.[47] Copyright 2021, Elsevier.

EBFC for electrochemical biosensing.[46,47] They encapsulated laccase (LAC) within ZIF-8, which was then combined with bacterial cellulose (BC)/carboxylated multi-walled carbon nanotubes (c-MWCNTs) to fabricate a BC/c-MWCNTs/ZIF-8@LAC electrode. The sensing set-up shown schematically in Fig. 4d consists of MWCNTs/ZIF-8@LAC electrodes (as both anode and cathode) with bisphenol A (BPA) and 2,2′-azinobis(ethylbenzothiazoline-6-sulfonate) as the anolyte and catholyte (ABTS, cathode mediator), respectively. The role of ABTS was to facilitate good electron transfer by exchanging electrons between the enzyme and the conducting support, thereby improving the power output. The ZIF-8 EBFC attained a maximum power density of 3.68 W m^{-3} and a detection limit of 1.95×10^{-3} mM BPA. The device also demonstrated extraordinary stability and consistent performance due to the protection enjoyed by the encapsulated LAC within ZIF-8. Moreover, the ZIF-8 EBFC sensor could also detect BPA in organic media with high percentage residual activity.[46]

In another study,[47] the same group fabricated a CA/ZIF-8@LAC/MWCNTs/Au electrode using the *in situ* assembly of ZIF-8@LAC on cellulose acetate (CA) membrane, followed by surface adsorption of multi-walled carbon nanotubes (MWCNT) and gold colloids. The SEM image and the photograph of the flexible electrode are shown in Fig. 4e and f, respectively. The dependence of glucose concentration on the open circuit potential of CA/ZIF-8@LAC/MWCNTs/Au through electrochemical impedance investigation was used to study the sensitivity of the ZIF-8 EBFC sensor. It gave a linear response to glucose concentration in the range 1 to 10 mM and showed continuous glucose detection for up to 15 h without a decrease in sensitivity due to the stability of the enzyme encapsulated within the cavities of ZIF-8. The fabrication of flexible biomineralized MOF electrodes are promising in the construction of wearable and implantable devices with long-term stability for biomedical applications.

(c) Non-enzymatic glucose detection. In a study performed by Shahrokhian *et al.*, HKUST-1 was utilized for high performance non-enzymatic glucose sensing.[101] In their study, the thin film of HKUST-1 was directly grown on the GCE substrate *via* three steps, as illustrated in Fig. 5a. The first step involved the electrodeposition of metallic copper clusters on the GCE surface, followed by the chemical conversion of the copper into $Cu(OH)_2$ nanotubes (NTs) and finally, the conversion of $Cu(OH)_2$ NTs into HKUST-1. The final step of this process can be expressed as a simple acid–base reaction, involving $Cu(OH)_2$ NTs and trimesic acid (H_3BTC). The authors also hypothesized that the residual $Cu(OH)_2$ can serve as a conductive binder, hence eliminating the need to use other insulating binders or conductive additives that could increase the resistivity of the electrode. The $Cu(OH)_2$ NTs also exhibited electrochemical activity toward glucose oxidation. As shown in the graph of Fig. 5b, the catalytic current of glucose oxidation was enhanced when HKUST-1 was used as the sensing element. This indicates that the MOFs have larger surface area and higher electrocatalytic activity toward the oxidation of glucose compared to the $Cu(OH)_2$ NTs. The surface area of the HKUST-1 film was also calculated to be 2.6 times higher than that of the $Cu(OH)_2$ NTs. The properties of the MOF toward glucose detection were

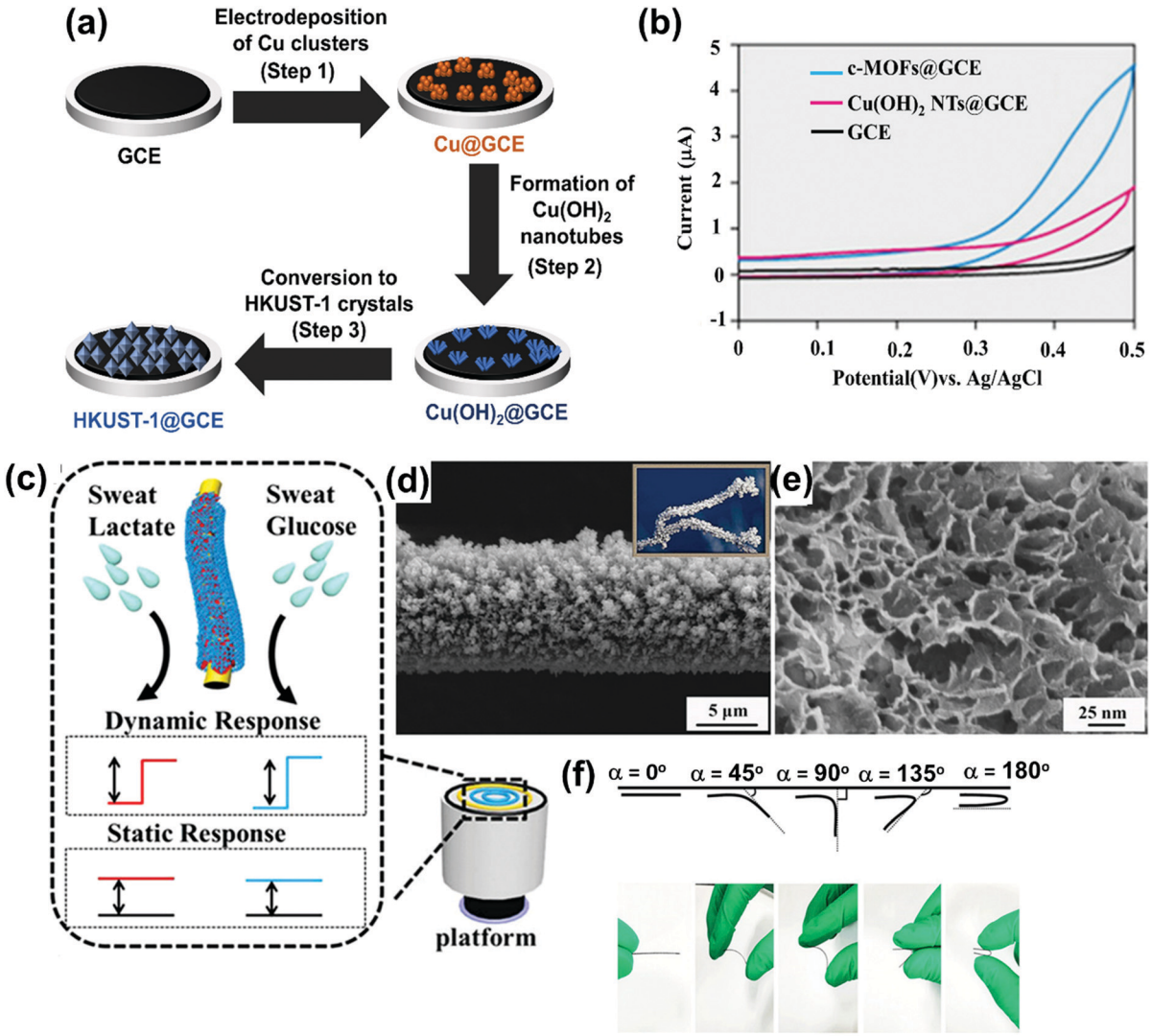

Fig. 5 (a) Schematic illustration for the fabrication of the HKUST-1 thin films on GCE from Step 1 to Step 3. (b) CV responses of bare GCE (black), $Cu(OH)_2$ NTs@GCE (pink) and HKUST-1@GCE (blue) obtained from chemically prepared $Cu(OH)_2$ in the presence of 0.27 mM glucose in 0.1 M NaOH solution; scan rate: 10 mV s^{-1}. Adapted with permission.[101] Copyright 2018, Elsevier. (c) Diagram of ACF-rGO/$Cu(INA)_2$ electrode showing the schematic design of ACF-rGO/$Cu(INA)_2$ and electrochemical response to lactate and glucose. (d and e) Top-sectional SEM images of the surface ACF-rGO/$Cu(INA)_2$, at (d) low magnification and (e) high magnification. (f) Optical images of flexible ACF-rGO/$Cu(INA)_2$. Reproduced with permission.[45] Copyright 2018, American Chemical Society.

investigated, which displayed a LOD of 0.6 μM (S/N = 3) and two linear ranges of concentration from 2.0 μM to 1.4 mM and 1.4 mM to 4.0 mM with sensitivities of 1044 and 682 μA mM^{-1} cm^{-2} respectively. The lower sensitivity over the latter range might be attributed to the slow adsorption of the glucose molecules at high concentration. Nevertheless, this sensor had better performance, such as lower LOD and wider linear range of concentrations compared to some previously reported copper-based non-enzymatic glucose sensors.[102,103]

Shahrokhian *et al.* also recently reported the fabrication of bimetallic NiCo-BTC on GCE that showed a higher sensitivity of 1789 μA mM^{-1} cm^{-2} to glucose due to the improved electrocatalytic properties of the bimetallic NiCo-BTC. They then fabricated a miniaturized device by depositing the same MOF on a graphitic screen-printed electrode (GSPE), which they demonstrated towards glucose sensing. The NiCo-BTC/GSPE had a sensitivity of 230.5 μA mM^{-1} cm^{-2} and a detection limit of 10.8 μM glucose.[104] An improvement in the electrocatalytic and electronic conducting properties of the MOF layer lead to better sensitivity in electrochemical detection. This was demonstrated by Xu *et al.* when they fabricated an electronically conducting bimetallic NiCo-HHTP MOF on a carbon cloth (CC) substrate for glucose sensing.[105] Ni/Co(HHTP)MOF/CC showed a sensitivity of 3250 μA mM^{-1} cm^{-2} towards glucose. The high sensitivity of Ni/Co(HHTP)MOF/CC is related to the excellent electrocatalytic properties and exceptional charge transfer kinetics due to the synergy in the electrocatalytic behaviours of both metals within the MOF structure and the overall high electronic conduction of the MOF, respectively.[105]

Wang *et al.* developed a non-enzymatic electrochemical sweat biosensor (Fig. 5c) using copper isonicotinate MOF ($Cu(INA)_2$) grown on the surface of a graphene-coated activated carbon fibre (ACF-rGO).[45] The surface of the ACF-rGO/$Cu(INA)_2$ composite as seen from the SEM image in Fig. 5d and e shows that $Cu(INA)_2$ has a rime-like morphology with hierarchical pores. The composite was applied in amperometric sensing of glucose and lactate in an acidic electrolyte showing excellent performance in the analysis of sweat lactate and glucose to obtain 9.99 and 0.50 mM, respectively. Moreover, ACF-rGO/$Cu(INA)_2$ was deposited on flexible substrates (see Fig. 5f), which is promising to directly deploy MOFs in non-invasive wearable sweat sensor systems such as body wear or wristbands for sporting activities or point of care diagnostics.

(d) Detection of imatinib. HKUST-1 is one of the most commonly studied MOFs for electrochemical applications due to its facile preparation and exposed metal sites.[106] Recently, Jalal *et al.* successfully developed an electrochemical sensor for the detection of imatinib (IMA) *via* the *in situ* growth of HKUST-1 on graphene oxide nanoribbon (GONR) modified GCE.[107] IMA is an anticancer drug and the ability to control the levels of this drug is required to provide dose optimization.[108] Besides showing good stability, reproducibility and repeatability, the as-prepared HKUST-1/GONRs/GCE sensor also recorded a LOD of 6 nM IMA and two linear ranges of 0.04 to 1.0 μM and 1.0 to 80 μM IMA. These properties outperformed most of the existing electrochemical sensors.[107] The GONRs are responsible for improving the electrochemical sensitivity of the MOF composites by facilitating the electron transfer between the target analyte and the electrode surface. Furthermore, the high surface area of the HKUST-1 provided abundant sites for the electrostatic interaction between the MOF and the IMA. This resulted in the enhanced oxidation peak current of IMA at the HKUST-1/GONRs/GCE composites. Owing to the synergistic effects of both the GONRs and the HKUST-1, a lower potential was required to achieve higher anodic current for the electrooxidation of IMA compared to using HKUST-1 only. Importantly, the sensitivity of the sensor is controlled by the thickness of the HKUST-1 film and the concentration of GONRs. Thicker films slow the electron transfer between the target analyte and the electrode, whereas high concentrations of GONRs will potentially block the pores of HKUST-1. Thus, it is crucial to optimize the reaction time for the *in situ* growth of HKUST-1 and the concentration of GONRs.[107]

(e) Detection of E. coli bacteria. Modified HKUST-1 with conductive additives can also be applied as an electrochemical biosensor for the highly sensitive detection of *E. coli* bacteria. In a study performed by Gupta *et al.*, HKUST-1 was mixed with polyaniline (PANI) on an ITO substrate before applying it as a biosensor.[75] This novel biosensor possessed a wide range of detection from 2.0 to 2.0×10^8 cfu mL^{-1}, low LOD of 2.0 cfu mL^{-1} and response times of approximately 2 min. Furthermore, the analyte concentration detected using the as-fabricated sensor agreed well with that obtained using the conventional colony counting method. These unprecedented performances are attributed to the effect of using conducting PANI and HKUST-1. In addition to introducing electrical conductivity to HKUST-1, PANI also assisted in the formation of homogenous thin films on the ITO while the large surface area of the HKUST-1 improved the anti-*E. coli* antibodies (Ab) loading, which are essential for the bacteria binding. The sensor also displayed long-term stability of up to at least 60 days of storage. With this simple synthesis approach, the development of such a sensor in the form of disposable strips becomes feasible.

2.2 Electronic sensors

The advancement of semiconductor and integrated circuit devices has accelerated the development of electronic chemical sensors. MOFs have been intensively researched for potential integration with electronic device technology.[32] Although most of the known MOFs are poor electronic conductors, which prevents direct interfacing with the electronic conducting physical components of devices, researchers have developed methods to exploit the sensing properties of MOFs through changes in their indirect electronic properties such as capacitance, resistance and field-effects.[30,31,34,109,110] Recent reports demonstrate the design of electronically conducting MOFs,[111] tuning electronic properties of intrinsically insulating MOFs,[112–115] and the understanding of charge transfer processes.[43,116] These studies are required to drive research towards the development of MOF-based electronic devices for chemical sensing technologies. In this sub-section, discussions will be focussed on proof-of-concept MOF-based electronic devices that have been deployed in chemical sensing.

2.2.1 Room temperature chemical capacitive sensors. A variety of devices have been fabricated to demonstrate the promise of MOFs towards chemical sensing based on the capacitance response of MOFs after their adsorption of molecular guests. Interdigitated electrode (IDE) chips are popular devices used for electrical transduction and can be readily modified with solid-state materials. Yassine *et al*. coated a rare earth (RE) metal centred MOF having face-centred cubic (**fcu**) topology, Yttrium-**fcu** fumarate (Y-fum-**fcu**-MOF), on IDE chips to make a capacitive sensor for H_2S detection.[52] The MOF IDE chip was fabricated through an *in situ* solvothermal synthesis and crystallization of Y-fum-**fcu** on the surface of an OH-terminated self-assembled monolayer functionalized IDE substrate. The Y-fum-**fcu**-MOF IDE sensor showed high response to H_2S compared to other gases including CH_4, NO_2, H_2 and toluene with a detection limit of 5.4 ppb H_2S (see Fig. 6a). This sensor maintained consistent performance over multiple cycles of testing and showed better stability than other MOF (ZIF-8 and Cu(II) terephthalate) IDEs which declined in performance due to the formation of metal sulphide. The unique structural formation within Y-fum-**fcu**-MOF consisting of a hexanuclear Y cluster bridged by short rigid fumarate linkers prevented the formation of yttrium(III) sulphide during prolonged exposure to H_2S (12 weeks) and ensured the steady performance of the Y-fum-**fcu**-MOF IDE sensor (Fig. 6a).[52]

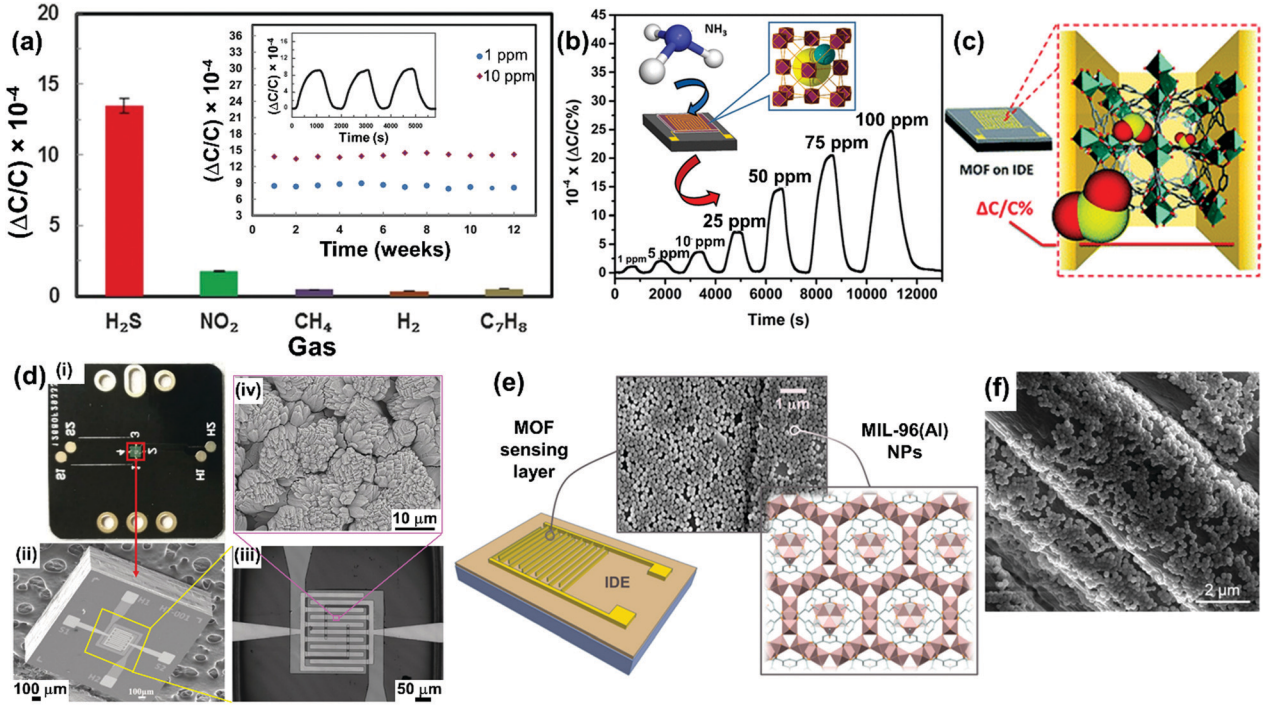

Fig. 6 (a) Selectivity of the Y-fum-**fcu**-MOF sensor to H_2S in the presence of NO_2, CH_4, H_2 and toluene at 10 ppm (inset: stability performance of Y-fum-**fcu**-MOF over 12 weeks (inset: reproducibility cycles for detection of 1 ppm of H_2S over 5000 s)). Adapted with permission.[52] Copyright 2016, Wiley-VCH. (b and c) Schematic diagrams of different RE-MOFs fabricated on IDE chips for capacitive sensing applications: (b) NDC-Y-**fcu**-MOF IDE sensor for NH_3 detection. Reproduced with permission.[53] Copyright 2017, American Chemical Society. (c) MFM-300 (In) MOF IDE capacitive sensor for SO_2 detection. Adapted with permission.[51] Copyright 2018, the Royal Society of Chemistry. (d) (i–iv) Mg–MOF-74 fabricated on IDE chip as a capacitive sensor for CO_2 and benzene vapour: (i) optical image of the IDE chip, (ii) a magnified optical image showing expanded view of the IDE chip, (iii) the SEM image of the IDE chip showing the Pt finger electrodes of the IDE chip and (iv) the SEM image showing the morphology of Mg–MOF-74 crystals grown on the IDE chip. Adapted with permission.[117] Copyright 2019, Wiley-VCH. (e) MIL-96(Al) IDE sensor for humidity sensing. Reproduced with permission.[118] Copyright 2020, American Chemical Society. (f) SEM images showing the surface of a linen fabric coated with MIL-96(Al) crystals as a TEX sensor for humidity detection. Reproduced with permission.[56] Copyright 2020, American Chemical Society.

Assen *et al.* integrated a similar MOF with IDE chips for capacitive sensing of NH_3.[53] The naphthalene-based Yttrium-**fcu**-MOF (NDC-Y-**fcu**-MOF) was grown on an IDE and exhibited selective recognition of ammonia gas with a detection limit of 0.1 ppm (see Fig. 6b). The sensor showed excellent selectivity to NH_3 in the presence of mixtures of NH_3 with CO_2 and various levels of humidity. The NDC-Y-**fcu**-MOF retained its chemical stability with sustained capacitive response to NH_3 for more than two weeks. Interestingly, the low detection limit was obtained at room temperature, thereby attracting opportunities to deploy NDC-Y-**fcu**-MOF in low temperature applications such as in breath analysis, ammonia detection for livestock protection, environmental monitoring and chemical leakage sensors in room temperature sensing applications.[53]

Chernikova *et al.* also fabricated an indium based MFM-300 (In) MOF IDE capacitive sensor for the detection of SO_2 gas, as shown in Fig. 6c, that had an outstanding performance at room temperature with a detection limit of 75 ppb.[51] The reported sensing response was due to excellent adsorption of SO_2 by MFM-300 (In) through hydrogen bonding interactions between the SO_2 with both the bridging –OH group of the inorganic cluster, $InO_4(OH)_2$ and the hydrogen atoms of the aromatic rings of the linker. The intermolecular interaction between the adsorbed SO_2 molecules also increased their loading within the MOF cavities.[119] This sensor displayed similar performance in both wet and dry conditions. Remarkably, the uptake and the capacitive response to SO_2 are greatly enhanced at high relative humidity due to the increased hydrogen bonding interaction of SO_2 with adsorbed water molecules without the collapse of the MOF structure.[51,119] Yuan *et al.* also deposited Mg–MOF-74 on an IDE chip (Fig. 6d) *via in situ* solvothermal crystallization of the MOF on the IDE substrate for room temperature sensing of CH_4, CO_2 and benzene vapour.[117] The Mg–MOF-74-IDE capacitive sensor exhibited a selective response to benzene and CO_2 over CH_4. CO_2 with a large quadruple moment and the π-electron-rich benzene molecules preferentially interact with the open metal sites of Mg–MOF-74 through strong physisorption and Lewis acid–based interactions, respectively. Moreover, the Mg–MOF-74-IDE capacitive sensor was subjected to post-synthetic ethylenediamine functionalization, which decreased its sensitivity to benzene vapour but improved selectivity toward CO_2 through strong amine–CO_2 interactions.[117]

Andrés *et al.* employed a similar device that they fabricated by depositing preformed MIL-96(Al) particles on an IDE using the Langmuir–Blodgett (LB) method for humidity sensing, shown in Fig. 6e.[118] The LB film deposition method is used

to fabricate close-packed MOF films through repeated immersion and withdrawal of the substrate from a suspension of the MOF that also contains amphiphilic substances at the air–water interface to induce ordering of the MOF crystals.[120] The MIL-96(Al) LB IDE device response to humidity was based on the affinity of MIL-96(Al) to water molecules and its high adsorption capacity. The sensor also shows high selectivity to water vapour in the presence of organic vapours. Moreover, the sensitivity of MIL-96(Al) LB IDE to water vapour was improved after the chemical vapour deposition of a hydrophobic porous poly(*para*-xylylene) film (Parylene C) on the surface of the MOF-IDE chip to ensure the stability of the MOF during multiple cycles of sensing and regeneration.[118] Rauf *et al.* later integrated the same MIL-96(Al) with textiles to fabricate a smart textile-based (TEX) sensor for humidity detection after the incorporation of MIL-96(Al) on fabric materials.[56] The MIL-96(Al) crystals were added to the thread of a conducting fabric using a vertical LB deposition technique. The SEM image in Fig. 6f shows the surface of the TEX linen fabric modified with MIL-96(Al) crystals. The response of the TEX sensor to water vapour was probed by measuring changes in the capacitance of the device which increased with increasing humidity. The presence of MIL-96(Al) on the TEX sensor causes high selectivity to water due to the hydrogen bonding alumina clusters of the MOF. The response of the TEX sensor is only lowered by increased temperature which signposts a promising application in wearable sensors for human respiration monitoring.[56]

2.2.2 Chemoresistive MOF sensors. Most MOFs are insulators, but they exhibit changes in resistance after adsorption of guest species, hence they have been investigated for use in chemoresistive devices. The sensing performance of such devices can be determined through either resistance measurements or direct conductivity studies.

(a) Resistance-switching memory MOF sensors. Resistive random-access memory (RRAM) devices belong to the family of non-volatile memory devices that have metal–insulator–metal structural arrangements and possess resistance-switching (RS) properties. Devices that exhibit RS properties undergo resistance fluctuations between two stable states, namely: high resistance (HRS) and low resistance states (LRS). Both HRS and LRS represent distinct logic states such as the (0, 1) binary codes that are applicable in computing and information storage.[121] RRAM devices are also promising in the development of portable and wearable sensors with inherent data storage capability to secure the user's privacy.[122]

RS properties have been studied in various MOFs and combined with their chemical sensitivity towards analytes can be used to develop wearable sensors with data storage features.[123–129] Pan *et al.* deposited HKUST-1 film on a gold-coated flexible polyethylene terephthalate (PET) substrate to form a Au/HKUST-1/Au device.[128] The device, with its current–voltage characteristic shown in Fig. 7a, was initially in a HRS due to the insulating property of HKUST-1 and then switched to the LRS after a biased voltage of 2 V was applied. The device can be reset (*i.e.* switching from LRS to HRS) by applying a biased

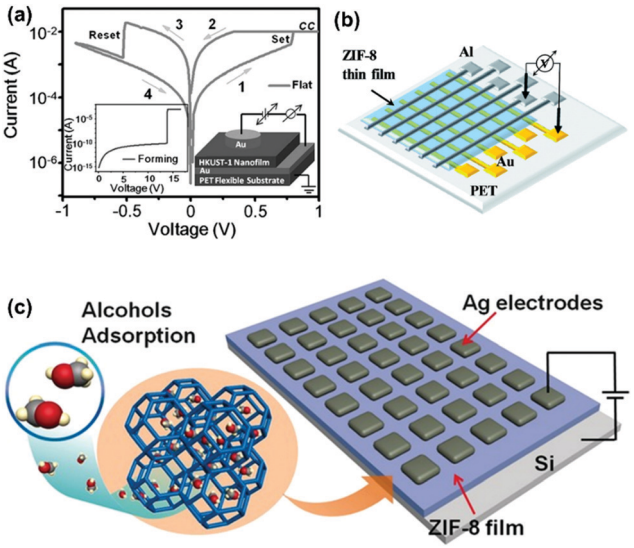

Fig. 7 (a) Current–voltage characteristics of the Au/HKUST-1/Au/PET flexible device (inset: schematic configuration and the forming process of the memory device). Stages 1 and 2 represent the switch from the initial HRS to LRS, respectively after applying voltage bias, while stages 3 and 4 indicate resetting from LRS to HRS, respectively after applying reverse voltage bias. Adapted with permission.[128] Copyright 2015, Wiley-VCH. (b) Schematic image of the matrix-formed ReRAM device with Al top and Au bottom electrodes, the ZIF-8 film sits on the PET substrate. Adapted with permission.[129] Copyright 2017, the Royal Society of Chemistry. (c) ZIF-8-based memory device arrays with alcohol-mediated properties. Adapted with permission.[54] Copyright 2016, Wiley-VCH.

voltage of −2 V. To understand the process, the authors proposed that RS occurred due to the presence of a charge transfer pathway from voltage-induced redox reactions of the MOF's metal centre leading to the instability of the negatively charged organic linkers to create a π-conjugated system. In the Au/HKUST-1/Au device schematically represented in Fig. 7b, the switching from the HRS to the LRS occurs due to the reduction of Cu^{2+} to metallic Cu, followed by the pyrolysis of the 1,3,5-benzene tricarboxylate linker to evolve CO_2 from the carboxylate group, which then leads to the creation of conjugated aromatic system for charge transport.[128] Park and Lee fabricated a ZIF-8 RS device by spreading the ZIF-8 film on gold-coated flexible substrates.[129] The RS behaviour of the ZIF-8 device was due to the redox activity of the organic linkers. The electron transfer from the Au layer after applying a voltage induced a redox reaction of the imidazole linker that facilitates the electron transport within the MOF structure and causing RS of the device.[129]

The chemical sensing demonstration of a MOF-based RS device was first reported by Liu *et al.*[54] They fabricated a ZIF-8-based RS memory device with an alcohol vapour recognition function by sandwiching the ZIF-8 film between Si and Ag electrodes (see Fig. 7c). The transition from the HRS to LRS occurred under an applied electric field. The mechanism for the RS behaviour was proposed to be due to the increased electronic conductivity of the ZIF-8 structure after the formation of Ag nanoparticles at the Ag-ZIF-8 interface through electro-migration and electron hopping. Moreover, the resistance states could be reversed by reversing the electric field. In the

chemical sensing application, the device showed varied resistance in the HRS region in proportion to different alcohol concentrations through the adsorption of alcohols into the cavities of the ZIF-8. The application of an electric field caused organization of the alcohol molecules within the pores by aligning their dipoles in the direction of the field inducing charge transfer and decreasing the resistance to a new (but lower) resistance state. The excellent sensing response to alcohol was also favoured by the hydrogen bonding interaction between the molecules. The viability of this device for wearable electronics was further demonstrated by fabrication on flexible substrates which showed similar alcohol response. Since the wearable sensor will be directly attached to the body, personal physiological data that are collected and processed may be stored within the device.[54,122]

(b) Electron conducting MOF sensors. The design and modification of electron conducting MOFs are actively investigated within the MOF community for potential electronic device implementation.[111,130–133] The design of electronically conducting MOFs is achieved from the combination of a variety of redox-active metal centres with specialized linkers having p-conjugated structures, such as HITP, THT (THT = 2,3,6,7,10,11-triphenylenehexathiol) and BHT (BHT = benzenehexathiol). The resulting MOF materials can exploit different types of charge transfer interactions, such as the π–π stacking and π–d conjugated structures, to adjust the Fermi levels and band gaps.[134] Huang *et al.* fabricated a crystalline CuBHT film that has the highest reported electronic conductivity with a value of 1580 S cm^{-1} and fast charge mobilities of 99 cm^2 V^{-1} s^{-1} for holes and 116 cm^2 V^{-1} s^{-1} for electrons.[135] Other interesting conducting MOF materials have been excellently reviewed by Sun *et al.*,[130] Xie *et al.*[111] and recently by Liu *et al.*[134] The success accomplished in this area of MOF materials science motivates the development of conducting MOF sensor arrays that can directly interface with conducting components of electronic devices by eliminating ohmic loss to achieve optimum sensor capability. The theoretical study by Gustafson and Wilmer indicates that the combination of different MOFs with dissimilar sensing preferences to analytes to make a sensor array could lead to the detection of a wide range of analytes and better selectivity than a single MOF system.[136] Campbell *et al.* fabricated a chemiresistive sensor array by depositing three isostructural conducting MOFs, namely: $Cu_3(HHTP)_2$, $Cu_3(HITP)_2$ and $Ni_3(HITP)_2$ on interdigitated gold electrodes for sensing of volatile organic compounds.[137] They devised a protocol to deposit the MOFs on an interdigitated gold electrode through a solvent-free mechanical abrasion of pelletised MOF that was placed inside a mechanical pencil holder. The compressed MOF inside the pencil holder was abraded into spaces between the fingers of the gold electrode (see Fig. 8a).

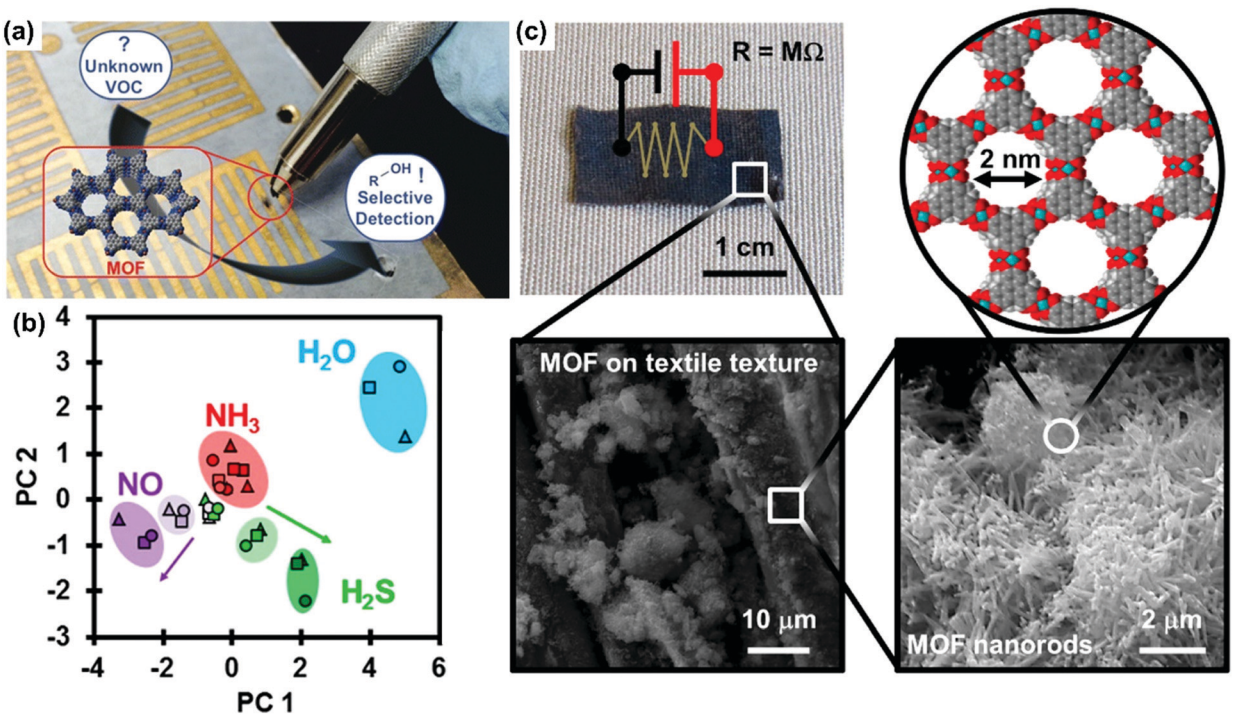

Fig. 8 (a) Photograph of conducting MOFs on interdigitated gold electrodes fabricated into a conducting MOF sensor array, shown schematically over the photo. Reproduced with permission.[137] Copyright 2015, American Chemical Society. (b) Principal component analysis demonstrating differentiation of analytes (3 arrays, 2 sensors each); NH_3 shown in red, NO in purple, H_2S in green and H_2O in blue, whereas Array #1 markers are circular, Array #2 are square and Array #3 are triangular. Reproduced with permission.[138] Copyright 2016, American Chemical Society. (c) Textiles coated with nanoporous MOF. Both macroscopic and molecular level detail is shown, from a photograph of cotton SOFT-sensor postreaction (top left), to scanning electron micrographs detailing MOF coating on fibres (bottom left) and characteristic MOF nanorod texture (bottom right), to a space-filling model of the MOF (top right). Reproduced with permission.[55] Copyright 2017, American Chemical Society.

Upon exposure of the Ni–MOF sensor to organic volatiles, the sensor showed an increased electronic conductance while the Cu–MOF-based sensors showed decreased conductance. This opposite direction in sensing response has been explained in terms of the different charge densities of the MOFs imposed by the different electronic states of the metal centres. The sensor array distinguished between the different families of organic vapours having different functional groups. The different interactions between the analytes and the organic linkers also contributed to the selectivity shown by the sensors.[137]

Smith *et al.* directly grew conducting isostructural Cu_3HHTP_2 and Ni_3HHTP_2 on the surface of graphite IDE deposited on a shrinkable polymer film through solvothermal synthesis to ensure good contact between the MOFs and the electrodes. Both sensors showed the ability to distinguish between NO, NH_3, H_2S and H_2O at different concentrations (Fig. 8b).[138] Smith and Mirica further demonstrated the practicality of integrating conducting MOFs with cotton fabric materials to fabricate electronic textile sensors. The textile sensors were fabricated by the self-assembly of Cu or Ni precursors with organic triphenylene-based ligand on the surface of cotton materials to give Self-Organized Frameworks on Textiles (SOFT) sensors (Fig. 8c).[55] The SOFT sensors were exposed to NO and H_2S at ppm level with detection limits of 160 ppb and 230 ppb, respectively. It is noteworthy that the sensors showed sustained performance in a humid environment (RH = 18%) and the Ni_3HITP_2 SOFT sensor showed high selectivity for NO.[55] Another class of electronic conducting 2D MOFs reported for their fast response and selectivity to analytes with potential for sensor fabrication are based on phthalocyanine (Pc) and naphthalocyanine (NPc) MOFs. The sensors developed from these MOFs also show consistent performance in humid environments. Meng *et al.* developed NiPc and NiNPc sensors and demonstrated them for the detection of NH_3, NO and H_2S with exceptionally low detection limits of 310–330 ppb (NH_3), 19–32 ppb (H_2S) and 1.0–1.1 ppb (NO).[139] Wang *et al.* performed a surface functionalization on their bimetallic $Ni_2[MPc(NH)_8]$ MOF using aliphatic hydrocarbon chains to devise a sensor capable of discriminating alcohols based on differences in polarity.[140]

2.2.3 Field-effect transistors (FETs) in MOF sensors. Field-effect transistors (FETs) are among the emerging microelectronic devices showing promise for various technological applications including integrated circuits, memory storage devices, radio frequency identification (RFID) tags, organic electronics, robotics and chemical and biochemical sensing.[141–145] They control the electrical properties of materials by employing an applied electric field. A typical FET device consists of four components including a substrate and three electrodes (gate, source and drain electrodes) as illustrated in Fig. 9a. Both the source and drain are semiconducting electrodes that are separated from the metallic gate by a gate oxide. The chemical sensing response of FETs is assessed from a change in either the gate-source voltage or drain–source currents.[146] For instance, in ion sensing, the chemical interaction of the analytes with a functional semiconductor substrate creates a concentration gradient leading to a chemical potential between the gate and the source (V_{GS}) that is measurable.[144] The incorporation of porous semiconducting substrates, such as MOFs, into FETs further provides easy accessibility and high charge mobility to chemical substances through rapid ionic/molecular transport resulting in significant electrical response. MOF-based FETs are promising as sensors due to their stability, sensitivity and suitability with low-cost and scalable assembly methods.[109]

Wu *et al.* incorporated a conducting $Ni_3(HITP)_2$ MOF in a FET to fabricate a p-type Ni–MOF-FET device that exhibited a discrete current on/off ratio and field-effect hole mobility of 48.6 $cm^2\ V^{-1}\ s^{-1}$.[147] Wang *et al.* applied the same Ni–MOF to fabricate a liquid-gated device for the detection of gluconic acid (Fig. 9b and c). As a promising glucose sensor, the device showed a decent response to gluconic acid to as low as 1 ppm. The device exhibited an increased charge mobility from 6.2 to 45.4 $cm^2\ V^{-1}\ s^{-1}$ for gluconic acid recognition mostly due to the excellent semiconducting behaviour and large surface area that provided accessible channels for charge transfer.[58] A similar p-type device was fabricated by Ingle *et al.* using $Ni_3(HHTP)_2$ MOF to attain a charge mobility of 8.5×10^{-2} $cm^2\ V^{-1}\ s^{-1}$ and was applied to sense SO_2 gas at 625 ppb.[148]

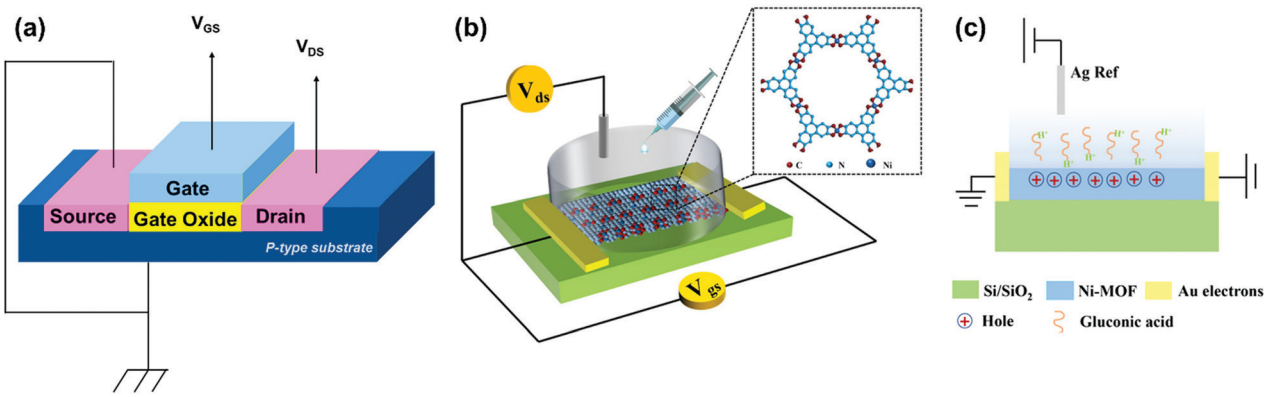

Fig. 9 (a) Schematic illustration of a four-terminal metal-oxide semiconductor field-effect transistor. V_{GS} and V_{DS} are the gate-to-source and drain-to-source voltages. (b) and (c) Schematic illustration of the Ni–MOF-FET (b) as a liquid-gated FET and (c) detecting gluconic acid under negative gate voltage. Reproduced with permission.[58] Copyright 2019, American Chemical Society.

The ability of MOF-FET sensors to cause charge mobility of analytes depends on accessible surface areas, ionic/molecular transport channels and electronic conductivity of MOFs. However, only a small fraction of MOFs possess the required electronic conductivity as the vast majority of MOFs are insulators that must be combined with conducting substances for FET applications.[149,150] Yet, Stassen *et al.* integrated an insulating MOF, UiO-66, with FETs for the field-effect detection of dimethyl methylphosphonate (DMMP).[151] DMMP is used as a chemical simulant for organophosphate nerve agents due to its lower toxicity.[152] They applied the Kelvin Probe technique which measures the contact potential difference (CPD) of two electrodes that were brought close but have no electrical contact. An electron flow can be observed from the electrode with a lower work-function to the other with higher work function when their Fermi-levels match.[151,153] The electrodes consist of a UiO-66-NH_2-coated Si electrode and a bare Si electrode. At different concentrations of DMMP, the changes in CPD could be observed. The UiO-66-FET device could sense DMMP due to a concentration change following their adsorption on the electrodes, which changes their work-function to allow the measurement of CPD. The UiO-66-FET device showed a detection limit of 3 ppb.[151]

2.3 Electromechanical sensors

Electromechanical devices are among the oldest and simplest of sensors, and are attractive for their high sensitivity (up to $\sim 10^{-21}$ g detection limit).[154] They can be considered as micro-analytical balances that respond to tiny changes in mass of the species deposited on a piezoelectric layer that is coated with an adsorbent film to produce measurable electrical signals.[155] The adsorbent films used with these sensors have consisted of a variety of materials including polymers, zeolites, carbon and metal oxides for the detection of gases and volatiles. Electromechanical devices, such as surface acoustic wave (SAW) devices and quartz crystal microbalances (QCMs), are more advanced and can be obtained from commercial vendors.[156]

MOFs are promising in the development of ultrasensitive and selective electromechanical sensors due to their exceptionally high surface area allowing analytes to concentrate in their pores and yield significant electromechanical responses.[13] This section presents an update on recent studies on the application of MOF-based electromechanical sensors which include SAW, QCM and microcantilever devices to sense various analytes.

2.3.1 MOF SAW sensors. In a MOF-SAW sensor, the MOF film is coated on the piezoelectric substrate that separates two sets of interdigital transducer (IDT) electrodes. The electrodes are connected by a radio frequency (RF) amplifier to create a resonant frequency. When the RF voltage passes through the IDT electrodes, a mechanical Rayleigh surface wave velocity and the corresponding resonant frequency are produced that propagate over the surface of the MOF film; these change in the presence of analytes for chemical sensing (see the schematic in Fig. 10a).

Conventional methods to attach MOFs on the surface of the piezoelectric layer are based on solvothermal growth through surface mounting using self-assembled monolayers, layer-by-layer growth and drop-casting of preformed crystals.[13,27] Recently, the acoustic wave generated by the RF amplifier was employed to grow MOF crystals directly on the surface of the piezoelectric substrate using an acoustomicrofluidic technique developed by Yeo *et al.*[60,61] In this method, SAW irradiation was used to initiate the reaction between MOF precursors that are present in a tiny droplet of the solution to crystallize HKUST-1 and Fe-MIL-88B separately on the piezoelectric surface of the SAW device. The generated acoustic wave from the resonant oscillating electric field source causes microscale mixing of the reactants present in the droplet and subsequently microcentrifugal flow to induce nucleation and crystallization of the MOFs on the surface of the piezoelectric substrate (Fig. 10b). The acoustic excitation causes alignment of the MOF crystals in a preferred orientation. The study further showed that the intense SAW oscillations can activate the MOF crystals by forcing out the solvent molecules from the pores. Although the study did not demonstrate the device for sensing, the method developed therein using acoustic irradiation to activate freshly synthesized MOFs on SAW devices is promising for future sensing applications.[61]

The response of MOF-based SAW devices to analytes depends on the accessibility of molecules to the pore apertures and the adsorption capability of the MOF layer. Paschke *et al.*[159] incorporated two Metal–organic Framework Ulm University (MFU)-type MOFs into SAW devices to impart selectivity to the already sensitive device. One MFU@SAW sensor was fabricated by incorporating MFU-4 ($Zn_5Cl_4(BBTA)_3$, $BBTA^{2-}$ = 1*H*,5*H*-benzo(1,2-*d*:4,5-*d*′)bistriazolate) into a SAW device through solvothermal growth. MFU has a narrow 2.5 Å pore opening allowing detection of small gas molecules such as CO_2, H_2, He, NH_3 and H_2O and for screening out larger molecules such as CH_4. For response to larger molecules, another type of MFU structure, MFU-4*l* ($Zn_5Cl_4(BTDD)_3$, $BTDD^{2-}$ = bis(1*H*-1,2,3-triazolato-[4,5-*b*],[4′,5′-*i*])dibenzo-[1,4]-dioxin), with a larger aperture of 9.1 Å was grown on the SAW device.[159]

2.3.2 MOF QCM sensors. In QCM devices, the MOF film is deposited on a gold electrode that is positioned at the centre of a circular quartz crystal. The frequency shifts depend on the slight changes in the mass of the MOF layer due to the adsorption of analytes (see Fig. 10a). The relationship between the frequency shift and the mass changes due to analyte adsorption is directly proportional as shown by Sauerbrey in eqn (1):[30,160]

$$\Delta f = -\frac{2f_0^2}{A\sqrt{\mu_q \rho_q}}\Delta m \quad (1)$$

where f_0 is the resonant frequency, A is the area of the quartz, Δm is the mass change of the active layer, μ_q is the shear modulus of the quartz and ρ_q is the density of the quartz.

The response of the MOF QCM sensor to analytes is primarily determined by the mass of the analyte, such that the heaviest molecule adsorbed by the MOF triggers the highest frequency change. However, specific chemical interactions

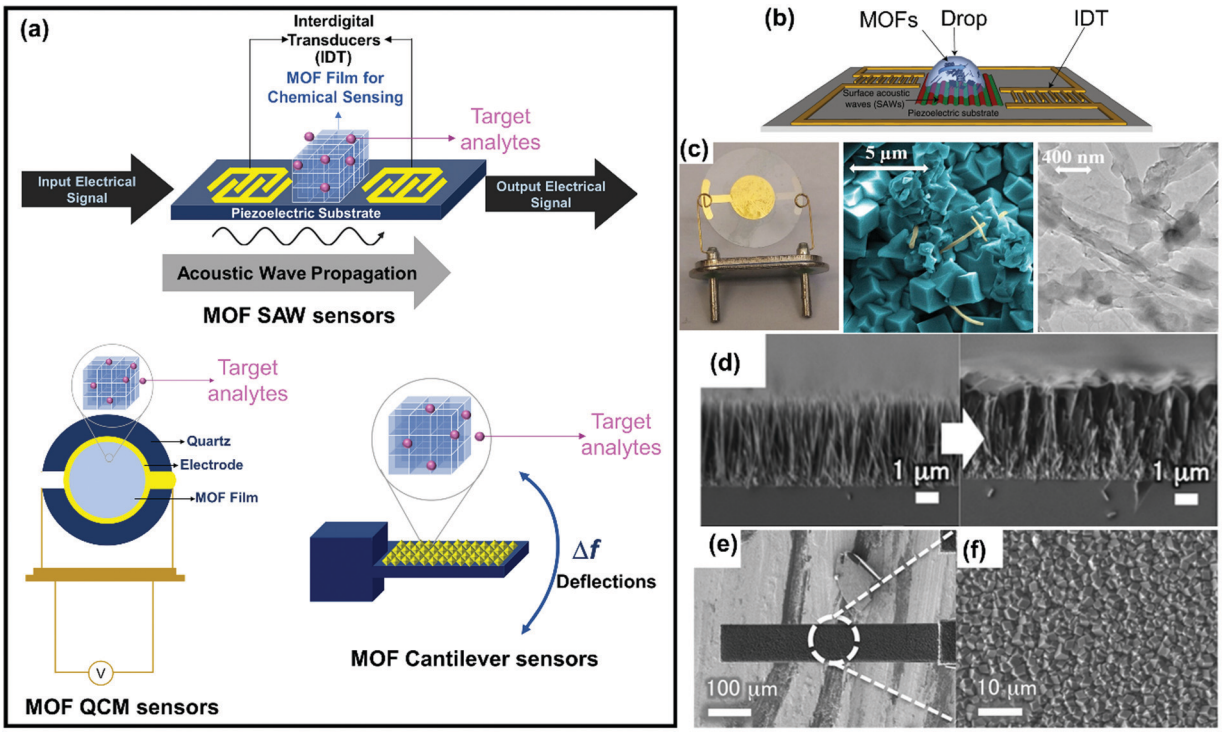

Fig. 10 (a) Schematics of different MOF-based electromechanical sensors studied recently. The sensitive MOF films are positioned between interdigital transducers that respond to acoustic wave irradiation in the MOF SAW sensors. In the QCM sensor, MOF films are coated on a gold substrate (electrode) to give changes in resonance frequency after molecular adsorption. MOF cantilever sensors produce deflections and changes in resonance frequency following changes in the effective mass of the microcantilever. (b) Illustration of the acoustomicrofluidic platform on which the MOF crystals are synthesized in the presence of an acoustic wave generated by applying an input voltage to a pair of offset IDTs patterned on the substrate. Reproduced with permission.[61] Copyright 2019, Springer Nature. (c) (left) Digital image of the QCM coated with HKUST-1 film, (middle) false colour SEM images of CNT-HKUST-1 composite, HKUST-1 is the cyan-coloured cubical crystal, while CNT is the yellow thread, (right) TEM image of the CNT-HKUST-1 composite showing cubical HKUST-1 crystals formed on CNT thread. Adapted with permission.[157] Copyright 2018, Elsevier. (d–f) SEM images of a ZIF-8 cantilever fabricated on a Si wafer: (d) side-view SEM image of the ZnO nanorods grown to 3.5 μm on a silicon wafer and cross-sectional SEM image of the corresponding ZIF-8 films after 1 h solvothermal reaction. (e) Top-view SEM image of a ZIF cantilever and (f) magnified image of the ZIF cantilever surface. Adapted with permission.[158] Copyright 2015, the Royal Society of Chemistry.

between the analyte and the secondary building units of MOFs further contributes to the adsorption of analytes which then determines the overall sensor response. Xu *et al.* exploited the strong affinity of Al(OH)(1,4-NDC) MOF to pyridine vapour to selectively detect pyridine from a group of vapours consisting of methanol, ethanol, acetone, THF, pyridine and water vapour using the QCM platform.[161] They demonstrated that the sensor could attain high sensitivity by activating the Al–MOF film prior to depositing it on the QCM device through solvent exchange of DMF with CH_2Cl_2. A sensitivity of 99.7 Hz ppm^{-1} was obtained with a detection limit of 40 ppb pyridine. The selective response of the Al–MOF QCM sensor to pyridine is favoured by the combination of hydrogen bonding with $Al(OH)_2O_4$ cluster and interaction with the NDC linker.[161] Haghighi and Zeinali also demonstrated their MIL-101(Cr) QCM sensor for improved sensing of pyridine with a sensitivity of 2.79 Hz ppm^{-1} and a detection limit of 1.6 ppm pyridine.[162] The MIL-101(Cr) QCM sensor was fabricated by drop-casting the MOF suspension on the Au substrate of the QCM device. The selected target vapours are both polar and non-polar and include methanol, ethanol, 2-propanol, *n*-hexane, dichloromethane, chloroform, acetone, tetrahydrofuran (THF) and pyridine. Although, all the molecules could be adsorbed into the MIL-101 pores due to its large cavities, the MIL-101(Cr) QCM sensor showed highest frequency change in the presence of pyridine due to a combination of its hydrogen bond interactions with the $Cr_3F(H_2O)_2O$ clusters of the MIL-101(Cr) and high molecular weight of pyridine.[162] The authors later reported a similar response of MIL-101(Cr) QCM sensor with formaldehyde and a sensitivity of 1.67 Hz ppm^{-1} and a detection limit of 1.79 ppm.[163] The MIL-101(Cr) QCM sensor exhibited long-term stability and retained its sensitivity to both pyridine and formaldehyde after two months.[162,163] Ma *et al.* integrated MOF-14 (Cu(BTB); BTB = 4,4′,4″-benzene-1,3,5-triyl-tribenzoate) with a QCM device to selectively detect benzene from a selected group of aromatic organic volatiles which included benzene, toluene, ethylbenzene and xylene (BTEX).[164] The MOF-14 QCM sensor showed sensitivity of 15 Hz ppm^{-1} with a detection limit of 500 ppb benzene. The selective response of the MOF-14 QCM sensor to benzene is due to its smaller size and lower steric hindrance than other members of the BTEX group that allows benzene to access and populate the pores of MOF-14. However, MOF-14 also adsorbs water vapour and CO_2, which interfered with the detection of the organic molecules.[164] The MOF-14 QCM device

is a promising sensor for monitoring the presence of benzene in the environment.

Composite materials of MOFs with other porous materials have been employed in the fabrication of QCM sensors in pursuit of improved sensitivity. Chappanda *et al.* reported a highly sensitive humidity HKUST-1/CNT QCM sensor. The composite was prepared by ultrasonic mixing of suspensions of CNT and HKUST-1 in isopropanol, followed by spin-coating on the Au substrate of the QCM device as shown in Fig. 10c. This study indicates that the combination of CNT to HKUST-1 reduces the particle size of the MOF resulting in increased water vapour adsorption. Low amounts of CNT could not reduce the particle size of HKUST-1 and did not result in improved sensitivity over the pristine HKUST-1 QCM sensor. Conversely, excess CNTs reduce the surface area of HKUST-1 and minimize the adsorption of water molecules. An optimum composition of the HKUST-1/CNT mixture was determined as 0.5 mg CNT per 2.5 mg HKUST-1 to attain a sensitivity of −141 Hz per % RH.[157]

Solution-phase sensing by MOF QCM sensors makes them versatile and promising for biochemical detection. Yang *et al.* developed a MOF-based enantioselective QCM sensor for the discrimination of Cysteine (Cys) enantiomers.[165] Tartaric acid-functionalized UiO-66-NH_2 was spin-coated on a QCM device to fabricate L- and D-UiO-tart@Au QCM sensors. The sensors showed selective response to the enantiomer with the same chiral configuration, *i.e.* L-UiO-tart@Au QCM showed preference to L-cys and *vice versa*. The selectivity for L-cys and D-cys was 5.97 and 5.63, respectively. The enantioselectivity was due to the hydrogen bonding interactions between the –OH of the tartrate group and the –SH of Cys, which depend on the absolute configurations of the UiO-66-tart layer and Cys.

The QCM sensors have received greater attention in the MOF community than their SAW counterparts due to their easy handling and flexibility to detect analytes in both gas and solution phases. However, they operate at lower natural frequencies and are less sensitive. The difference in the sensing capabilities of MOF SAW and QCM devices was investigated by Devkota *et al.* in the detection of CO_2 and CH_4.[166] The individual sensors were fabricated by *in situ* growth of ZIF-8 from its precursors directly on the surface of the piezoelectric substrate of the devices. They reported that both sensors exhibited selective response to CO_2 over CH_4, due to the higher molecular weight of CO_2. However, the ZIF-8 SAW sensor exhibited higher sensitivity than the ZIF-8 QCM sensor over similar thickness of the ZIF-8 film.[166] Moreover, both sensors are promising for monitoring greenhouse gases.

2.3.3 MOF cantilever sensors. Microcantilevers can leverage the structural flexibility of MOFs to become highly sensitive devices. Molecules adsorbed on the surface of the sensing layer cause either frequency shifts (dynamic mode) or surface stress (static mode).[167] The sensing in the dynamic mode is similar to those observed in the SAW and QCM devices since changes in resonance frequencies are seen with adsorption of molecules (Fig. 10a). However, for the static mode, the sensing layer deflects upon molecular adsorption. The presence of a structurally flexible adsorbent coating provides additional sensitivity to the sensor. MOFs that yield a mechanical response upon molecular adsorption are compatible with microcantilevers to operate in the static mode. An example of such is MIL-53 (Cr or Al), which expands and compresses after the adsorption and desorption of guest molecules, respectively, without collapse of the framework.[168–170] A MIL-53(Al) based microcantilever was fabricated and studied by Yim *et al.* for the detection of CO, CO_2, N_2 and Ar using both sensing modes. Their study showed that the static mode gave a higher response than the dynamic mode due to the intrinsic flexibility of MIL-53(Al).[171] Yim *et al.* further investigated the flexible pore property of ZIF-8 in a ZIF-8 cantilever sensor. They fabricated a ZIF-8 microcantilever sensor from the reaction of ZnO that was grown on a Si cantilever with 2-methylimidazole. The SEM images obtained during the fabrication of ZIF-8 cantilever is shown in Fig. 10(d–f).[158] The sensor was exposed to different alcohols (methanol, ethanol and 1-propanol) to cause frequency shifts and deflection of the ZIF-8 cantilever. Since resonance frequency is inversely proportional to the square root of the mass difference of the MOF film due to analyte adsorption,[167] the largest deflection was observed for methanol that has the least molecular mass.[158] Also, the critical alcohol vapour concentration required to cause the cantilever deflection decreased with increasing hydrophobicity, due to the hydrophobic nature of ZIF-8.[158]

MOF-based electromechanical sensors utilize the most important property of MOFs; high surface areas therefore offering extraordinary sensitivity and selectivity to analytes. More studies into these class of sensors are required, particularly to investigate the adaptability of several MOF materials with SAW and cantilever devices and to explore their versatility in chemical sensing. Also, the combination of electromechanical capabilities with both electrochemical and electronic sensing to create electrical sensor arrays is promising to develop highly sensitive MOF-based recognition platforms for chemical and biochemical applications.[172]

2.4 Optical sensors

Generally, an optical sensor comprises of a light source, a light modulator (which changes wave properties of the radiated light oscillations such as intensity, polarisation, frequency and phase) and an optical element to guide the light from the source through the modulator to a detector. Optical fibre sensors are attractive for their portability and immunity to electromagnetic interferences, which give them an advantage over their electronic counterparts. Thus, they can be used under harsh conditions such as explosive environments. Also, since the optical communications do not require electrical components, the application of optical sensors does not pose safety threats. Optical fibre sensors may be classified into either extrinsic or intrinsic sensors as illustrated in Fig. 11a and b. MOFs have been integrated with optical fibre devices both as extrinsic and intrinsic sensors to minimize optical losses for enhanced sensitivity and selectivity.

2.4.1 Intrinsic MOF-based optical fibre sensor. An intrinsic optical fibre sensor actively participates in sensing by acting as the light modulator while propagating the light within the fibre.[175] Nazari *et al.* fabricated a UiO-66-based intrinsic optical fibre sensor by coating UiO-66 on a perpendicularly cleaved end-face of an optical fibre (Fig. 11c) for the aqueous detection of Rhodamine-B (Rh-B).[176] The overall light intensity indicates the sensitivity of the UiO-66 device towards Rh-B, which changes with the variation in the wavelength of the light source. The total intensity analyzed by an optical processor was estimated from the separate back-reflection light intensities from the MOF–fibre interface and the MOF–water interface. The shifts in the interferograms towards the longer wavelengths signalled the detection of Rh-B as the concentration increased.[176] The same sensor was applied in a light-triggered release of 5-fluorouracil that was trapped within the UiO-66 cavities.[173]

A similar device was constructed by incorporating a single crystal MOF to an end face of the optical fibre instead of using a polycrystalline MOF coating on the fibre. Zhu *et al.* attached a HKUST-1 single crystal to one end of an optical fibre for the detection of nitrobenzene (Fig. 11d). The device produces a polarised light signal which is promising as an in-line polarizer micro sensor.[70] However, the performance of the sensor declined in the long-term due to the poor stability of HKUST-1. To fabricate an intrinsic MOF-based optical fibre sensor for CO_2, Kim *et al.* combined the total internal reflection property of an optical fibre with the ultra-porosity of ZIF-8 by cladding the fibre with ZIF-8 (Fig. 11e). ZIF-8 served to selectively adsorb gaseous molecular targets while the sensitivity of the device can be measured from the changes in the refractive index of the MOF film. In this device, optical modulation occurred within the fibre core. The sensor also showed a rapid response and high selectivity to CO_2.[69] The same group later performed a post-synthetic modification of the ZIF-8 layer with hydrophobic oleylamine to minimize the interference of moisture during CO_2 sensing, while increasing the sensitivity of ZIF-8-optical fibre device to CO_2 and improving the moisture stability of the device.[177]

2.4.2 Extrinsic MOF-based optical fibre sensor. An extrinsic fibre sensor passively participates in chemical sensing since it only serves as an optical mediator between the analyte and external instrumentation for signal detection. After light extraction from the optical fibre, modulation is performed in a

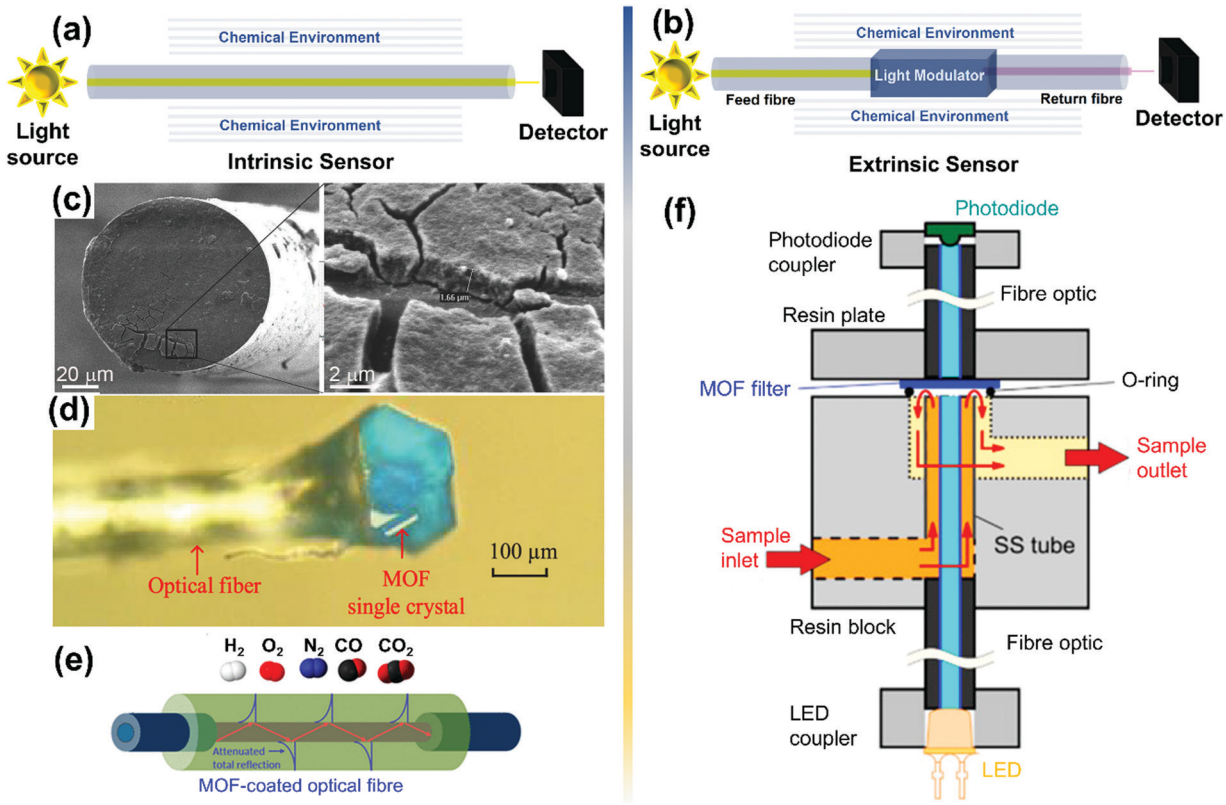

Fig. 11 (a) Schematic of an intrinsic optical fibre sensor in which the light propagating along the fibre axis is modulated either directly through its chemical environments or environmentally induced optical path length changes within the fibre itself. (b) Schematic of an extrinsic optical fibre sensor in which light modulation is performed within a sensing material connected to the fibre. The fibre only serves to propagate the incoming light from the source and the extracted light toward the detector. (c) SEM images of UiO-66 optical fibre thin film with its cross-section view showing its thickness. Adapted with permission.[173] Copyright 2016, Wiley-VCH. (d) An optical microscope image of a prototype single crystal MOF sensor. Reproduced with permission.[70] Copyright 2019, American Chemical Society. (e) Schematic diagram of an optical fibre sensor integrated with ZIF-8 thin film. Reproduced with permission.[69] Copyright 2018, American Chemical Society. (f) Schematic of the CuBTC filter fibre optic gas sensing device. Reproduced with permission.[174] Copyright 2015, Elsevier.

different medium (Fig. 11b). Ohira *et al.* developed an extrinsic optical gas sensor by integrating a CuBTC filter into an optical fibre for trace level moisture detection in purified industrial gases.[174] The CuBTC filter was sandwiched between the ends of two fibre optics that are connected to a light-emitting diode (LED) source and photodiode detector, respectively (Fig. 11f). Moisture detection is determined from absorbance measurements by observing the colour changes of CuBTC from light-blue to deep-blue after moisture adsorption. The sensitivity of this device is affected by the gas flow rate or the nature of the industrial gas, except NH_3 which gives a similar response due to its affinity to the Cu^{2+} centre of the MOF. However, the interference of NH_3 can be resolved by noting that NH_3 was adsorbed faster than water by CuBTC under similar conditions. The detection limit of NH_3 (1.8 ppm) is lower than moisture (85 ppm).[174]

2.4.3 Optical fibre grating MOF sensors. Optical fibre grating sensors are a type of optical fibre sensor that consists of a grating with periodic variation of refractive index within the fibre core to act as a spectral filter that reflects light of a specific wavelength while transmitting other wavelengths. The fibre gratings control the properties of light propagating within the fibre that involves the periodic changes of the refractive index of the fibre core that forms a modulated pattern along the fibre axis. The periodic fibre grating (PFG) devices are classified into two: (1) the short-period gratings (SPG) which have a sub-micrometre period and (2) the long-period gratings (LPG) which have periods in the range 100 μm to 1 mm.[178] There are only a few studies on the integration of MOFs into PFG devices with more focus on the LPG. A schematic diagram of a MOF–LPG hybrid is shown in Fig. 12a. The LPG cause periodic changes in refractive indices of the fibre core through coupling of the core mode to the co-propagating cladding modes of the fibre. This coupling yields a transmittance spectrum as a series of attenuation bands with corresponding central wavelengths, each band representing coupling to a different cladding mode. Hromadka *et al.* coated LPG with MOFs having periods of approximately 110 μm to sense alcohols,[66] volatile organic compounds[67] and CO_2.[68] High sensitivity can be attained at a phase-matching turning point (PMTP) by precisely adjusting the grating periods and tuning the thickness of the MOF layers. Wu *et al.* showed that with an increased period, improved sensitivity could be attained.[179] The PMTP is the wavelength (λ) at which minimum energy is coupled from the core to the cladding mode of the fibre according to:

$$\lambda = [n_{\text{eff}}(\text{core}) - n_{\text{eff}}(\text{cladding})]\Lambda \quad (2)$$

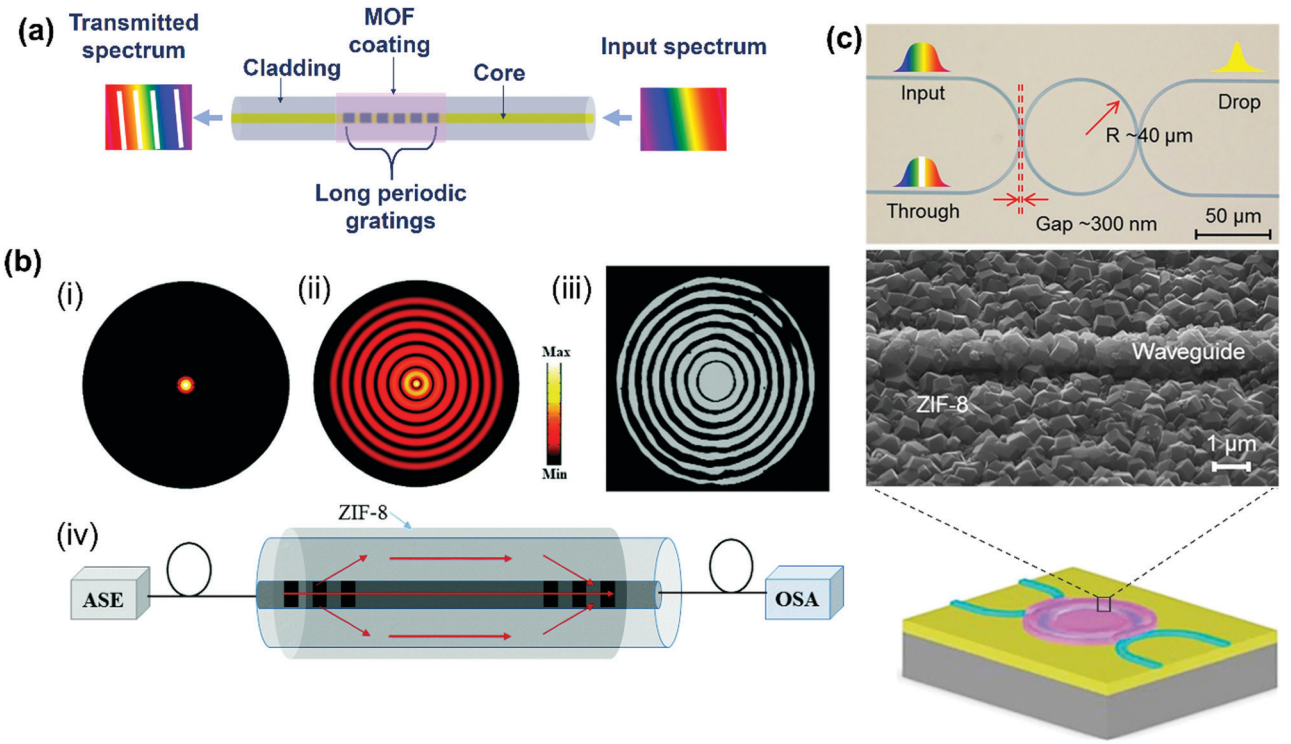

Fig. 12 (a) Schematic diagram of MOF-coated LPG showing the input and the transmitted spectra. (b) (i) Electric field distribution of the fundamental mode (LP_{01}, core mode) and (ii) higher-order mode (LP_{08}, cladding mode); (iii) near-field image of the LP_{08} mode pattern obtained with an infrared camera; (iv) schematic diagram of the fibre Mach–Zehnder interferometer with cascaded LPGs. ASE: amplified spontaneous emission light source; OSA: optical spectrum analyzer. Reproduced with permission.[179] Copyright 2020, the Royal Society of Chemistry. (c) Top: Schematic diagram of the hybrid micro-ring resonator MOF sensor showing the optical fibre connections. The micro-ring resonator was coupled with two bus waveguides that have two integrated inversed-tip couplers for input and output of optical signals from and to optical fibres; middle: SEM image of a section of the ZIF-8 film coated on the hybrid micro-ring resonator device; bottom: schematic diagram of the hybrid micro-ring resonator MOF sensor. Adapted with permission.[71] Copyright 2017, Springer Nature.

where n_{eff}(core) and n_{eff}(cladding) represent the effective refractive index of the core and cladding, respectively. Λ is the period of LPG.[66–68,179]

The response of the device was measured through the changes in central wavelengths, which are sensitive to their chemical environments. The MOF films on the optical fibres provide increased presence of analytes around the cladding mode by adsorbing and concentrating molecules within their pores. Wu *et al.* also exploited both the light-vapour and the ZIF-8-vapour interactions to modulate the refractive index in their fabricated Mach–Zehnder interferometer as shown in Fig. 12b through the manipulation of the co-propagating cladding mode, LP_{08}. They showed that the vapour adsorption by ZIF-8 caused significant changes in the refractive index of the fibre. The changes in the refractive index prompted an increased power of the evanescent field in ZIF-8 to sense the vapours.[179]

2.4.4 MOF-based micro-ring resonators. Tao *et al.* incorporated ZIF-8 into a micro-ring resonator device shown in Fig. 12c for the sensing of volatile organic compounds.[71] A micro-ring resonator is an optical waveguide consisting of at least one closed loop in which light propagates and consists of a coupling unit to access the loop.[180] The response of the device to vapours is defined by a spectra shift which is caused by changes in the refractive index. The micro-ring ZIF-8 resonator can sense the sub-ppm level of organic vapours due to the large surface area of the MOF and high adsorption of the organic vapours.[71]

2.4.5 MOF films as diffracting surfaces. The colour changes from diffraction gratings are promising in chemical sensing to promote the integration of MOFs with optoelectronic devices. Faustini *et al.* fabricated optical diffracting nanopatterned ZIF-8/TiO_2 composite film using soft lithography. ZIF-8 crystals were deposited on a patterned TiO_2 surface that provides the optical index contrast. The diffracted light can be captured by a smartphone camera and is further processed to obtain diffraction luminance intensity. Following the adsorption of organic vapour molecules, there is a decrease in the optical index contrast between ZIF-8 and TiO_2 that leads to reduced luminance intensity.[181] A crack-patterning technique was also used to prepare a MOF-based diffracting surface for an organic vapour sensor. Colloidal ZIF-8 (32 nm) and MIL-101 particles (about 25 nm) were dip-coated on different surfaces including flat and the interior of tubular substrates. At low relative humidity (<10%), crack patterns were obtained *via* evaporation of the colloidal solution and excellent control over periodicity was achieved by dip-coating at different speeds. The patterned MOF films showed photonic behaviour due to their ability to diffract light. Signal transduction is based on the changes in refractive indices due to interaction with molecules and it is related to the diffraction intensities.[182]

2.4.6 MOF colloidal crystal films and devices. The combination of the high surface area of MOFs with the opalescence of their colloidal crystal films is useful for the optical recognition of chemicals. The response to gas-phase analytes is due to changes in the refractive indices of the MOF colloidal crystal films following the adsorption of guest molecules. Since pores of MOFs are expected to be free of organic volatiles before sensing, analyte adsorption will change the overall refractive indices of the MOF film due to refractive index contributions from adsorbed molecules during sensing. Hence, a change in the photonic stopband of the periodic MOF structure can be observed after the adsorption of guest molecules by the photonic MOF. The shifts in the photonic stopband positions ($\Delta\lambda$) are usually obtained from UV-Vis reflectance or transmission measurements.[183] The sensing response of the colloidal crystal MOF film is directly correlated to the magnitude of $\Delta\lambda$. Avci *et al.* exposed a ZIF-8 colloidal crystal film to water and simple alcohols including methanol, ethanol, iso-propanol and *n*-butanol. The film showed largest $\Delta\lambda$ to *n*-butanol and no change to water.[184] The organization of crystals of a MOF film layer added to an optical device has been shown to improve the sensitivity of the sensor.

Chocarro-Ruiz *et al.* fabricated a ZIF-8 based optical sensor for CO_2 by depositing self-assembled ZIF-8 nanocrystals on a bimodal waveguide (BiMW) interferometer as shown in Fig. 13a. The sensor response is based on adsorption of CO_2 by ZIF-8 which significantly changes the refractive index of the device. High sensitivity to CO_2 was obtained *via* coating of a transparent film of self-assembled ZIF-8 nanoparticles (size: 32 $\pm$ 5 nm) on the surface of the BiMW waveguides to achieve high optical transmittance at 660 nm. This was followed by a protective coating of the ZIF-8 film with polydimethylsiloxane to prevent cracking of the ZIF-8 layer that causes the loss of optical transmission during activation and sensing. The limit of detection of CO_2 by the sensor was 774 ppm at 278 K.[185]

Zhang *et al.* fabricated periodic UiO-66 structures from crystals of different sizes. They tested the response of the UiO-66 films to saturated organic vapours and found that their performance is related to the crystal sizes of UiO-66 present in the self-assembled films. Of the seven different colloidal crystal UiO-66 films exposed to ethanol vapour, the results in Fig. 13b indicate that periodic structures consisting of the smallest crystals (380 nm) have the largest spectra shift, fastest response and shortest recovery time due to the largest surface area.[186]

To expand the range of applicability of MOF-based colloidal crystal sensors and exploit the high surface areas of MOFs towards the detection of low amounts of chemicals, it is important to tune the sensitivity of the films such that low concentrations of analytes should yield measurable $\Delta\lambda$. High sensitivity performance for vapour sensing have been reported for MOF-coated silica or polystyrene colloidal crystals but may be improved when template-free MOF colloidal crystals are used due to higher porosity. The high sensitivity of template-free MOF colloidal crystals will depend on whether there is a high degree of colloidal ordering, high surface area, the molecular size of the analytes is small enough to access the MOF cavities and the resolution of the spectrophotometer.[186,188,189]

Alternatively, it is possible to exploit the high surface area of MOFs toward achieving the low-level detection by template-free colloidal crystals by coupling them with fluorescent-based detection. Enhanced fluorescence of a Nile Red dye adsorbed

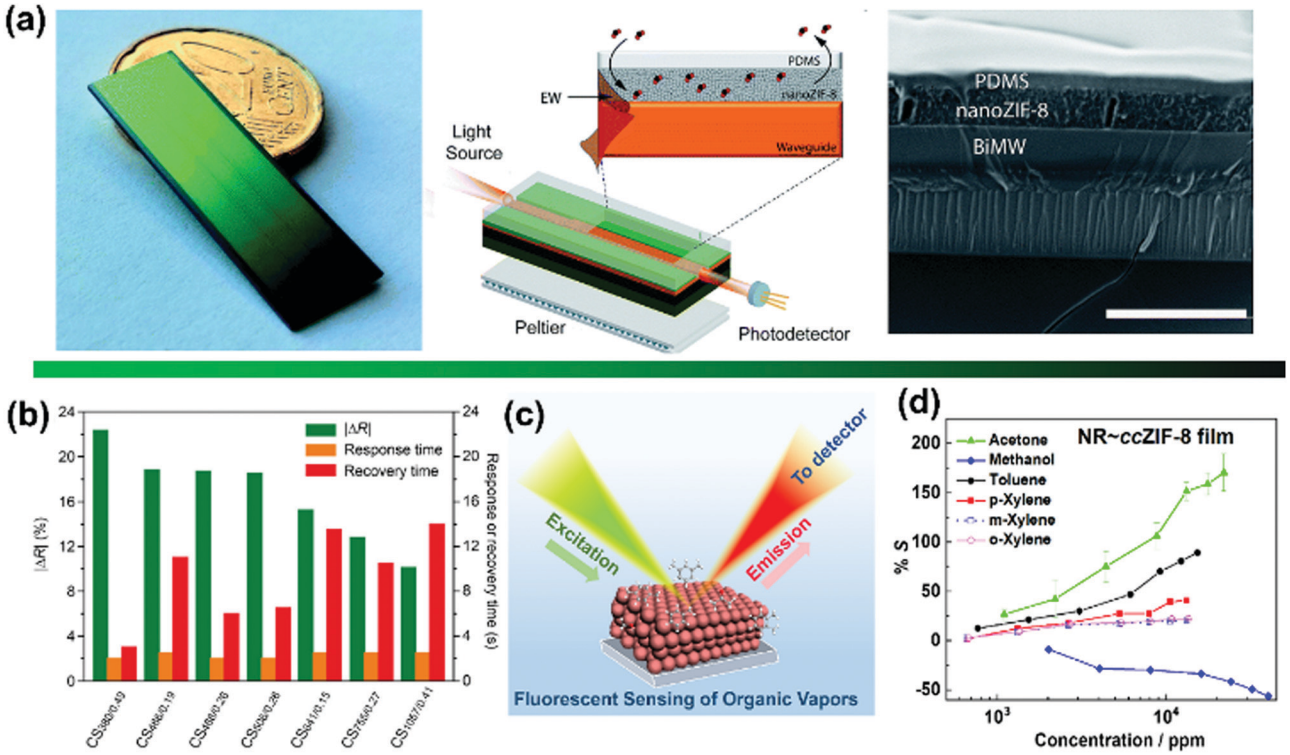

Fig. 13 (a) (left) Photo of a chip containing 20 BiMW sensors; (middle) schematic of the nanoZIF-8-based BiMW sensor and (right) FE-SEM image (side view) of the nanoZIF-8-based BiMW sensor, showing the layers of nanoZIF-8 and PDMS built on top of the waveguide. Scale bar: 5 μm. Reproduced with permission.[185] Copyright 2018, the Royal Society of Chemistry. (b) Maximum absolute reflectance changes (|Δ*R*|), response times and recovery times of MOF sensors (*i.e.*, $CS_{380/0.49}$, $CS_{466/0.19}$, $CS_{468/0.26}$, $CS_{506/0.26}$, $CS_{641/0.15}$, $CS_{755/0.27}$ and $CS_{1057/0.41}$) for the saturated ethanol vapour. Adapted with permission.[186] Copyright 2019, American Chemical Society. (c) Illustration of fluorescent sensing of organic vapours by NR∼ccZIF-8 film and (d) fluorescent response of the NR∼ccZIF-8 film to different concentrations of acetone, methanol, toluene, *p*-, *o*- and *m*-xylene vapours at 298 K. The negative % *S* values indicate fluorescent quenching while positive values show the fluorescent intensity increase. Adapted with permission.[187] Copyright 2020, Wiley-VCH.

into a periodic ZIF-8 structure (NR∼ccZIF-8 film) when exposed to organic vapours was recently reported (Fig. 13c).[187] After carefully matching the photonic stopband of ZIF-8 with the emission wavelength of Nile Red, the NR∼ccZIF-8 film showed a 200-fold enhanced fluorescence compared to Nile Red adsorbed on a disordered ZIF-8 film. The enhanced fluorescence occurred due to the overlap of the leaky mode of the ZIF-8 colloidal crystal with the emission energy of the Nile Red. The sensitivity of the NR∼ccZIF-8 film to low concentrations of acetone, methanol, toluene and xylene isomers at room temperature was obtained from fluorescent intensity changes (see Fig. 13d). Detection limits of 60 ppm and 95 ppm for acetone and toluene, respectively, were obtained. The NR∼ccZIF-8 film also distinguished between vapour adsorbates through vapochromic response at higher vapour concentrations.[187] This study should inspire other combinations of fluorophores with photonic MOF systems for various fluorescent sensing applications.

2.5 Current limitations of each sensing method

In the previous sections, different proof-of-concept MOF devices have been evaluated from electrochemical, electronic, electromechanical and optical sensing platforms. The performance of MOF devices across the four platforms is encouraging and signals their readiness for integration with wearable and field-deployable sensors. However, there remain a few issues that should be addressed to expand the library of MOFs that can be integrated with devices.

Electrochemical sensing that occurs in an aqueous environment requires water-stable MOFs. However, only a few families of MOFs are stable in humid environments. Post-synthetic functionalization through well-controlled incorporation of hydrophobic moieties may be required to enhance the stabilities of various hydrolytic-vulnerable MOFs. The synthetic protocols should be carefully performed to allow analytes unrestricted access to the pores, channels and chemical recognition groups.[190]

Another challenge with electrochemical sensing is the poor electronic conduction in MOFs that limits their performance. This is also problematic for some types of electronic sensing. Current efforts to develop protocols to design electron conducting or semiconducting MOFs and to modify the existing insulating ones will greatly benefit both the electronic and electrochemical sensing platforms. However, the best of the recently developed conducting MOFs are nonporous or have low surface areas.[134] Therefore, a compromise between large surface areas and electronic conductivity should be reached to obtain a suitable material for a specific electronic-based sensing applications.

Electromechanical sensors utilize the large surface areas of MOFs to attain exceptional sensitivity to analytes. Molecular adsorption capacity of MOFs and the molecular weights of the analytes are the key factors that determine the sensing performance on this platform. However, a major limitation is the lack of selectivity between molecular species having identical molecular mass in a mixture of analytes. This issue may be addressed by designing the pores of MOFs to discriminate between molecules based on structural and chemical differences such as molecular geometry, chirality and polarity rather than molecular mass.

Interestingly for optical sensing, light interacts with almost any type of MOF. The changes accompanying chemical sensing can be obtained through signals produced from light absorption, transmittance, diffraction, refraction and luminescence. However, a major challenge is how to magnify sensing responses generated within small devices based on the various light-MOF interactions. Addressing this issue could require subtle material design or using an appropriate optical technique to extract signals. For example, the fluorescent response from a solid-state device can be low due to weak excitation sources, possible optical loss resulting from scattering of the incident light and the quantum yield of the active material. Hence, MOFs could be designed or post-synthetically modified by incorporating light extracting groups to maximize optical excitation and produce measurable fluorescent signals for applications in small analytical sensing devices.

3 Smartphones in MOF-based sensing

The introduction and evolution of mobile phone technology is one of the most remarkable achievements of the 21st century that has had significant global impact. Smartphones are mobile phones with integrated computer and internet capabilities that can perform many advanced functions besides phone call exchange, such as high pixel imaging, sensing of physical parameters and coordinates, due to their high microprocessing strength, networking and image recognition properties.[191] Li *et al.* recently reviewed the sensing applications of smartphones from their installed physical sensors. Their studies showed that smartphones can detect chemicals through various modes depending on the type of physical sensor that is activated.[192] Rezazadeh *et al.* also recently compiled and reviewed how different functions of smartphones are applied in qualitative and quantitative chemical analysis.[193] The combination of MOF-based sensing with mobile devices technology is a promising area that is expected to experience significant growth within the next few years.

3.1 MOF optical sensing using smartphones

The chemical sensing response from MOFs can be obtained and processed by smartphones through their inbuilt sensors and microprocessors. For example, for the ZIF-8/TiO_2 diffraction grating film that consists of a 200 nm feature replicated over an area of 1 cm^2 of a selected substrate shown in Fig. 14a, the diffracted light was detected by the charge coupled device (CCD) camera installed in a smartphone. During chemical sensing, the CCD camera estimates the changes in the diffraction efficiency due to variation in the refractive index of the ZIF-8/TiO_2 film.[181]

The refractive index of the ZIF-8/TiO_2 film changed due to the exposure of the film to styrene and isopropanol vapours at room temperature. The changes in luminance of the film due to vapour uptake was measured by the CCD camera and the photo image of the film after vapour exposure could be processed by the smartphone. This study demonstrates that a simple smartphone camera can give chemical sensing results that agree with those from the bench-top ellipsometer.[181]

Spectroscopy can be also be combined with smartphones to access their inbuilt light and image recognition features for chemical sensing. Different sensing platforms have leveraged these features to perform MOF-based detection of chemical and biochemical analytes. A simple spectroscopic technique that has been used many times is colorimetric sensing that is based on visual observation of chemical changes to the MOF after interactions with analytes. Colour changes of the active MOF film at different analyte concentrations may be captured with smartphones that could then be analysed to evaluate the sensing performance. Kou *et al.* combined their fabricated biomimetic MOF colorimetric paper with a smartphone for the detection of biomolecules such as glucose, uric acid, lactose and urea.[195] The smartphone-assisted biomimetic MOF nanoreactor colorimetric paper is promising for point-of-care technology and personal diagnosis. The molecular recognition in this device was driven by the cascade reactions occurring within the micropores of ZIF-8, which was catalyzed by the enzymes encapsulated in the MOF. These reactions result in colour changes on the paper strip that can be inspected by the naked eye but also with a specialized app installed on the smartphone that works with the camera.[195]

The smartphone-based spectroscopic approach can exploit the fluorescent detection technique, which is more sensitive than colorimetry since it relies on the fluorescence emission of the active MOF. Zeng *et al.* performed a ppm level detection of fluoride ions through a Lewis acid–base interaction with mixed lanthanide MOFs consisting of triazine-based ligands (Tb/Eu(TATB)). The sensing performance of Tb/Eu(TATB) in the presence of F^- was assessed with a fluorometer while a smartphone captured the digital image of the light emitted from the MOF. The red-green-blue (RGB) values of the images were identified with the aid of an installed app to calibrate the MOF/smartphone device for further detection of F^- from drinking water samples.[196] Other fluorescent-based smartphone sensing approaches have been reported.[197–199] Chemical sensing may be performed through the excitation of fluorescent MOFs by a commercial UV light emitting diode and the luminescent emissions detected by a light sensor installed with the smartphone camera. Zhao *et al.* demonstrated this by constructing a portable homemade device equipped with capabilities to measure luminescent signals of MIL-53(Fe)–OH suspensions for sensing Fe^{3+} and to transmit the optical

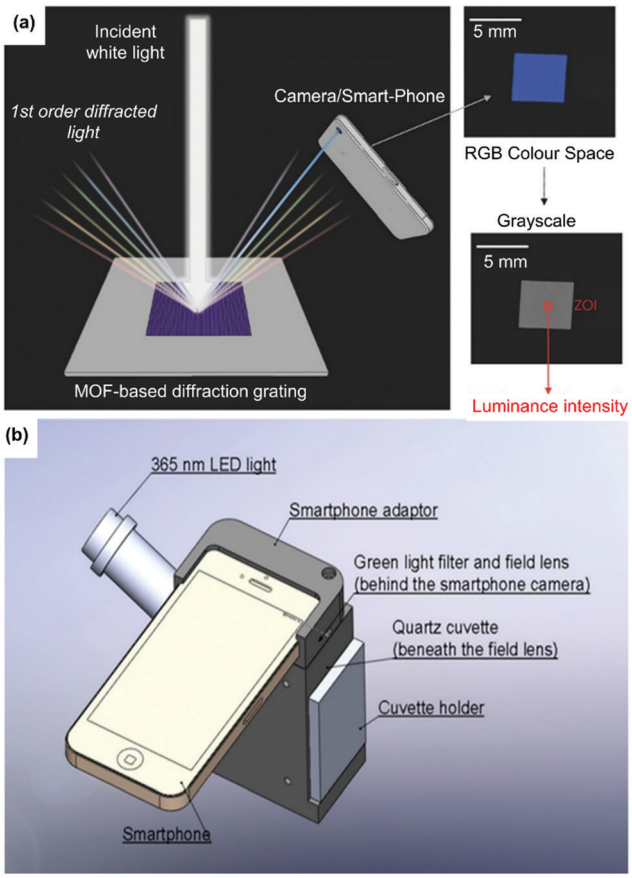

Fig. 14 (a) Illustration of the experimental set-up for the detection using a smartphone camera and the photographs of the diffracting grating in colour and grayscale taken by a smartphone photo camera. Reproduced with permission.[181] Copyright 2015, Wiley-VCH. (b) Diagram of the smartphone fluorescent reader. Reproduced with permission.[194] Copyright 2019, Elsevier.

information to a smartphone, as shown in Fig. 14b. The smartphone was fit into a light-proof box equipped with a green light filter that interfaces with the smartphone camera and a cuvette holder. The LED light of the smartphone functions as the excitation light source. The emission light passes through the green filter and is then captured with the smartphone camera to be analysed with a dedicated app.[194]

3.2 MOF electrochemical sensing using smartphone

Smartphone-based optical sensing involves changes in the optical and spectroscopic properties of the MOF after exposure to analytes that are captured through the CCD camera and processed by the appropriate image recognition software installed on the phone. Whereas, in electrochemical sensing, the smartphone acts as a miniature electrochemical analyser to which an electrochemical module is attached. The electrochemical module consists of a test strip that is fabricated by depositing the sensitive MOF on specialized electrodes that are joined to electronic accessories.[200] Xu *et al.* constructed a smartphone-controlled electrochemical sensor that consisted of a module which could achieve a two-way communication with the smartphone for the detection of heavy metal ions through differential pulse voltammetry.[201] The test strips were made by depositing reduced graphene oxide (rGO), polyethyleneimine (PEI) with SMOF (a composite of UiO-66-NH_2 and single walled carbon nanotubes) on screen-printed carbon electrodes (SPCE). The function of UiO-66-NH_2 was to capture and bind to different metal ions, while the other components of the test strip provided the required electrical conductivity to produce measurable signals that can be transferred to the smartphone. An installed application controlled the device and transformed the electrical signals into output data that was displayed as a voltammogram on the smartphone screen in real-time, as shown in Fig. 15a.

In another study, Zhu and co-workers fabricated a wearable smartphone-controlled electrochemical ZIF-67 sweatband sensor for the analysis of perspiration glucose as shown in Fig. 15b.[202] The glucose detection is a nonenzymatic reaction that is based on water splitting-assisted electrocatalytic oxidation of glucose on Pd@ZIF-67 which is deposited on a conducting polymer substrate. The sweatband electrochemical module consisting of Pd@ZIF-67 electrode and flexible printed circuit board was connected to the smartphone through Bluetooth wireless communication. This system is promising for non-invasive glucose monitoring by a nonenzymatic process that can be achieved due to the unique electrocatalytic water-splitting glucose oxidation of ZIF-67.

4 Promising sensing applications of MOF devices and future outlook

MOF sensing devices are promising in five major areas of public health and environmental safety comprising of point-of-care diagnosis, food security, environmental monitoring, defence and artificial intelligence.

4.1 Point-of-care testing and diagnostics

Many recent studies have focussed on the design and the implementation of wearable MOF-based sensors for point-of-care (POC) testing and diagnostics. Functional devices are fabricated through the integration of MOF materials with biocompatible substrates that can then be deployed for detecting important biomarkers and monitoring the physiological conditions of the users. Wu *et al.* fabricated a transparent electronic and flexible Ni–MOF film for the detection of NH_3, CO and O_2.[59] The nickel catecholate (Ni-Cat-1) MOF was grown epitaxially on a single-layer-graphene (SLG) that was coated on PET and polydimethylsiloxane substrates. The thickness of the Ni-CAT-1-on-SLG layer was controlled to ensure the transparency of the film while the polymer substrates provide flexibility (Fig. 16a and b). The visible light transparency of the film may be explored for optical recognition purposes. However, the sensor response to different gases was measured from the changes in its electrical conductivity at room temperature. The presence of the Ni-CAT-1 MOF provides molecular recognition capability to the sensor. The alignment between the lattice structure of Ni-CAT-1 with graphene lead to a high

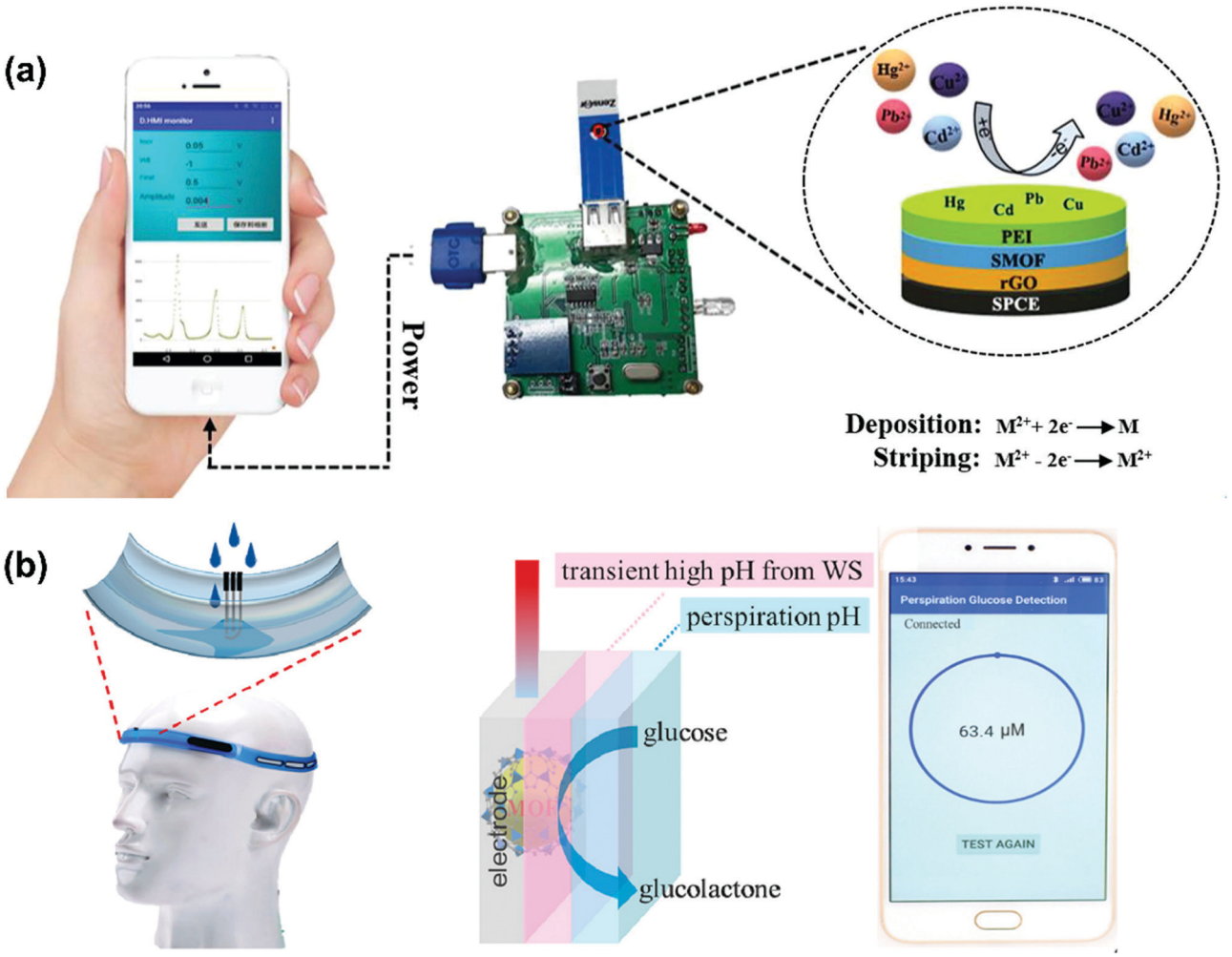

Fig. 15 (a) Schematic representation of the quantitative point-of-care testing system and the simultaneous detection of multiple metal ions by the rGO/SMOF/PEI-modified screen-printed carbon electrodes. Reproduced with permission.[201] Copyright 2020, Elsevier. (b) Sweatband with electrochemical sensor for perspiration glucose sensing: non-enzymatic glucose sensing method with the water splitting-assisted electrocatalytic reaction on the MOF-based electrode; a photograph of the smartphone with an app for the perspiration analysis. The sensor was connected to the smartphone *via* Bluetooth. Adapted with permission.[202] Copyright 2019, American Chemical Society.

electronically conducting composite. Limited film thickness of the Ni-CAT-1-on-SLG composite and the flexibility of the polymer substrate render the Ni-CAT-1-on-SLG device promising as a wearable electronic sensor for indicating the blood ammonia level in the body.[59,203]

The combination of MOF sensors with smartphone technologies has been demonstrated in advancing POC testing. The widespread use of smartphones has inspired an emerging field of mobile health in which the medical and public health practices are supported by mobile devices.[206] A simple demonstration of MOF–smartphone-based diagnosis was reported by Leelasree *et al.* in the application of their prototypical HKUST-1-modified face mask used to monitor breathing patterns in sleep apnoea diagnosis (Fig. 16c).[204] The face mask coated with a HKUST-1/MoS_2 composite has excellent recognition for water vapour due to the high adsorption capacity of HKUST-1. The vapour is then transported to the MoS_2 layer that is acting as a charge carrier in the device for electronic sensing. The prototype was assembled by connecting the face mask to a smartphone through an Arduino Bluetooth wireless technology.[204] Additional promising smartphone based POC demonstrations by MOF sensors are indicated in Table 2 from summarising different sensing platforms.

Another milestone in the demonstration of MOF devices for POC testing and diagnosis was reported by Ling *et al.*, which showed the prospects of implantable electrochemical MOF sensors for monitoring biomolecules in body fluids.[205] They fabricated implantable electrochemical sensor arrays using a combination of different enzyme-encapsulated Co and Cu-based MOFs with flexible electronics for the detection of biochemical species in the blood and interstitial fluids. Different enzyme@MOF suspensions were prepared in Nafion solutions and drop-cast onto screen-printed silver/carbon electrodes using thin PET substrates as flexible supports. The sensors were implanted on different parts of a live animal for *in vivo* detection of biomolecules from various organs and

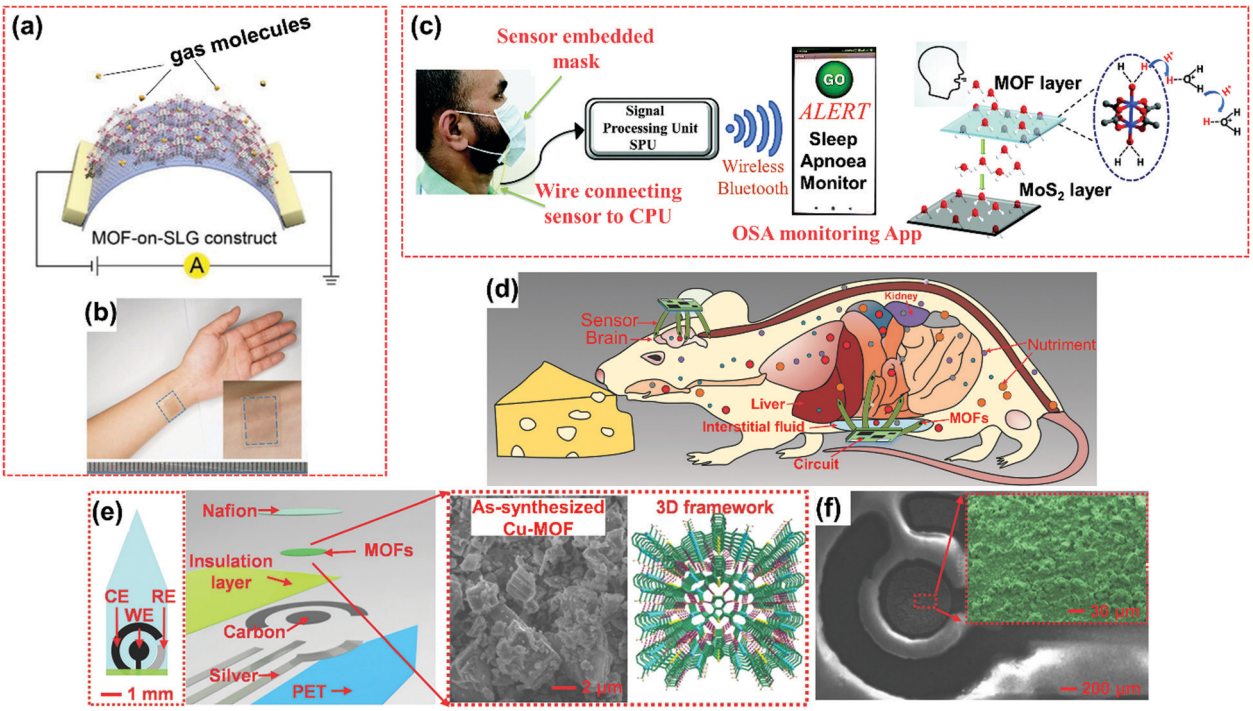

Fig. 16 (a and b) Ni-CAT-1-on-SLG construct with 25 nm thickness on transparent flexible polymers for personal electronics. (a) Illustration of the flexible device composed of Ni-CAT-1-on-SLG construct. (b) Photograph of Ni-CAT-1-on-SLG device attached to the skin of a human arm using PDMS as the substrate. Adapted with permission.[59] Copyright 2020, Wiley-VCH. (c) Schematic illustration of the face mask with the embedded HKUST-1-MoS_2 device showing real time operation using a smartphone device. Breath sensing mechanism in the HKUST-1-MoS_2 integrated device. Adsorption and transfer of water molecules from the MOF to the MoS_2 layer and the mechanism of proton conduction in the MOF layer involving proton transfer from acidic water molecules coordinated to the metal cluster to the solvent molecules present in the channels. Only one cluster has been shown for clarity. Reproduced with permission.[204] Copyright 2020, the Royal Society of Chemistry. (d) The schematic of flexible MOF-modified sensors for nutrient sensing (e) multilayer structure of the MOF electrochemical sensor, in which a MOF layer is integrated. SEM micrograph of Cu–MOF before grinding is shown on the left and a 3D framework structure of Cu–MOF through hydrogen bonds is shown on the right. (f) SEM micrographs of the Cu–MOF nanoparticles on the surface of an electrode. Adapted with permission.[205] Copyright 2018, Wiley-VCH.

interstitial fluids (Fig. 16d–f). The MOFs used in this experiment demonstrated structural stability during the electrochemical measurements which lasted for 20 days, thereby also ensuring that the metal ions did not leach into the biological systems to cause cytotoxicity.

Currently, there are many risks surrounding the clinical application of implantable devices including infections, blood clotting, inflammation and tissue growth around the implanted device. Just as in drug delivery applications of MOFs,[229] a careful selection of MOFs can be made to minimise potential biological risks from the building units of the MOF or other accessories that make up the device. The chemical stability of the MOFs in the presence of body fluids should also be considered to ensure sustained performance of the sensor. Although research on MOF-based implantable sensors is relatively new, these sensors are showing promise in the advancement of biomedical and clinical practices.[230–232]

4.2 Food security

The detection of harmful chemicals in plant and animal products ensures food safety and protects the consumers. MOFs have been deployed to detect, adsorb and disarm toxic agrochemicals that are present in plants and to promote livestock wellbeing.[233] The function of MOFs in food analysis, chemical sensing, food preservation, food packaging and cleaning has been reviewed by Wang *et al.*[234] Typical MOF devices that have recently been studied for food safety are highlighted in Table 2. Sustainable agriculture is currently pursued to promote the quality of life of the current and future global population. Smart farming using farm-deployable MOF devices and information technology will revolutionize sustainable agriculture for food and environmental safety.[235]

4.3 Environmental monitoring

Large surface areas and high molecular adsorption capacity are important properties of MOFs that differentiate them from other solid-state materials. The effectiveness of bulk MOF materials to remediate environmentally unfriendly chemicals has inspired the fabrication of different types of devices. Excellent reviews have thoroughly discussed MOF devices for environmental applications.[236–238] Examples of recently developed MOF sensor devices are included in Table 2. New directions should focus on driving MOF sensors towards consumer needs, which could be either as simple as digitalized face masks and clothing for assessing indoor/outdoor air quality or as advanced as MOF-integrated unmanned aerial vehicles.[239–242]

Table 2 Applications of various field-deployable MOF devices to sense important biological, organic and inorganic analytes

Application	Sensor	Analyte	Sensing platform	Ref.
POC diagnostics	Co–MOF integrated carbon cloth/paper hybrid electrochemical button-sensor	Glucose	Electrochemical	207
POC diagnostics	Smartphone-assisted rGO/SMOF/PEI	Heavy metals	Electrochemical	201
POC diagnostics	Acetylcholinesterase/Zn–MOF EμAD	Chlorpyrifos	Electrochemical	208
POC diagnostics	BC/c-MWCNTs/ZIF-8@LAC biofuel cell sensor	Bisphenol A	Electrochemical	46
POC diagnostics	CA/ZIF-8@LAC/MWCNTs/Au biofuel cell sensor	Glucose	Electrochemical	47
POC diagnostics	ACF-rGO/$Cu(INA)_2$ sensor	Glucose from sweat	Electrochemical	106
POC diagnostics	Trx-1 and ADAM17cyto-ZIF-8 IDE device	Protein–protein (ADAM17cyto) interactions	Electrochemical	209
POC diagnostics	Smartphone-assisted HKUST-1-MoS_2 face mask sensor	Sleep apnoea diagnosis	Electronic	204
POC diagnostics	ZIF-8@antibody plasmonic biochip	Goat anti-rabbit IgG	Optical	210
POC diagnostics	ZIF-8@antibody plasmonic biochips	Neutrophil gelatinase associated lipocalin (NGAL)	Optical	211
POC diagnostics	Smartphone-assisted Ln^{3+}–MOF sensor	Phenylamine and 1-naphthol in human urine	Optical	212 and 213
POC diagnostics	Smartphone-assisted 1-OHP@Co/Tb-DPA sensor	pH	Optical	214
POC diagnostics	Smartphone-assisted 2-D Co–MOF sensor	Blood glucose	Optical	215
POC diagnostics	GOx-Eu^{3+}@UMOF Logic Detector	Glucose	Optical	216
POC diagnostics	GOx@Zr-PCN-222(Fe) microfluidic μPADs	Glucose	Optical	217
POC diagnostics	Smartphone-assisted GOx/HRP@ZIF-8 paper biosensor	Glucose	Optical	195
POC diagnostics	Smartphone-assisted μPADs	Glucose	Optical	218
POC diagnostics	GOx/HRP@ZIF-8 microfluidic biosensor	Glucose	Optical	219
POC diagnostics	Smartphone-assisted NH_2–Cu–MOF sensors	Alkaline phosphatase activity	Optical	198
POC diagnostics	Smartphone-assisted Eu^{3+}/Sc–MOF	Phenylglyoxylic acid	Optical	199
POC diagnostics	Apt/HRP@MAF-7 colorimetric device	Antibiotics	Optical	220
Food security	AChE/Z1200/EμPAD device	Chlorpyrifos in tomatoes	Electrochemical	221
Food security	Smartphone-integrated logic platform with binary UiO-66-NH_2/Eu^{3+}@MOF-808 paper indicator	Phosphate	Optical	222
Food security	Cu-Based surface-anchored MOF sensor array on quartz crystal microbalance	Volatile plant oils	Electromechanical	223
Food security	AChE/Cys/aAuNR/MOF/ITO bioprobe	Organophosphate pesticides	Electrochemical	224
Food security	Eu–BCA MOF thin-film	Nitrofuran antibiotics in animals	Optical	225
Food security	Au@ZIF-8 SERS paper	putrescine and cadaverine detection from spoilt food	Optical	226
Food security	Fe-MIL-88NH_2-Pt aptasensor	Kanamycin in milk	Optical	227
Food security	NDC-Y-**fcu**-MOF IDE sensor	NH_3 for livestock protection	Electronic	53
Environmental monitoring	NH_2-MIL-53(Al)-Matrimid/CMOS device	Alcohol vapour	Electronic	228
Environmental monitoring	Cu_3HHTP_2/Ni_3HHTP_2 IDE chip	NH_3, H_2S and NO	Electronic	138
Environmental monitoring	MFM-300 (In)/IDE	SO_2	Electronic	51
Environmental monitoring	MIL-96(Al)/IDE	Humidity	Electronic	118
Environmental monitoring	$Ni_3(HITP)_2$ SOFT sensor	NO	Electronic	55
Environmental monitoring	MIL-96(Al) smart textile-based (TEX) sensor	Humidity	Electronic	56
Environmental monitoring	Smartphone-assisted ZIF-8/TiO_2	Styrene	Optical	181
Environmental monitoring	UiO-66 optical fibre	Rh B	Optical	176
Environmental monitoring	UiO-66 optical fibre	5-Fluorouracil	Optical	173
Environmental monitoring	HKUST-1 single crystal optical fibre	Nitrobenzene	Optical	177
Environmental monitoring	ZIF-8 micro-ring resonator sensor	Various organic vapours	Optical	71
Environmental monitoring	NanoZIF-8-based BiMW sensor	CO_2	Optical	185

4.4 Defence and security applications

The global events of chemical attacks and explosions in the last decade, such as the terrorist attacks in Brussels and France in 2015 using the toxin triacetone triperoxide, the deployment of nerve agents in Syria in 2018 and the 2020 Beirut explosion from a large storage of ammonium nitrate, indicate the realities of the times we are in. Terrorism and diverse crimes have also become global threats to public safety. Remarkably, many

studies have demonstrated the potential of MOFs to adsorb and detoxify chemical warfare agents.[243–252] The excellent performance of MOFs demonstrated in these studies should motivate researchers to investigate the production of MOF-based portable catalytic sensors to assist the military in combating chemical warfare on the frontline and for the protection of civilians. These sensors may include MOF-integrated military wearables: helmet, personal digital assistants, smart wristwatch and wristbands. Also, other devices such as MOF-based smart gloves for narcotics sensing, portable electronics for explosives detection and miniaturized spectrometers can assist the law enforcement agents to effectively fight crimes and terrorism.

4.5 Artificial intelligence and robotics

Advances in computer technology are currently driving the development of industrial automation. Computers are programmed to learn cognitive behaviours of humans and to perform several tasks without human aid. In the MOF field, machine intelligence has been explored to envisage the properties of new materials and their potential applications.[253–258] Computer-guided research in machine intelligence will be crucial in the near future for materials screening to identify exceptionally performing MOFs and to predict ideal structure–property–performance relationships to design new sensors. The combination of the predictive strength of machine learning with advanced manufacturing and engineering technology should accelerate the mass production of MOF sensors for various applications. Moreover, computer-guided MOF research should extend to robotics to design machines with multifunctional chemical features that can simulate human/mammalian senses, such as strong 'sense of smell' provided by MOF-based electronic nose, electronic eye for optical sensing, electronic tongue for liquid/ion detection, electronic ears for acoustic detection of chemicals and chemically sensitive skin provided by MOF-based electronic skin.[59,223,259–261] Therefore, the integration of MOF sensors with artificial intelligence and robotics will aid the advancement of other areas such as food security, environmental monitoring and defence.

5 Conclusion

Over the last 25 years, the field of MOFs has continued to grow and increase in diversity due to the evolution of new materials. MOFs possess modifiable structures to incorporate chemical recognition groups, large surface areas for adsorption, uniform pore structure to control mass transport and a wide range of physical properties including chemoresistive, electronic and optical properties, making them ideal for chemical sensing. This review has examined the latest progress on the application of MOF films and proof-of-concept devices in chemical sensing. The development of wearable and hand-held MOF sensors for on-site analyte detection across the four major sensing platforms, namely: electronic, electrochemical, electromechanical and optical sensing are currently pursued within the MOF sensing community, which is indicative of the prospects of the combination of MOFs with portable optoelectronic gadgets. A major challenge regarding the integration of the majority of MOFs into analytical devices is their instability in the environments of application. The instability of some MOFs to air and water will hinder their performance in sensing devices despite their other advantageous properties. Only a few families of MOFs such as the ZIFs, Al-based MOFs, Matériaux de l'Institut Lavoisier MOFs and Zr-based MOFs, consisting of either high valent metal centres or imidazolate, terephthalate and other hydrophobic linkers, have shown extraordinary stability in humid conditions. Great efforts within the MOF community to enhance MOF stability include the synthesis of MOF composites with hydrophobic materials having exceptional stability even under extreme acidic and alkaline conditions.[190] Poor electronic conductivity is another key issue that affects charge transfer in MOFs and limits their performance in electrochemical sensing. This is usually addressed through either MOF designs using electron conducting ligands and appropriate metal centres or through the fabrication of MOF composites with suitable electron conducting materials.[111]

The mass production of MOF sensing devices to reach the end users will rely on key developments: the use of computer-guided research in artificial intelligence to screen materials to identify high performing MOFs; the advancement in large-scale synthesis of MOFs using flow chemistry; and advanced MOF film fabrication techniques such as lithography and vapour deposition methods.[262–264] It is also important for future studies to investigate the techno-economics of MOF device fabrication by taking advantage of the available computational tools to simplify MOF synthesis and materials processing towards the development of highly performing and affordable sensors. Based on the current success of MOF sensing capability and the microprocessing strength of smartphones, future MOF devices are likely to play key roles in the revolution of healthcare, smart farming, environmental monitoring, defence and artificial intelligence. Therefore, mobile devices such as smartphones, computer tablets, personal digital assistants, wristwatches, aerial drones and robots are all likely candidates for future integration with functional MOFs.

Conflicts of interest

There is nothing to declare.

Acknowledgements

J. F. O. thanks Dr Mehran Ghasemlou, RMIT University for assistance with graphic designs. C. M. D. acknowledges support through the Veski Inspiring Women Fellowship.

References

1 O. M. Yaghi and H. Li, *J. Am. Chem. Soc.*, 1995, **117**, 10401–10402, DOI: 10.1021/ja00146a033.

2 H. Li, M. Eddaoudi, M. O'Keeffe and O. M. Yaghi, *Nature*, 1999, **402**, 276–279, DOI: 10.1038/46248.
3 M. Kindo, T. Yoshitomi, H. Matsuzaka, S. Kitagawa and K. Seki, *Angew. Chem., Int. Ed. Engl.*, 1997, **36**, 1725–1727, DOI: 10.1002/anie.199717251.
4 H. C. Zhou, J. R. Long and O. M. Yaghi, *Chem. Rev.*, 2012, **112**, 673–674, DOI: 10.1021/cr300014x.
5 H. C. Zhou and S. Kitagawa, *Chem. Soc. Rev.*, 2014, **43**, 5415–5418, DOI: 10.1039/C4CS90059F.
6 H. Furukawa, K. E. Cordova, M. O'Keeffe and O. M. Yaghi, *Science*, 2013, **341**, 1230444, DOI: 10.1126/science.1230444.
7 J. Li, X. Wang, G. Zhao, C. Chen, Z. Chai, A. Alsaedi, T. Hayat and X. Wang, *Chem. Soc. Rev.*, 2018, **47**, 2322–2356, DOI: 10.1039/C7CS00543A.
8 J.-R. Li, R. J. Kuppler and H.-C. Zhou, *Chem. Soc. Rev.*, 2009, **38**, 1477–1504, DOI: 10.1039/B802426J.
9 X. Zhao, Y. Wang, D.-S. Li, X. Bu and P. Feng, *Adv. Mater.*, 2018, **30**, 1705189, DOI: 10.1002/adma.201705189.
10 Y. Xu, Q. Li, H. Xue and H. Pang, *Coord. Chem. Rev.*, 2018, **376**, 292–318, DOI: 10.1016/j.ccr.2018.08.010.
11 L. Jiao, Y. Wang, H.-L. Jiang and Q. Xu, *Adv. Mater.*, 2018, **30**, 1703663, DOI: 10.1002/adma.201703663.
12 J. Gascon, A. Corma, F. Kapteijn and F. X. Llabrés i Xamena, *ACS Catal.*, 2014, **4**, 361–378, DOI: 10.1021/cs400959k.
13 L. E. Kreno, K. Leong, O. K. Farha, M. Allendorf, R. P. Van Duyne and J. T. Hupp, *Chem. Rev.*, 2012, **112**, 1105–1125, DOI: 10.1021/cr200324t.
14 S. Wu, H. Min, W. Shi and P. Cheng, *Adv. Mater.*, 2020, **32**, 1805871, DOI: 10.1002/adma.201805871.
15 A. Amini, S. Kazemi and V. Safarifard, *Polyhedron*, 2020, **177**, 114260, DOI: 10.1016/j.poly.2019.114260.
16 O. S. Wolfbeis, *Angew. Chem., Int. Ed.*, 2013, **52**, 9864–9865, DOI: 10.1002/anie.201305915.
17 M. D. Allendorf, A. Schwartzberg, V. Stavila and A. A. Talin, *Chem. – Eur. J.*, 2011, **17**, 11372–11388, DOI: 10.1002/chem.201101595.
18 D. Zacher, O. Shekhah, C. Wöll and R. A. Fischer, *Chem. Soc. Rev.*, 2009, **38**, 1418–1429, DOI: 10.1039/B805038B.
19 A. Bétard and R. A. Fischer, *Chem. Rev.*, 2012, **112**, 1055–1083, DOI: 10.1021/cr200167v.
20 D. Bradshaw, A. Garai and J. Huo, *Chem. Soc. Rev.*, 2012, **41**, 2344–2381, DOI: 10.1039/C1CS15276A.
21 P. Falcaro, D. Buso, A. J. Hill and C. M. Doherty, *Adv. Mater.*, 2012, **24**, 3153–3168, DOI: 10.1002/adma.201200485.
22 P. Falcaro, R. Ricco, C. M. Doherty, K. Liang, A. J. Hill and M. J. Styles, *Chem. Soc. Rev.*, 2014, **43**, 5513–5560, DOI: 10.1039/C4CS00089G.
23 R. Dong, T. Zhang and X. Feng, *Chem. Rev.*, 2018, **118**, 6189–6235, DOI: 10.1021/acs.chemrev.8b00056.
24 M. Zhao, Y. Huang, Y. Peng, Z. Huang, Q. Ma and H. Zhang, *Chem. Soc. Rev.*, 2018, **47**, 6267–6295, DOI: 10.1039/C8CS00268A.
25 M. Wang, R. Dong and X. Feng, *Chem. Soc. Rev.*, 2021, **50**, 2764–2793, DOI: 10.1039/D0CS01160F.
26 G. Chakraborty, I.-H. Park, R. Medishetty and J. J. Vittal, *Chem. Rev.*, 2021, **121**, 3751–3891, DOI: 10.1021/acs.chemrev.0c01049.
27 C. Crivello, S. Sevim, O. Graniel, C. Franco, S. Pané, J. Puigmartí-Luis and D. Muñoz-Rojas, *Mater. Horiz.*, 2021, **8**, 168–178, DOI: 10.1039/D0MH00898B.
28 J. Ren and T.-C. Jen, *Coord. Chem. Rev.*, 2021, **430**, 213734, DOI: 10.1016/j.ccr.2020.213734.
29 M. Faustini, *Nat. Mater.*, 2021, **20**, 8–9, DOI: 10.1038/s41563-020-00837-9.
30 I. Stassen, N. Burtch, A. Talin, P. Falcaro, M. Allendorf and R. Ameloot, *Chem. Soc. Rev.*, 2017, **46**, 3185–3241, DOI: 10.1039/C7CS00122C.
31 W. T. Koo, J. S. Jang and I. D. Kim, *Chem*, 2019, **5**, 1938–1963, DOI: 10.1016/j.chempr.2019.04.013.
32 L. T. Zhang, Y. Zhou and S. T. Han, *Angew. Chem., Int. Ed.*, 2021, **60**, 2–23, DOI: 10.1002/anie.202006402.
33 M. D. Allendorf, R. Dong, X. Feng, S. Kaskel, D. Matoga and V. Stavila, *Chem. Rev.*, 2020, **120**, 8581–8640, DOI: 10.1021/acs.chemrev.0c00033.
34 A. Chidambaram and K. C. Stylianou, *Inorg. Chem. Front.*, 2018, **5**, 979–998, DOI: 10.1039/C7QI00815E.
35 Y. Zhang, S. Yuan, G. Day, X. Wang, X. Yang and H. C. Zhou, *Coord. Chem. Rev.*, 2018, **354**, 28–45, DOI: 10.1016/j.ccr.2017.06.007.
36 W. P. Lustig, S. Mukherjee, N. D. Rudd, A. V. Desai, J. Li and S. K. Ghosh, *Chem. Soc. Rev.*, 2017, **46**, 3242–3285, DOI: 10.1039/C6CS00930A.
37 E. A. Dolgopolova, A. M. Rice, C. R. Martin and N. B. Shustova, *Chem. Soc. Rev.*, 2018, **47**, 4710–4728, DOI: 10.1039/C7CS00861A.
38 R. Haldar, L. Heinke and C. Wöll, *Adv. Mater.*, 2020, **32**, 1905227, DOI: 10.1002/adma.201905227.
39 J. Liu and C. Wöll, *Chem. Soc. Rev.*, 2017, **46**, 5730–5770, DOI: 10.1039/C7CS00315C.
40 P. Kumar, A. Deep and K. H. Kim, *Trends Anal. Chem.*, 2015, **73**, 39–53, DOI: 10.1016/j.trac.2015.04.009.
41 H. Y. Li, S. N. Zhao, S. Q. Zang and J. Li, *Chem. Soc. Rev.*, 2020, **49**, 6364–6401, DOI: 10.1039/C9CS00778D.
42 X. Fang, B. Zong and S. Mao, *Nano-Micro Lett.*, 2018, **10**, 64, DOI: 10.1007/s40820-018-0218-0.
43 W. H. Li, W. H. Deng, G. E. Wang and G. Xu, *EnergyChem*, 2020, **2**, 100029, DOI: 10.1016/j.enchem.2020.100029.
44 Ü. Anik, S. Timur and Z. Dursun, *Microchim. Acta*, 2019, **186**, 196, DOI: 10.1007/s00604-019-3321-0.
45 Z. Wang, T. Liu, M. Asif, Y. Yu, W. Wang, H. Wang, F. Xiao and H. Liu, *ACS Appl. Mater. Interfaces*, 2018, **10**, 27936–27946, DOI: 10.1021/acsami.8b07868.
46 X. Li, D. Li, Y. Zhang, P. Lv, Q. Feng and Q. Wei, *Nano Energy*, 2020, **68**, 104308, DOI: 10.1016/j.nanoen.2019.104308.
47 X. Li, Q. Feng, K. Lu, J. Huang, Y. Zhang, Y. Hou, H. Qiao, D. Li and Q. Wei, *Biosens. Bioelectron.*, 2021, **171**, 112690, DOI: 10.1016/j.bios.2020.112690.
48 H. Yuan, J. Tao, N. Li, A. Karmakar, C. Tang, H. Cai, S. J. Pennycook, N. Singh and D. Zhao, *Angew. Chem., Int. Ed.*, 2019, **58**, 14089–14094, DOI: 10.1002/anie.201906222.
49 M. S. Hosseini, S. Zeinali and M. H. Sheikhi, *Sens. Actuators, B*, 2016, **230**, 9–16, DOI: 10.1016/j.snb.2016.02.008.

50 S. Homayoonnia and S. Zeinali, *Sens. Actuators, B*, 2016, **237**, 776–786, DOI: 10.1016/j.snb.2016.06.152.
51 V. Chernikova, O. Yassine, O. Shekhah, M. Eddaoudi and K. N. Salama, *J. Mater. Chem. A*, 2018, **6**, 5550–5554, DOI: 10.1039/C7TA10538J.
52 O. Yassine, O. Shekhah, A. H. Assen, Y. Belmabkhout, K. N. Salama and M. Eddaoudi, *Angew. Chem., Int. Ed.*, 2016, **55**, 15879–15883, DOI: 10.1002/anie.201608780.
53 A. H. Assen, O. Yassine, O. Shekhah, M. Eddaoudi and K. N. Salama, *ACS Sens.*, 2017, **2**, 1294–1301, DOI: 10.1021/acssensors.7b00304.
54 Y. Liu, H. Wang, W. Shi, W. Zhang, J. Yu, B. K. Chandran, C. Cui, B. Zhu, Z. Liu, B. Li, C. Xu, Z. Xu, S. Li, W. Huang, F. Huo and X. Chen, *Angew. Chem., Int. Ed.*, 2016, **55**, 8884–8888, DOI: 10.1002/anie.201602499.
55 M. K. Smith and K. A. Mirica, *J. Am. Chem. Soc.*, 2017, **139**, 16759–16767, DOI: 10.1021/jacs.7b08840.
56 S. Rauf, M. T. Vijjapu, M. A. Andrés, I. Gascón, O. Roubeau, M. Eddaoudi and K. N. Salama, *ACS Appl. Mater. Interfaces*, 2020, **12**, 29999–30006, DOI: 10.1021/acsami.0c07532.
57 L. J. Small, R. C. Hill, J. L. Krumhansl, M. E. Schindelholz, Z. Chen, K. W. Chapman, X. Zhang, S. Yang, M. Schröder and T. M. Nenoff, *ACS Appl. Mater. Interfaces*, 2019, **11**, 27982–27988, DOI: 10.1021/acsami.9b09938.
58 B. Wang, Y. Luo, B. Liu and G. Duan, *ACS Appl. Mater. Interfaces*, 2019, **11**, 35935–35940, DOI: 10.1021/acsami.9b14319.
59 J. Wu, J. Chen, C. Wang, Y. Zhou, K. Ba, H. Xu, W. Bao, X. Xu, A. Carlsson, S. Lazar, A. Meingast, Z. Sun and H. Deng, *Adv. Sci.*, 2020, **7**, 1903003, DOI: 10.1002/advs.201903003.
60 H. Ahmed, X. Yang, Y. Ehrnst, N. N. Jeorje, S. Marqus, P. C. Sherrell, A. E. Ghazaly, J. Rosen, A. R. Rezk and L. Y. Yeo, *Nanoscale Horiz.*, 2020, **5**, 1050–1057, DOI: 10.1039/D0NH00171F.
61 H. Ahmed, A. R. Rezk, J. J. Richardson, L. K. Macreadie, R. Babarao, E. L. H. Mayes, L. Lee and L. Y. Yeo, *Nat. Commun.*, 2019, **10**, 2282, DOI: 10.1038/s41467-019-10173-5.
62 C. Yim, M. Lee, W. Kim, S. Lee, G.-H. Kim, K. T. Kim and S. Jeon, *Chem. Commun.*, 2015, **51**, 6168–6171, DOI: 10.1039/C5CC01315A.
63 X.-Y. Xu and B. Yan, *J. Mater. Chem. C*, 2018, **6**, 1863–1869, DOI: 10.1039/C7TC05204A.
64 Y. Xing, L. Shi, J. Yan and Y. Chen, *ChemistrySelect*, 2020, **5**, 3946–3952, DOI: 10.1002/slct.201904131.
65 R. Singh, G. Souillard, L. Chassat, Y. Gao, X. Mulet and C. M. Doherty, *Adv. Sustainable Syst.*, 2020, 2000059, DOI: 10.1002/adsu.202000059.
66 J. Hromadka, B. Tokay, S. James, R. P. Tatam and S. Korposh, *Sens. Actuators, B*, 2015, **221**, 891–899, DOI: 10.1016/j.snb.2015.07.027.
67 J. Hromadka, B. Tokay, R. Correia, S. P. Morgan and S. Korposh, *Sens. Actuators, B*, 2018, **260**, 685–692, DOI: 10.1016/j.snb.2018.01.015.
68 J. Hromadka, B. Tokay, R. Correia, S. P. Morgan and S. Korposh, *Sens. Actuators, B*, 2018, **255**, 2483–2494, DOI: 10.1016/j.snb.2017.09.041.
69 K.-J. Kim, P. Lu, J. T. Culp and P. R. Ohodnicki, *ACS Sens.*, 2018, **3**, 386–394, DOI: 10.1021/acssensors.7b00808.
70 C. Zhu, J. A. Perman, R. E. Gerald, S. Ma and J. Huang, *ACS Appl. Mater. Interfaces*, 2019, **11**, 4393–4398, DOI: 10.1021/acsami.8b19775.
71 J. Tao, X. Wang, T. Sun, H. Cai, Y. Wang, T. Lin, D. Fu, L. L. Y. Ting, Y. Gu and D. Zhao, *Sci. Rep.*, 2017, **7**, 41640, DOI: 10.1038/srep41640.
72 D. F. Pozo-Ayuso, M. Castaño-Álvarez and A. Fernández-la-Villa, in *Laboratory Methods in Dynamic Electroanalysis*, ed. M. T. Fernandez Abedul, Elsevier, 2020, pp. 57–65.
73 F. R. Simões and M. G. Xavier, Electrochemical Sensors, in *Nanoscience and its Applications*, ed. A. L. Da Róz, M. Ferreira, F. de Lima Leite and O. N. Oliveira, William Andrew Publishing, 2017, pp. 155–178.
74 C.-H. Chuang and C.-W. Kung, *Electroanalysis*, 2020, **32**, 1885–1895, DOI: 10.1002/elan.202060111.
75 A. Gupta, S. K. Bhardwaj, A. L. Sharma, K.-H. Kim and A. Deep, *Environ. Res.*, 2019, **171**, 395–402, DOI: 10.1016/j.envres.2019.01.049.
76 H. A. Schulze, B. Hoppe, M. Schäfer, D. P. Warwas and P. Behrens, *ChemNanoMat*, 2019, **5**, 1159–1169, DOI: 10.1002/cnma.201900110.
77 X. Tu, Y. Xie, X. Ma, F. Gao, L. Gong, D. Wang, L. Lu, G. Liu, Y. Yu and X. Huang, *J. Electroanal. Chem.*, 2019, **848**, 113268, DOI: 10.1016/j.jelechem.2019.113268.
78 Y. Dong, C. Duan, Q. Sheng and J. Zheng, *Analyst*, 2019, **144**, 521–529, DOI: 10.1039/C8AN01641K.
79 S. Lu, M. Hummel, K. Chen, Y. Zhou, S. Kang and Z. Gu, *Electrochem. Commun.*, 2020, **114**, 106715, DOI: 10.1016/j.elecom.2020.106715.
80 Y. Li, W. Ye, Y. Cui, B. Li, Y. Yang and G. Qian, *J. Mol. Struct.*, 2020, **1209**, 127986, DOI: 10.1016/j.molstruc.2020.127986.
81 H. X. Dai, W. J. Lü, X. W. Zuo, Q. Zhu, C. J. Pan, X. Y. Niu, J. J. Liu, H. L. Chen and X. G. Chen, *Biosens. Bioelectron.*, 2017, **95**, 131–137, DOI: 10.1016/j.bios.2017.04.021.
82 Y. Zhou, C. Li, Y. Hao, B. Ye and M. Xu, *Talanta*, 2018, **188**, 282–287, DOI: 10.1016/j.talanta.2018.05.078.
83 Y. Zheng and Z. Ma, *Biosens. Bioelectron.*, 2019, **129**, 42–49, DOI: 10.1016/j.bios.2019.01.016.
84 K.-O. Honikel, *Meat Sci.*, 2008, **78**, 68–76, DOI: 10.1016/j.meatsci.2007.05.030.
85 R. Mo, X. Wang, Q. Yuan, X. Yan, T. Su, Y. Feng, L. Lv, C. Zhou, P. Hong, S. Sun, Z. Wang and C. Li, *Sensors*, 2018, **18**, 1986, DOI: 10.3390/s18071986.
86 H. Winnischofer, S. de Souza Lima, K. Araki and H. E. Toma, *Anal. Chim. Acta*, 2003, **480**, 97–107, DOI: 10.1016/S0003-2670(02)01594-5.
87 C.-W. Kung, T.-H. Chang, L.-Y. Chou, J. T. Hupp, O. K. Farha and K.-C. Ho, *Electrochem. Commun.*, 2015, **58**, 51–56, DOI: 10.1016/j.elecom.2015.06.003.
88 C.-W. Kung, Y.-S. Li, M.-H. Lee, S.-Y. Wang, W.-H. Chiang and K.-C. Ho, *J. Mater. Chem. A*, 2016, **4**, 10673–10682, DOI: 10.1039/C6TA02563C.

89 Y.-S. Chang, J.-H. Li, Y.-C. Chen, W. H. Ho, Y.-D. Song and C.-W. Kung, *Electrochim. Acta*, 2020, **347**, 136276, DOI: 10.1016/j.electacta.2020.136276.
90 C. C. Winterbourn, in *Methods in Enzymology*, ed. E. Cadenas and L. Packer, Academic Press, 2013, vol. 528, pp. 3–25.
91 Y. Zhou, C. Li, Y. Hao, B. Ye and M. Xu, *Talanta*, 2018, **188**, 282–287, DOI: 10.1016/j.talanta.2018.05.078.
92 E. Biemmi, C. Scherb and T. Bein, *J. Am. Chem. Soc.*, 2007, **129**, 8054–8055, DOI: 10.1021/ja0701208.
93 K. S. Park, Z. Ni, A. P. Côté, J. Y. Choi, R. Huang, F. J. Uribe-Romo, H. K. Chae, M. O'Keeffe and O. M. Yaghi, *Proc. Natl. Acad. Sci. U. S. A.*, 2006, **103**, 10186–10191, DOI: 10.1073/pnas.0602439103.
94 K. Liang, R. Ricco, C. M. Doherty, M. J. Styles, S. Bell, N. Kirby, S. Mudie, D. Haylock, A. J. Hill, C. J. Doonan and P. Falcaro, *Nat. Commun.*, 2015, **6**, 7240, DOI: 10.1038/ncomms8240.
95 Z. Fan, J. Wang, Y. Nie, L. Ren, B. Liu and G. Liu, *J. Electrochem. Soc.*, 2015, **163**, B32, DOI: 10.1149/2.0531603jes.
96 Q. Zhang, L. Zhang, H. Dai, Z. Li, Y. Fu and Y. Li, *J. Electroanal. Chem.*, 2018, **823**, 40–46, DOI: 10.1016/j.jelechem.2018.04.015.
97 R. C. Hoft, M. J. Ford, A. M. McDonagh and M. B. Cortie, *J. Phys. Chem. C*, 2007, **111**, 13886–13891, DOI: 10.1021/jp072494t.
98 S. C. Barton, J. Gallaway and P. Atanassov, *Chem. Rev.*, 2004, **104**, 4867–4886, DOI: 10.1021/cr020719k.
99 A. J. Bandodkar, J.-M. You, N.-H. Kim, Y. Gu, R. Kumar, A. M. V. Mohan, J. Kurniawan, S. Imani, T. Nakagawa, B. Parish, M. Parthasarathy, P. P. Mercier, S. Xu and J. Wang, *Energy Environ. Sci.*, 2017, **10**, 1581–1589, DOI: 10.1039/C7EE00865A.
100 C. Gu, L. Bai, L. Pu, P. Gai and F. Li, *Biosens. Bioelectron.*, 2021, **176**, 112907, DOI: 10.1016/j.bios.2020.112907.
101 S. Shahrokhian, E. Khaki Sanati and H. Hosseini, *Biosens. Bioelectron.*, 2018, **112**, 100–107, DOI: 10.1016/j.bios.2018.04.039.
102 S. G. Leonardi, S. Marini, C. Espro, A. Bonavita, S. Galvagno and G. Neri, *Microchim. Acta*, 2017, **184**, 2375–2385, DOI: 10.1007/s00604-017-2232-1.
103 Y. Fan, X. Yang, Z. Cao, S. Chen and B. Zhu, *J. Appl. Electrochem.*, 2015, **45**, 131–138, DOI: 10.1007/s10800-014-0779-7.
104 M. Ezzati, S. Shahrokhian and H. Hosseini, *ACS Sustainable Chem. Eng.*, 2020, **8**, 14340–14352, DOI: 10.1021/acssuschemeng.0c03806.
105 Z. Xu, Q. Wang, H. Zhangsun, S. Zhao, Y. Zhao and L. Wang, *Food Chem.*, 2021, **349**, 129202, DOI: 10.1016/j.foodchem.2021.129202.
106 C. H. Hendon and A. Walsh, *Chem. Sci.*, 2015, **6**, 3674–3683, DOI: 10.1039/C5SC01489A.
107 N. Rezvani Jalal, T. Madrakian, A. Afkhami and A. Ghoorchian, *ACS Appl. Mater. Interfaces*, 2020, **12**, 4859–4869, DOI: 10.1021/acsami.9b18097.
108 N. Iqbal and N. Iqbal, *Chemother. Res. Pract.*, 2014, **2014**, 1–9, DOI: 10.1155/2014/357027.
109 M. G. Campbell and M. Dincă, *Sensors*, 2017, **17**, 1108, DOI: 10.3390/s17051108.
110 M. Ko, L. Mendecki and K. A. Mirica, *Chem. Commun.*, 2018, **54**, 7873–7891, DOI: 10.1039/C8CC02871K.
111 L. S. Xie, G. Skorupskii and M. Dincă, *Chem. Rev.*, 2020, **120**, 8536–8580, DOI: 10.1021/acs.chemrev.9b00766.
112 D. Ray, S. Goswami, J. Duan, J. T. Hupp, C. J. Cramer and L. Gagliardi, *Chem. Mater.*, 2021, **33**, 1182–1189, DOI: 10.1021/acs.chemmater.0c03855.
113 E. A. Dolgopolova, A. J. Brandt, O. A. Ejegbavwo, A. S. Duke, T. D. Maddumapatabandi, R. P. Galhenage, B. W. Larson, O. G. Reid, S. C. Ammal, A. Heyden, M. Chandrashekhar, V. Stavila, D. A. Chen and N. B. Shustova, *J. Am. Chem. Soc.*, 2017, **139**, 5201–5209, DOI: 10.1021/jacs.7b01125.
114 Z. Xia, X. Jia, X. Ge, C. Ren, Q. Yang, J. Hu, Z. Chen, J. Han, G. Xie, S. Chen and S. Gao, *Angew. Chem., Int. Ed.*, 2021, **60**, 10228–10238, DOI: 10.1002/anie.202100123.
115 C.-W. Kung, P.-C. Han, C.-H. Chuang and K. C.-W. Wu, *APL Mater.*, 2019, **7**, 110902, DOI: 10.1063/1.5125487.
116 M. V. Winkle and D. K. Bediako, *ACS Cent. Sci.*, 2021, **7**, 14–16, DOI: 10.1021/acscentsci.0c01625.
117 H. Yuan, J. Tao, N. Li, A. Karmakar, C. Tang, H. Cai, S. J. Pennycook, N. Singh and D. Zhao, *Angew. Chem., Int. Ed.*, 2019, **58**, 14089–14094, DOI: 10.1002/anie.201906222.
118 M. A. Andrés, M. T. Vijjapu, S. G. Surya, O. Shekhah, K. N. Salama, C. Serre, M. Eddaoudi, O. Roubeau and I. Gascón, *ACS Appl. Mater. Interfaces*, 2020, **12**, 4155–4162, DOI: 10.1021/acsami.9b20763.
119 M. Savage, Y. Cheng, T. L. Easun, J. E. Eyley, S. P. Argent, M. R. Warren, W. Lewis, C. Murray, C. C. Tang, M. D. Frogley, G. Cinque, J. Sun, S. Rudić, R. T. Murder, M. J. Benham, A. N. Fitch, A. J. Blake, A. J. Ramirez-Cuesta, S. Yang and M. Schröder, *Adv. Mater.*, 2016, **28**, 8705–8711, DOI: 10.1002/adma.201602338.
120 J. Benito, M. Fenero, S. Sorribas, B. Zornoza, K. J. Msayib, N. B. Mckeown, C. Téllez, J. Coronas and I. Gascón, *Colloids Surf., A*, 2015, **470**, 161–170, DOI: 10.1016/j.colsurfa.2015.01.082.
121 M. Lanza, H.-S. P. Wong, E. Pop, D. Ielmini, D. Strukov, B. C. Regan, L. Larcher, M. A. Villena, J. J. Yang, L. Goux, A. Belmonte, Y. Yang, F. M. Puglisi, J. Kang, B. Magyari-Köpe, E. Yalon, A. Kenyon, M. Buckwell, A. Mehonic, A. Shluger, H. Li, T.-H. Hou, B. Hudec, D. Akinwande, R. Ge, S. Ambrogio, J. B. Roldan, E. Miranda, J. Suñe, K. L. Pey, X. Wu, N. Raghavan, E. Wu, W. D. Lu, G. Navarro, W. Zhang, H. Wu, R. Li, A. Holleitner, U. Wurstbauer, M. C. Lemme, M. Liu, S. Long, Q. Liu, H. Lv, A. Padovani, P. Pavan, I. Valov, X. Jing, T. Han, K. Zhu, S. Chen, F. Hui and Y. Shi, *Adv. Electron. Mater.*, 2019, **5**, 1800143, DOI: 10.1002/aelm.201800143.
122 M. Wang and D. Kerr, *Wearable Technologies: Concepts, Methodologies, Tools, and Applications*, IGI Global, 2018, pp. 65–83, DOI: 10.4018/978-1-5225-5484-4.ch005.

123 Z. Yao, L. Pan, L. Liu, J. Zhang, Q. Lin, Y. Ye, Z. Zhang, S. Xiang and B. Chen, *Sci. Adv.*, 2019, **5**, eaaw4515, DOI: 10.1126/sciadv.aaw4515.

124 Z. Wang, D. Nminibapiel, P. Shrestha, J. Liu, W. Guo, P. G. Weidler, H. Baumgart, C. Wöll and E. Redel, *ChemNanoMat*, 2016, **2**, 67–73, DOI: 10.1002/cnma.201500143.

125 N. T. T. Hoang, H. T. Le, K. H. T. Ta, Y. Thi, L. H. T. Nguyen, T. L. H. Doan, C. K. Fang, S. Hwang, B. T. Phan and N. K. Pham, *Org. Electron.*, 2021, **93**, 106136, DOI: 10.1016/j.orgel.2021.106136.

126 L. G. S. Albano, T. P. Vello, D. H. S. de Camargo, R. M. L. da Silva, A. C. M. Padilha, A. Fazzio and C. C. B. Bufon, *Nano Lett.*, 2020, **20**, 1080–1088, DOI: 10.1021/acs.nanolett.9b04355.

127 H. Ohara, S. Yamamoto, D. Kuzuhara, T. Koganezawa, H. Oikawa and M. Mitsuishi, *ACS Appl. Mater. Interfaces*, 2020, **12**, 50784–50792, DOI: 10.1021/acsami.0c13016.

128 L. Pan, Z. Ji, X. Yi, X. Zhu, X. Chen, J. Shang, G. Liu and R.-W. Li, *Adv. Funct. Mater.*, 2015, **25**, 2677–2685, DOI: 10.1002/adfm.201500449.

129 M. J. Park and J. S. Lee, *RSC Adv.*, 2017, **7**, 21045–21049, DOI: 10.1039/C6RA28361F.

130 L. Sun, M. G. Campbell and M. Dincă, *Angew. Chem., Int. Ed.*, 2016, **55**, 3566–3579, DOI: 10.1002/anie.201506219.

131 V. Stavila, A. A. Talin and M. D. Allendorf, *Chem. Soc. Rev.*, 2014, **43**, 5994–6010, DOI: 10.1039/C4CS00096J.

132 L. Sun, C. H. Hendon, S. S. Park, Y. Tulchinsky, R. Wan, F. Wang, A. Walsh and M. Dincă, *Chem. Sci.*, 2017, **8**, 4450–4457, DOI: 10.1039/C7SC00647K.

133 S. K. Bhardwaj, N. Bhardwaj, R. Kaur, J. Mehta, A. L. Sharma, K.-H. Kim and A. Deep, *J. Mater. Chem. A*, 2018, **6**, 14992–15009, DOI: 10.1039/C8TA04220A.

134 H. Liu, Y. Wang, Z. Qin, D. Liu, H. Xu, H. Dong and W. Hu, *J. Phys. Chem. Lett.*, 2021, **12**, 1612–1630, DOI: 10.1021/acs.jpclett.0c02988.

135 X. Huang, P. Sheng, Z. Tu, F. Zhang, J. Wang, H. Geng, Y. Zou, C. Di, Y. Yi, Y. Sun, W. Xu and D. Zhu, *Nat. Commun.*, 2015, **6**, 7408, DOI: 10.1038/ncomms8408.

136 J. A. Gustafson and C. E. Wilmer, *J. Phys. Chem. C*, 2017, **121**, 6033–6038, DOI: 10.1021/acs.jpcc.6b09740.

137 M. G. Campbell, S. F. Liu, T. M. Swager and M. Dincă, Chemiresistive Sensor Arrays from Conductive 2D Metal–Organic Frameworks, *J. Am. Chem. Soc.*, 2015, **137**, 13780–13783, DOI: 10.1021/jacs.5b09600.

138 M. K. Smith, K. E. Jensen, P. A. Pivak and K. A. Mirica, *Chem. Mater.*, 2016, **28**, 5264–5268, DOI: 10.1021/acs.chemmater.6b02528.

139 Z. Meng, A. Aykanat and K. Mirica, *J. Am. Chem. Soc.*, 2019, **141**, 2046–2053, DOI: 10.1021/jacs.8b11257.

140 M. Wang, Z. Zhang, H. Zhong, X. Huang, W. Li, M. Hambsch, P. Zhang, Z. Wang, P. S. Petkov, T. Heine, S. C. B. Mannsfeld, X. Feng and R. Dong, *Angew. Chem., Int. Ed.*, 2021, DOI: 10.1002/anie.202104461.

141 Y. Guo, G. Yu and Y. Liu, *Adv. Mater.*, 2010, **22**, 4427–4447, DOI: 10.1002/adma.201000740.

142 P. F. Baude, D. A. Ender, M. A. Haase, T. W. Kelley, D. V. Muyres and S. D. Theiss, *Appl. Phys. Lett.*, 2003, **82**, 3964–3966, DOI: 10.1063/1.1579554.

143 T. Someya, T. Sekitani, S. Iba, Y. Kato, H. Kawaguchi and T. Sakurai, *Proc. Natl. Acad. Sci. U. S. A.*, 2004, **101**, 9966–9970, DOI: 10.1073/pnas.0401918101.

144 R. J. W. Lugtenberg, M. M. G. Antonisse, R. J. M. Egberink, J. F. J. Engbersen and D. N. Reinhoudt, *J. Chem. Soc., Perkin Trans. 2*, 1996, 1937–1941, DOI: 10.1039/P29960001937.

145 E. L. Gui, L. J. Li, K. Zhang, Y. Xu, X. Dong, X. Ho, P. S. Lee, J. Kasim, Z. X. Shen, J. A. Rogers and S. G. Mhaisalkar, *J. Am. Chem. Soc.*, 2007, **129**, 14427–14432, DOI: 10.1021/ja075176g.

146 *Chemical Sensors: Fundamentals of Sensing Materials Volume 1: General Approaches*, ed. G. Korotcenkov, Momentum Press, 2010, vol. 1.

147 G. Wu, J. Huang, Y. Zang, J. He and G. Xu, *J. Am. Chem. Soc.*, 2017, **139**, 1360–1363, DOI: 10.1021/jacs.6b08511.

148 N. Ingle, P. Sayyad, G. Bodkhe, M. Mahadik, A. G. Theeazen, S. Shirsat and M. D. Shirsat, *Appl. Phys. A: Mater. Sci. Process.*, 2020, **126**, 723, DOI: 10.1007/s00339-020-03907-6.

149 Z. G. Gu, S. C. Chen, W. Q. Fu, Q. Zheng and J. Zhang, *ACS Appl. Mater. Interfaces*, 2017, **9**, 7259–7264, DOI: 10.1021/acsami.6b14541.

150 G. A. Bodkhe, M. A. Deshmukh, H. K. Patil, S. M. Shirsat, V. Srihari, K. K. Pandey, G. Panchal, D. M. Phase, A. Mulchandani and M. D. Shirsat, *J. Phys. D: Appl. Phys.*, 2019, **52**, 335105, DOI: 10.1088/1361-6463/ab1987.

151 I. Stassen, B. Bueken, H. Reinsch, J. F. M. Oudenhoven, D. Wouters, J. Hajek, V. Van Speybroeck, N. Stock, P. M. Vereecken, R. Van Schaijk and D. De Vos, *Chem. Sci.*, 2016, **7**, 5827–5832, DOI: 10.1039/C6SC00987E.

152 B. R. Pinkard, S. Shetty, J. C. Kramlich, P. G. Reinhall and I. V. Novosselov, *J. Phys. Chem. A*, 2020, **124**, 8383–8389, DOI: 10.1021/acs.jpca.0c05104.

153 J. Janata and M. Josowicz, *Anal. Chem.*, 1997, **69**, 293A–296A, DOI: 10.1021/ac9716237.

154 Y. T. Yang, C. Callegari, X. L. Feng, K. L. Ekinci and M. L. Roukes, *Nano Lett.*, 2006, **6**, 583–586, DOI: 10.1021/nl052134m.

155 P. Gründler, *Chemical Sensors: An Introduction for Scientists and Engineers*, Springer Science & Business Media, 2007.

156 G. Korotcenkov, in *Handbook of Gas Sensor Materials: Properties, Advantages and Shortcomings for Applications Volume 1: Conventional Approaches*, ed. G. Korotcenkov, Springer, New York, NY, 2013, pp. 307–328.

157 K. N. Chappanda, O. Shekhah, O. Yassine, S. P. Patole, M. Eddaoudi and K. N. Salama, *Sens. Actuators, B*, 2018, **257**, 609–619, DOI: 10.1016/j.snb.2017.10.189.

158 C. Yim, M. Lee, W. Kim, S. Lee, G.-H. Kim, K. T. Kim and S. Jeon, *Chem. Commun.*, 2015, **51**, 6168–6171, DOI: 10.1039/C5CC01315A.

159 B. Paschke, A. Wixforth, D. Denysenko and D. Volkmer, *ACS Sens.*, 2017, **2**, 740–747, DOI: 10.1021/acssensors.7b00014.

160 V. G. Sauerbrey, *Z. Phys.*, 1959, **155**, 206–222, DOI: 10.1007/BF01337937.
161 F. Xu, L. Sun, P. Huang, Y. Sun, Q. Zheng, Y. Zou, H. Chu, E. Yan, H. Zhang, J. Wang and Y. Du, *Sens. Actuators, B*, 2018, **254**, 872–877, DOI: 10.1016/j.snb.2017.07.026.
162 E. Haghighi and S. Zeinali, *RSC Adv.*, 2019, **9**, 24460–24470, DOI: 10.1039/C9RA04152D.
163 E. Haghighi and S. Zeinali, *Microporous Mesoporous Mater.*, 2020, **300**, 110065, DOI: 10.1016/j.micromeso.2020.110065.
164 Z. Ma, T. Yuan, Y. Fan, L. Wang, Z. Duan, W. Du, D. Zhang and J. Xu, *Sens. Actuators, B*, 2020, 127365, DOI: 10.1016/j.snb.2019.127365.
165 X.-L. Yang, R.-B. Zang, R. Shao, R.-F. Guan and M.-H. Xie, *J. Hazard. Mater.*, 2021, **413**, 125467, DOI: 10.1016/j.jhazmat.2021.125467.
166 J. Devkota, K. J. Kim, P. R. Ohodnicki, J. T. Culp, D. W. Greve and J. W. Lekse, *Nanoscale*, 2018, **10**, 8075–8087, DOI: 10.1039/C7NR09536H.
167 K. M. Goeders, J. S. Colton and L. A. Bottomley, *Chem. Rev.*, 2008, **108**, 522–542, DOI: 10.1021/cr0681041.
168 A. Ghysels, L. Vanduyfhuys, M. Vandichel, M. Waroquier, V. Van Speybroeck and B. Smit, *J. Phys. Chem. C*, 2013, **117**, 11540, DOI: 10.1021/jp311601q.
169 A. V. Neimark, F. X. Coudert, C. Triguero, A. Boutin, A. H. Fuchs, I. Beurroies and R. Denoyel, *Langmuir*, 2011, **27**, 4734–4741, DOI: 10.1021/la200094x.
170 A. Boutin, F.-X. Coudert, M.-A. Springuel-Huet, A. V. Neimark, G. Férey and A. H. Fuchs, *J. Phys. Chem. C*, 2010, **114**, 22237–22244, DOI: 10.1021/jp108710h.
171 C. Yim, M. Lee, M. Yun, G.-H. Kim, K. T. Kim and S. Jeon, *Sci. Rep.*, 2015, **5**, 10674, DOI: 10.1038/srep10674.
172 N. L. Torad, S. Zhang, W. A. Amer, M. M. Ayad, M. Kim, J. Kim, B. Ding, X. Zhang, T. Kimura and Y. Yamauchi, *Adv. Mater. Interfaces*, 2019, **6**, 1900849, DOI: 10.1002/admi.201900849.
173 M. Nazari, M. Rubio-Martinez, G. Tobias, J. P. Barrio, R. Babarao, F. Nazari, K. Konstas, B. W. Muir, S. F. Collins, A. J. Hill, M. C. Duke and M. R. Hill, *Adv. Funct. Mater.*, 2016, **26**, 3244–3249, DOI: 10.1002/adfm.201505260.
174 S.-I. Ohira, Y. Miki, T. Matsuzaki, N. Nakamura, Y. Sato, Y. Hirose and K. Toda, *Anal. Chim. Acta*, 2015, **886**, 188–193, DOI: 10.1016/j.aca.2015.05.045.
175 R. A. Potyrailo, S. E. Hobbs and G. M. Hieftje, *Fresenius' J. Anal. Chem.*, 1998, **362**, 349–373, DOI: 10.1007/s002160051086.
176 M. Nazari, M. A. Forouzandeh, C. M. Divarathne, F. Sidiroglou, M. R. Martinez, K. Konstas, B. W. Muir, A. J. Hill, M. C. Duke, M. R. Hill and S. F. Collins, *Opt. Lett.*, 2016, **41**, 1696–1699, DOI: 10.1364/OL.41.001696.
177 K.-J. Kim, J. T. Culp, P. R. Ohodnicki, P. C. Cvetic, S. Sanguinito, A. L. Goodman and H. T. Kwon, *ACS Appl. Mater. Interfaces*, 2019, **11**, 33489–33496, DOI: 10.1021/acsami.9b12052.
178 F. Baldini, M. Brenci, F. Chiavaioli, A. Giannetti and C. Trono, *Anal. Bioanal. Chem.*, 2012, **402**, 109–116, DOI: 10.1007/s00216-011-5492-3.
179 J. Wu, W. Zhang, Y. Wang, B. Li, T. Hao, Y. Zheng, L. Jiang, K. Chen and K. Seng Chiang, *Nanoscale*, 2020, **12**, 9991–10000, DOI: 10.1039/C9NR09061D.
180 W. Bogaerts, P. D. Heyn, T. V. Vaerenbergh, K. D. Vos, S. K. Selvaraja, T. Claes, P. Dumon, P. Bienstman, D. V. Thourhout and R. Baets, *Laser Photonics Rev.*, 2012, **6**, 47–73, DOI: 10.1002/lpor.201100017.
181 O. Dalstein, D. R. Ceratti, C. Boissière, D. Grosso, A. Cattoni and M. Faustini, *Adv. Funct. Mater.*, 2016, **26**, 81–90, DOI: 10.1002/adfm.201503016.
182 O. Dalstein, E. Gkaniatsou, C. Sicard, O. Sel, H. Perrot, C. Serre, C. Boissière and M. Faustini, *Angew. Chem., Int. Ed.*, 2017, **56**, 14011, DOI: 10.1002/anie.201706745.
183 G. Lu, O. K. Farha, L. E. Kreno, P. M. Schoenecker, K. S. Walton, R. P. V. Duyne and J. T. Hupp, *Adv. Mater.*, 2011, **23**, 4449–4452, DOI: 10.1002/adma.201102116.
184 C. Avci, I. Imaz, A. Carné-Sánchez, J. A. Pariente, N. Tasios, J. Pérez-Carvajal, M. I. Alonso, A. Blanco, M. Dijkstra, C. López and D. Maspoch, *Nat. Chem.*, 2018, **10**, 78–84, DOI: 10.1038/nchem.2875.
185 B. Chocarro-Ruiz, J. Pérez-Carvajal, C. Avci, O. Calvo-Lozano, M. Isabel Alonso, D. Maspoch and L. M. Lechuga, *J. Mater. Chem. A*, 2018, **6**, 13171–13177, DOI: 10.1039/C8TA02767F.
186 R. Zhang, D. Zhang, Y. Yao, Q. Zhang, Y. Xu, Y. Wu, H. Yu and G. Lu, *ACS Appl. Mater. Interfaces*, 2019, **11**, 21010–21017, DOI: 10.1021/acsami.9b05933.
187 J. F. Olorunyomi, M. M. Sadiq, M. Batten, K. Konstas, D. Chen, C. M. Doherty and R. A. Caruso, *Adv. Opt. Mater.*, 2020, **8**, 2000961, DOI: 10.1002/adom.202000961.
188 J. Cui, N. Gao, C. Wang, W. Zhu, J. Li, H. Wang, P. Seidel, B. Jan Ravoo and G. Li, *Nanoscale*, 2014, **6**, 11995–12001, DOI: 10.1039/C4NR03095H.
189 L. Li, X. Jiao, D. Chen, B. V. Lotsch and C. Li, *Chem. Mater.*, 2015, **27**, 7601–7609, DOI: 10.1021/acs.chemmater.5b02476.
190 M. Ding, Z. Cai and H.-L. Jiang, *Chem. Sci.*, 2019, **10**, 10209–10230, DOI: 10.1039/C9SC03916C.
191 S. Majumder and M. J. Deen, *Sensors*, 2019, **19**, 2164, DOI: 10.3390/s19092164.
192 F. Li, Y. Bao, D. Wang, W. Wang and L. Niu, *Sci. Bull.*, 2016, **61**, 190–201, DOI: 10.1007/s11434-015-0954-1.
193 M. Rezazadeh, S. Seidi, M. Lid, S. Pedersen-Bjergaard and Y. Yamini, *TrAC, Trends Anal. Chem.*, 2019, **118**, 548–555, DOI: 10.1016/j.trac.2019.06.019.
194 Y. Zhao, H. Ouyang, S. Feng, Y. Luo, Q. Shi, C. Zhu, Y.-C. Chang, L. Li, D. Du and H. Yang, *Anal. Chim. Acta*, 2019, **1077**, 160–166, DOI: 10.1016/j.aca.2019.05.062.
195 X. Kou, L. Tong, Y. Shen, W. Zhu, L. Yin, S. Huang, F. Zhu, G. Chen and G. Ouyang, *Biosens. Bioelectron.*, 2020, **156**, 112095, DOI: 10.1016/j.bios.2020.112095.
196 X. Zeng, J. Hu, M. Zhang, F. Wang, L. Wu and X. Hou, *Anal. Chem.*, 2020, **92**, 2097–2102, DOI: 10.1021/acs.analchem.9b04598.
197 C.-Y. Zhu, Z. Wang, J.-T. Mo, Y.-N. Fan and M. Pan, *J. Mater. Chem. C*, 2020, **8**, 9916–9922, DOI: 10.1039/D0TC02391D.

198 L. Hou, Y. Qin, J. Li, S. Qin, Y. Huang, T. Lin, L. Guo, F. Ye and S. Zhao, *Biosens. Bioelectron.*, 2019, **143**, 111605, DOI: 10.1016/j.bios.2019.111605.
199 X. Lian, T. Miao, X. Xu, C. Zhang and B. Yan, *Biosens. Bioelectron.*, 2017, **97**, 299–304, DOI: 10.1016/j.bios.2017.06.018.
200 J. Guo, *Anal. Chem.*, 2016, **88**, 11986–11989, DOI: 10.1021/acs.analchem.6b04345.
201 Z. Xu, Z. Liu, M. Xiao, L. Jiang and C. Yi, *Chem. Eng. J.*, 2020, **394**, 124966, DOI: 10.1016/j.cej.2020.124966.
202 X. Zhu, S. Yuan, Y. Ju, J. Yang, C. Zhao and H. Liu, *Anal. Chem.*, 2019, **91**, 10764–10771, DOI: 10.1021/acs.analchem.9b02328.
203 T. R. Veltman, C. J. Tsai, N. Gomez-Ospina, M. W. Kanan and G. Chu, *ACS Sens.*, 2020, **5**, 2415–2421, DOI: 10.1021/acssensors.0c00480.
204 T. Leelasree, V. Selamneni, T. Akshaya, P. Sahatiya and H. Aggarwal, *J. Mater. Chem. B*, 2020, **8**, 10182–10189, DOI: 10.1039/D0TB01748E.
205 W. Ling, G. Liew, Y. Li, Y. Hao, H. Pan, H. Wang, B. Ning, H. Xu and X. Huang, *Adv. Mater.*, 2018, **30**, 1800917, DOI: 10.1002/adma.201800917.
206 C. S. Wood, M. R. Thomas, J. Budd, T. P. Mashamba-Thompson, K. Herbst, D. Pillay, R. W. Peeling, A. M. Johnson, R. A. McKendry and M. M. Stevens, *Nature*, 2019, **566**, 467–474, DOI: 10.1038/s41586-019-0956-2.
207 X. Wei, J. Guo, H. Lian, X. Sun and B. Liu, *Sens. Actuators, B*, 2021, **329**, 129205, DOI: 10.1016/j.snb.2020.129205.
208 S. Nagabooshanam, S. Roy, A. Mathur, I. Mukherjee, S. Krishnamurthy and L. M. Bharadwaj, *Sci. Rep.*, 2019, **9**, 1–9, DOI: 10.1038/s41598-019-56510-y.
209 L. D. Trino, L. G. S. Albano, D. C. Granato, A. G. Santana, D. H. S. de Camargo, C. C. Correa, C. C. B. Bufon and A. F. P. Leme, *Chem. Mater.*, 2021, **33**, 1293–1306, DOI: 10.1021/acs.chemmater.0c04201.
210 C. Wang, L. Wang, S. Tadepalli, J. J. Morrissey, E. D. Kharasch, R. R. Naik and S. Singamaneni, *ACS Sens.*, 2018, **3**, 342–351, DOI: 10.1021/acssensors.7b00762.
211 C. Wang, S. Tadepalli, J. Luan, K. K. Liu, J. J. Morrissey, E. D. Kharasch, R. R. Naik and S. Singamaneni, *Adv. Mater.*, 2017, **29**, 1604433, DOI: 10.1002/adma.201604433.
212 S. J. Qin and B. Yan, *Sens. Actuators, B*, 2018, **259**, 125–132, DOI: 10.1016/j.snb.2017.12.060.
213 S. J. Qin and B. Yan, *Anal. Chim. Acta*, 2018, **259**, 82–89, DOI: 10.1016/j.aca.2018.01.041.
214 L. Yu, Q. Zheng, D. Wu and Y. Xiao, *Sens. Actuators, B*, 2019, **294**, 199–205, DOI: 10.1016/j.snb.2019.05.037.
215 H. A. J. Al Lawati and J. Hassanzadeh, *Anal. Chim. Acta*, 2020, **1139**, 15–26, DOI: 10.1016/j.aca.2020.09.026.
216 Y. Zhang and B. Yan, *Nanoscale*, 2019, **11**, 22946–22953, DOI: 10.1039/C9NR06475C.
217 G. C. Ilacas, A. Basa, K. J. Nelms, J. D. Sosa, Y. Y. Liu and F. A. Gomez, *Anal. Chim. Acta*, 2019, **1055**, 74–80, DOI: 10.1016/j.aca.2019.01.009.
218 I. Ortiz-Gómez, A. Salinas-Castillo, A. G. García, J. A. Álvarez-Bermejo, I. D. Orbe-Payá, A. Rodríguez-Diéguez and L. F. Capitán-Vallvey, *Microchim. Acta*, 2017, **185**, 47, DOI: 10.1007/s00604-017-2575-7.
219 M. Mohammad, A. Razmjou, K. Liang, M. Asadnia and V. Chen, *ACS Appl. Mater. Interfaces*, 2018, **11**, 1807–1820, DOI: 10.1021/acsami.8b16837.
220 L. Wang, G. Liu, Y. Ren, Y. Feng, X. Zhao, Y. Zhu, M. Chen, F. Zhu, Q. Liu and X. Chen, *Anal. Chem.*, 2020, **92**, 14259–14266, DOI: 10.1021/acs.analchem.0c03723.
221 S. Nagabooshanam, S. Sharma, S. Roy, A. Mathur, S. Krishnamurthy and L. M. Bharadwaj, *IEEE Sens. J.*, 2021, **21**, 4129–4134, DOI: 10.1109/JSEN.2020.3030034.
222 K. Yi, X. Zhang and L. Zhang, *Sci. Total Environ.*, 2021, **772**, 144952, DOI: 10.1016/j.scitotenv.2021.144952.
223 S. Okur, Z. Zhang, M. Sarheed, P. Nick, U. Lemmer and L. Heinke, *Sens. Actuators, B*, 2020, **306**, 127502, DOI: 10.1016/j.snb.2019.127502.
224 I. Mukherjee, T. Basu and L. M. Bharadwaj, *Nanoscale*, 2020, **12**, 21719–21733, DOI: 10.1039/D0NR04480F.
225 F. Zhang, H. Yao, T. Chu, G. Zhang, Y. Wang and Y. Yang, *Chem. – Eur. J.*, 2017, **23**, 10293, DOI: 10.1002/chem.201701852.
226 H. Kim, B. T. Trinh, K. H. Kim, J. Moon, H. Kang, K. Jo, R. Akter, J. Jeong, E. K. Lim, J. Jung and H. S. Choi, *Biosens. Bioelectron.*, 2021, **179**, 113063, DOI: 10.1016/j.bios.2021.113063.
227 Q. Luan, N. Gan, Y. Cao and T. Li, *J. Agric. Food Chem.*, 2017, **65**, 5731–5740, DOI: 10.1021/acs.jafc.7b02139.
228 S. Sachdeva, S. J. H. Koper, A. Sabetghadam, D. Socco, D. J. Gravesteijn, F. Kapteijn, E. J. R. Sudhölter, J. Gascon and L. C. P. M. de Smet, *ACS Appl. Mater. Interfaces*, 2017, **9**, 24926–24935, DOI: 10.1021/acsami.7b02630.
229 H. D. Lawson, S. P. Walton and C. Chan, *ACS Appl. Mater. Interfaces*, 2021, **13**, 7004–7020, DOI: 10.1021/acsami.1c01089.
230 M. J. Neufeld, B. R. Ware, A. Lutzke, S. R. Khetani and M. M. Reynolds, *ACS Appl. Mater. Interfaces*, 2016, **8**, 19343–19352, DOI: 10.1021/acsami.6b05948.
231 M. J. Neufeld, A. Lutzke, J. B. Tapia and M. M. Reynolds, *ACS Appl. Mater. Interfaces*, 2017, **9**, 5139–5148, DOI: 10.1021/acsami.6b14937.
232 M. J. Neufeld, A. Lutzke, W. M. Jones and M. M. Reynolds, *ACS Appl. Mater. Interfaces*, 2017, **9**, 35628–35641, DOI: 10.1021/acsami.7b11846.
233 D. W. Sun, L. Huang, H. Pu and J. Ma, *Chem. Soc. Rev.*, 2021, **50**, 1070–1110, DOI: 10.1039/C9CS00829B.
234 P. L. Wang, L. H. Xie, E. A. Joseph, J. R. Li, X. O. Su and H. C. Zhou, *Chem. Rev.*, 2019, **119**, 10638–10690, DOI: 10.1021/acs.chemrev.9b00257.
235 A. Walter, R. Finger, R. Huber and N. Buchmann, *Proc. Natl. Acad. Sci. U. S. A.*, 2017, **114**, 6148–6150, DOI: 10.1073/pnas.1707462114.
236 M. Woellner, S. Hausdorf, N. Klein, P. Mueller, M. W. Smith and S. Kaskel, *Adv. Mater.*, 2018, **30**, 1704679, DOI: 10.1002/adma.201704679.
237 R. Ricco, M. J. Styles and P. Falcaro, *Metal–organic Frameworks (MOFs) for Environmental Applications*, Elsevier, 2019, pp. 383–426, DOI: 10.1016/B978-0-12-814633-0.00012-0.

238 S. Kempahanumakkagari, K. Vellingiri, A. Deep, E. E. Kwon, N. Bolan and K.-H. Kim, *Coord. Chem. Rev.*, 2018, **357**, 105–129, DOI: 10.1016/j.ccr.2017.11.028.

239 Y. Zhang, S. Yuan, X. Feng, H. Li, J. Zhou and B. Wang, *J. Am. Chem. Soc.*, 2016, **138**, 5785–5788, DOI: 10.1021/jacs.6b02553.

240 P. Li, J. Li, X. Feng, J. Li, Y. Hao, J. Zhang, H. Wang, A. Yin, J. Zhou, X. Ma and B. Wang, *Nat. Commun.*, 2019, **10**, 2177, DOI: 10.1038/s41467-019-10218-9.

241 Y. Chen, S. Zhang, S. Cao, S. Li, F. Chen, S. Yuan, C. Xu, J. Zhou, X. Feng, X. Ma and B. Wang, *Adv. Mater.*, 2017, **29**, 1606221, DOI: 10.1002/adma.201606221.

242 J. Ruiz-Jimenez, N. Zanca, H. Lan, M. Jussila, K. Hartonen and M. L. Riekkola, *J. Chromatogr. A*, 2019, **1597**, 202–208, DOI: 10.1016/j.chroma.2019.04.009.

243 Z. Chen, K. Ma, J. J. Mahle, H. Wang, Z. H. Syed, A. Atilgan, Y. Chen, J. H. Xin, T. Islamoglu, G. W. Peterson and O. K. Farha, *J. Am. Chem. Soc.*, 2019, **141**, 20016, DOI: 10.1021/jacs.9b11172.

244 C. Montoro, F. Linares, E. Q. Procopio, S. Senkovska, S. Kaskel, S. Galli, N. Masciocchi, E. Barea and J. A. Navarro, *J. Am. Chem. Soc.*, 2011, **133**, 11888–11891, DOI: 10.1021/ja2042113.

245 Z. Chen, K. Ma, J. J. Mahle, H. Wang, Z. H. Syed, A. Atilgan, Y. Chen, J. H. Xin, T. Islamoglu, G. W. Peterson and O. K. Farha, *J. Am. Chem. Soc.*, 2019, **141**, 20016–20021, DOI: 10.1021/jacs.9b11172.

246 M. W. Terban, S. K. Ghose, A. M. Plonka, D. Troya, P. Juhás, R. E. Dinnebier, J. J. Mahle, W. O. Gordon and A. I. Frenkel, *Chem. Commun.*, 2021, **4**, 2, DOI: 10.1038/s42004-020-00439-1.

247 T. Islamoglu, A. Atilgan, S.-Y. Moon, G. W. Peterson, J. B. DeCoste, M. Hall, J. T. Hupp and O. K. Farha, *Chem. Mater.*, 2017, **29**, 2672–2675, DOI: 10.1021/acs.chemmater.6b04835.

248 A. Atilgan, T. Islamoglu, A. J. Howarth, J. T. Hupp and O. K. Farha, *ACS Appl. Mater. Interfaces*, 2017, **9**, 24555–24560, DOI: 10.1021/acsami.7b05494.

249 S. Goswami, C. E. Miller, J. L. Logsdon, C. T. Buru, Y.-L. Wu, D. N. Bowman, T. Islamoglu, A. M. Asiri, C. J. Cramer, M. R. Wasielewski, J. T. Hupp and O. K. Farha, *ACS Appl. Mater. Interfaces*, 2017, **9**, 19535–19540, DOI: 10.1021/acsami.7b07055.

250 J. E. Mondloch, M. J. Katz, W. C. Isley III, P. Ghosh, P. Liao, W. Bury, G. W. Wagner, M. G. Hall, J. B. DeCoste, G. W. Peterson, R. Q. Snurr, C. J. Cramer, J. T. Hupp and O. K. Farha, *Nat. Mater.*, 2015, **14**, 512–516, DOI: 10.1038/nmat4238.

251 Y. Liu, A. J. Howarth, N. A. Vermeulen, S. Y. Moon, J. T. Hupp and O. K. Farha, *Coord. Chem. Rev.*, 2017, **346**, 101–111, DOI: 10.1016/j.ccr.2016.11.008.

252 N. S. Bobbitt, M. L. Mendonca, A. J. Howarth, T. Islamoglu, J. T. Hupp, O. K. Farha and R. Q. Snurr, *Chem. Soc. Rev.*, 2017, **46**, 3357–3385, DOI: 10.1039/C7CS00108H.

253 S. Chong, S. Lee, B. Kim and J. Kim, *Coord. Chem. Rev.*, 2020, **423**, 213487, DOI: 10.1016/j.ccr.2020.213487.

254 X. Zhang, K. Zhang, H. Yoo and Y. Lee, *ACS Sustainable Chem. Eng.*, 2021, **9**, 2872–2879, DOI: 10.1021/acssuschemeng.0c08806.

255 X. Zhang, K. Zhang and Y. Lee, *ACS Appl. Mater. Interfaces*, 2020, **12**, 734–743, DOI: 10.1021/acsami.9b17867.

256 Z. Shi, W. Yang, X. Deng, C. Cai, Y. Yan, H. Liang, Z. Liu and Z. Qiao, *Mol. Syst. Des. Eng.*, 2020, **5**, 725–742, DOI: 10.1039/D0ME00005A.

257 R. Batra, C. Chen, T. G. Evans, K. S. Walton and R. Ramprasad, *Nat. Mach. Intell.*, 2020, **2**, 704–710, DOI: 10.1038/s42256-020-00249-z.

258 G. Borboudakis, T. Stergiannakos, M. Frysali, E. Klontzas, I. Tsamardinos and G. E. Froudakis, *npj Comput. Mater.*, 2017, **3**, 40, DOI: 10.1038/s41524-017-0045-8.

259 J. A. Gustafson and C. E. Wilmer, *Sens. Actuators, B*, 2018, **267**, 483–493, DOI: 10.1016/j.snb.2018.04.049.

260 S. Okur, P. Qin, A. Chandresh, C. Li, Z. Zhang, U. Lemmer and L. Heinke, *Angew. Chem., Int. Ed.*, 2021, **60**, 3566–3571, DOI: 10.1002/anie.202013227.

261 G. Gaal, T. A. da Silva, V. Gaal, R. C. Hensel, L. R. Amaral, V. Rodrigues and A. Riul Jr, *Front. Chem.*, 2018, **6**, 151, DOI: 10.3389/fchem.2018.00151.

262 Z. Shi, W. Yang, X. Deng, C. Cai, Y. Yan, H. Liang, Z. Liu and Z. Qiao, *Mol. Syst. Des. Eng.*, 2020, **5**, 725–742, DOI: 10.1039/D0ME00005A.

263 M. Rubio-Martinez, M. P. Batten, A. Polyzos, K.-C. Carey, J. I. Mardel, K.-S. Lim and M. R. Hill, *Sci. Rep.*, 2014, **4**, 5443, DOI: 10.1038/srep05443.

264 C. A. M. de la Huerta, V. H. Nguyen, A. Sekkat, C. Crivello, F. Toldra-Reig, P. B. Veiga, S. Quessada, C. Jimenez and D. Muñoz-Rojas, *Adv. Mater. Technol.*, 2020, **5**, 2000657, DOI: 10.1002/admt.202000657.